

AD-A064 055

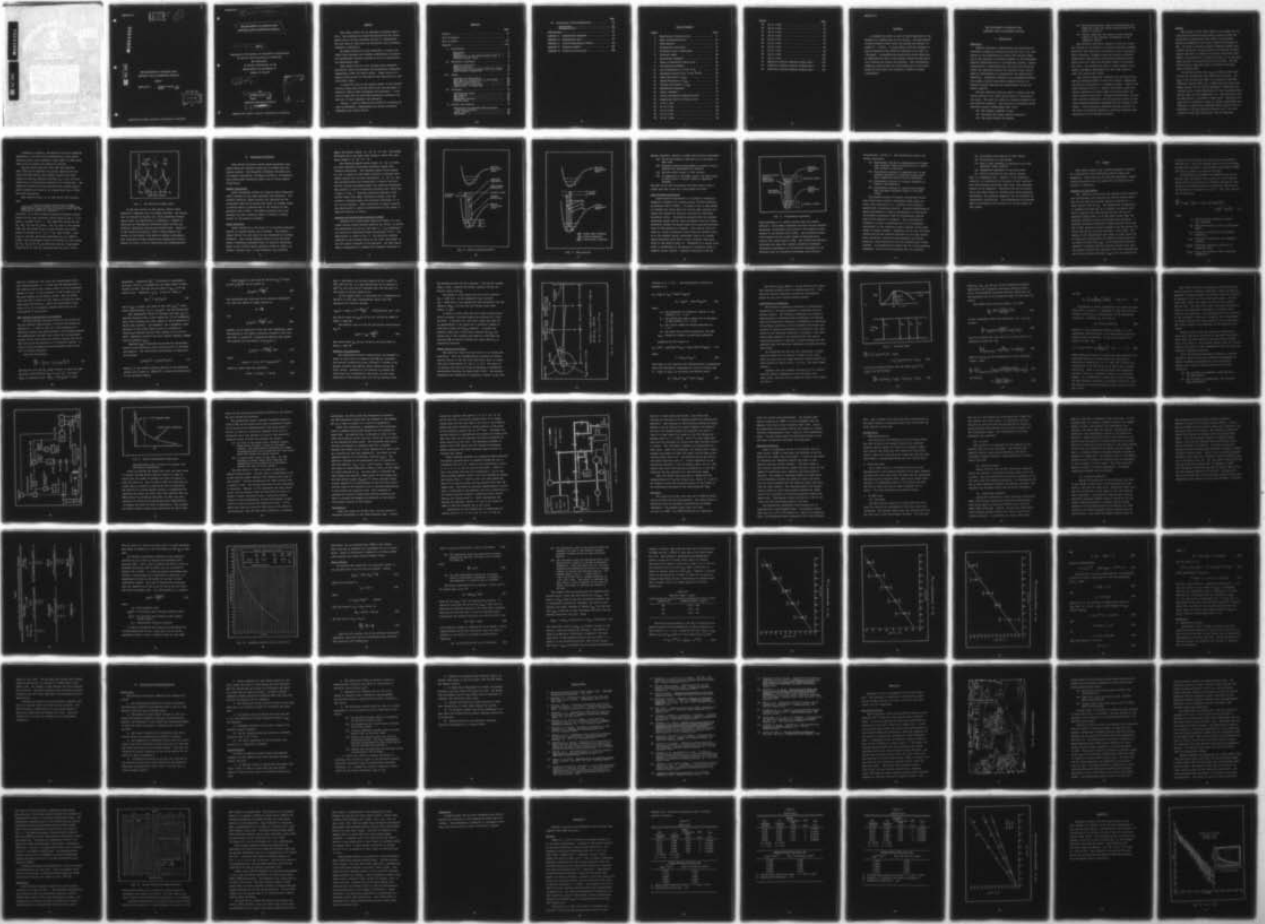
AIR FORCE INST OF TECH WRIGHT-PATTERSON AFB OHIO' SCH--ETC F/G 7/2  
THE MEASUREMENT OF QUENCHING RATE CONSTANTS USING FLUORSCENCE E--ETC(U)  
DEC 78 F GARCIA

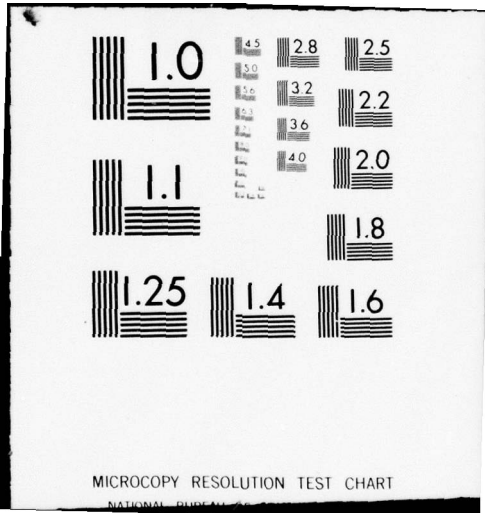
UNCLASSIFIED

AFIT-6EP/PH/78-3

NL

1 of 2  
AD  
A064055





MICROCOPY RESOLUTION TEST CHART

NATIONAL BUREAU OF STANDARDS-1963-A

GEP/PH/78-3

LEVEL #

①

ADA064055

DDC FILE COPY.

THE MEASUREMENT OF QUENCHING RATE  
CONSTANTS USING FLUORESCENCE EMISSION

THESIS

GEP/PH/78-3

Freddie Garcia, Jr.  
Major USAF

DDC  
RECEIVED  
JAN 31 1979  
A

14 AFIT-GEP/PH/78-3

6 THE MEASUREMENT OF QUENCHING RATE  
CONSTANTS USING FLUORESCENCE EMISSION.

9 Master's THESIS

Presented to the Faculty of the School of Engineering  
of the Air Force Institute of Technology  
Air University  
in Partial Fulfillment of the  
Requirements for the Degree of  
Master of Science

12 119 p.

10 by  
Freddie Garcia, Jr

Major USAF

Graduate Engineering Physics

11 December 1978

ABSTRACT	
NTIS	Write Section <input checked="" type="checkbox"/>
DDC	Write Section <input type="checkbox"/>
ORIGINATOR	<input type="checkbox"/>
JUSTIFICATION	
BY	
SYSTEMS	
DATE	
A	

Approved for public release; distribution unlimited

012 225

Gae

## Preface

This thesis effort was an extremely rewarding experience. The knowledge and experience gained from the experimental effort and the personnel involved is immeasurable. The many hours of hard work and frustration were handsomely rewarded at completion.

My humble thanks go to Paul Schreiber, a unique individual whose patience and in-depth understanding of physics and experimental analysis provided me with an appreciation for experimental work.

Many thanks also go to Dr. Rajendra Gupta (Arkansas University) whose encouragement and experimental background tremendously aided the thesis effort. Thanks also go to Captain Allen Hunter who provided me the opportunity to take this thesis topic.

I would also like to pay special thanks to Sig Kizirnis and Don Linder whose time and effort kept the equipment in excellent working order throughout the experiment. I wish also to thank the Air Force Aero Propulsion Laboratory for the loan of their equipment and personnel.

Lastly, I wish to thank my wife Renee for providing me with encouragement, understanding and typing assistance throughout this thesis effort.

## Contents

	Page
Preface . . . . .	ii
List of Figures . . . . .	v
List of Tables . . . . .	vii
Abstract . . . . .	viii
I. Introduction . . . . .	1
Background . . . . .	1
Purpose . . . . .	3
Improvements to the Wharton Effort (Ref 3) . . . . .	4
Nitrogen Dioxide (NO <sub>2</sub> ) . . . . .	4
II. Diagnostic Techniques . . . . .	8
Doppler Velocimetry . . . . .	8
Raman Scattering . . . . .	8
Coherent-Anti-Stokes Raman Scattering (CARS) . . . . .	9
Laser-Induced Fluorescence . . . . .	12
III. Theory . . . . .	16
Statement of the Problem . . . . .	16
Rate Equation Relationship to Experiment . . . . .	20
Diffusion Considerations . . . . .	23
Photon Counting Statistics . . . . .	24
Applications to Combustion . . . . .	27
IV. Procedure . . . . .	33
Experimental Method . . . . .	33
Gas Handling . . . . .	37
Dye Laser . . . . .	40
Background Counting . . . . .	41
Problem Areas . . . . .	42
V. Results and Analysis . . . . .	47
Calculation of Quenching Rate Constants and Cross-Sections . . . . .	47
Error Analysis . . . . .	51
Discussion . . . . .	59

	Page
VI. Conclusions and Recommendations . . . . .	63
Conclusions . . . . .	63
Recommendations . . . . .	64
Bibliography . . . . .	67
Appendix A: Experimental Equipment . . . . .	70
Appendix B: Experimental Data . . . . .	81
Appendix C: Plotted Experimental Results . . . . .	86
Appendix D: Computer Program . . . . .	102
Appendix E: Probability Derivation . . . . .	106

List of Figures

Figure		Page
1	NO <sub>2</sub> Potential Energy Curves . . . . .	7
2	Raman Scattering Process . . . . .	10
3	CARS Sequence . . . . .	11
4	Fluorescence Scattering . . . . .	13
5	Collection Optics Solid Angle . . . . .	25
6	Two-Level Model . . . . .	28
7	Electronics Schematic . . . . .	34
8	Delay of Exponential Decay Curve . . . . .	35
9	Gas Handling Schematic . . . . .	39
10	Noise Comparison at 5 Torr of N <sub>2</sub> . . . . .	46
11	Quenching Constant Plot of Ref 29:720 . . . . .	50
12	Argon Deviations in T <sub>eff</sub> . . . . .	55
13	Helium Deviations in T <sub>eff</sub> . . . . .	56
14	Nitrogen Deviations in T <sub>eff</sub> . . . . .	57
15	Experimental Equipment . . . . .	71
16	Optics Schematic . . . . .	75
17	Filter Transmission Characteristics . . . . .	77
18	Regression Curves of Foreign Gases . . . . .	85
19	Ar at 1 Torr . . . . .	87
20	Ar at 2 Torr . . . . .	88
21	Ar at 3 Torr . . . . .	89
22	Ar at 4 Torr . . . . .	90
23	Ar at 5 Torr . . . . .	91

Figure		Page
24	He at 1 Torr . . . . .	92
25	He at 2 Torr . . . . .	93
26	He at 3 Torr . . . . .	94
27	He at 4 Torr . . . . .	95
28	He at 5 Torr . . . . .	96
29	N <sub>2</sub> at 1 Torr . . . . .	97
30	N <sub>2</sub> at 2 Torr . . . . .	98
31	N <sub>2</sub> at 3 Torr . . . . .	99
32	N <sub>2</sub> at 4 Torr . . . . .	100
33	N <sub>2</sub> at 5 Torr . . . . .	101
34	Effective Lifetime Computer Program Page 1 . .	103
35	Effective Lifetime Computer Program Page 2 . .	104
36	Effective Lifetime Computer Program Page 3 . .	105

Abstract

A tuneable dye laser is used to excite  $\text{NO}_2$  while in the presence of a foreign gas (Ar, He and  $\text{N}_2$ ). The  $\text{NO}_2$  pressure is held constant (mTorr) while the foreign gas pressure is varied (1 - 5 Torr). A single photon counting technique is used to measure an  $\text{NO}_2$  effective lifetime on the order of 1 microsec. A quenching rate constant for each foreign gas is calculated by using a relationship between the  $\text{NO}_2$  effective lifetime and foreign gas pressure. The corresponding quenching cross-section for each foreign gas is also determined and the results are compared to those of another investigator.

THE MEASUREMENT OF QUENCHING RATE  
CONSTANTS USING FLUORESCENCE EMISSION

I. Introduction

Background

Improved production, understanding and utilization of combustion systems for military and civilian use is of vital concern to the conservation of fossil fuel derived energy and to the reduction of pollution products in the atmosphere. Complete characterization of the molecular kinetics, species concentrations, temperatures and flow velocities occurring within the combustion process are currently being investigated by experimentalists (diagnostics) and theoreticians (modeling). Combustion diagnostics and combustion modeling are closely related fields whose combined efforts are directed towards improving the understanding of the combustion process.

The most effective method by which to analyze the combustion process is to probe various parts of the flame or jet plume. The probe can either be intrusive (material) or non-intrusive (optical). The intrusive or perturbing probe possesses several disadvantages (Ref 1:74):

- (a) The temporal response is poor.
- (b) The probe size limits spatial resolution.
- (c) The probe disturbs the medium.

- (d) The combined chemical reaction between probe and flame will alter the species concentration of the medium of interest.
- (e) Present probes may not survive or give accurate results in the strenuous environments of new combustion systems.

The practical limitations imposed on intrusive probes are overcome by non-intrusive or optical diagnostic methods which have been enhanced by the advent of laser technology. Laser technology, although costly and requiring elaborate experimental configurations has provided combustion diagnostics with the ideal non-perturbing probe; the tuneable dye laser. The tuneable dye laser is ideal because it can produce narrowband wavelengths and large peak powers in short (ns) pulses (Ref 2:863).

Four optical diagnostic processes are currently being used for characterization of the flow velocity, temperature and species concentrations of combustion media. They are all laser processes known as: Doppler velocimetry, Raman scattering, Coherent-Anti-Stokes Raman Scattering (CARS) and Laser-induced fluorescence. Although each diagnostic process offers distinct advantages only the quenching aspects of the laser induced fluorescence technique will be studied in this report. The fluorescence technique naturally provides for the study of quenching parameters, which are important characteristics of the combustion process.

### Purpose

The purpose of this thesis effort is to modify and use a previously developed single photon counting scheme and experimental configuration (Ref 3:39) to characterize quenching parameters of the laser induced fluorescence of  $\text{NO}_2$ . By using a selected incident wavelength ( $4368\text{\AA}$ ) from a tuneable dye laser, the  $\text{NO}_2$  molecule (at constant 19 mTorr partial pressure) is raised to an excited electronic level ( $\text{NO}_2^*$ ) in the presence of a foreign gas (He, Ar, or  $\text{N}_2$ ) whose total pressure is varied from one to five Torr. The  $\text{NO}_2^*$  fluorescence is detected across a broadband wavelength region ( $5430\text{\AA} \pm 15\text{\AA}$ ).

An effective decay time ( $T_{\text{eff}}$ ) of  $\text{NO}_2^*$  to other lower levels will be found for each foreign gas pressure. The  $T_{\text{eff}}$  (5 per foreign gas) which is a function of the  $\text{NO}_2^*$  radiative lifetime ( $10\mu\text{s} \leq T_r \leq 210\mu\text{s}$ ) and the foreign gas number density will be used to determine a quenching rate constant  $K_q(T)$  at room temperature (T) and a quenching cross-section  $\sigma_q(T)$  at room temperature (T). The collection time per data point is a minimum of three hours. Each  $K_q(T)$  and  $\sigma_q(T)$  will be compared to those of another investigator who performed a steady state experiment which requires a priori knowledge of the  $\text{NO}_2$  radiative lifetime ( $T_r$ ). An error analysis of the  $K_q(T)$  values will also be performed.

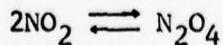
### Improvements to the Wharton Effort (Ref 3)

The single photon counting scheme (Method II) developed by Wharton (Ref 3:38) has been modified and improved in order to facilitate the quenching analysis of  $\text{NO}_2$ . The areas improved/modified are as follows:

- (a) Completely redesigned the gas handling system. The new system design allows improved gas evacuation (to  $10^{-7}$  Torr), improved pressure monitoring instrumentation and better techniques for the introduction of a foreign gas. Also new are gas flow tubing connections; Cajon, Varion and Swagelok fittings.
- (b) Added a Turbo Molecular Pump for continuous system evacuation.
- (c) Added a new Time-To-Pulse Height Converter (TPHC) to extend into the experimentally required micro-second range.
- (d) Redesigned a new sample tube to improve fluorescence collection.

### Nitrogen Dioxide ( $\text{NO}_2$ )

$\text{NO}_2$  exists as a stable polyatomic gaseous molecule with 17 electrons and  $\text{N}_2\text{O}_4$  as a stable dimer (no visible absorption). In the ground state  $\text{NO}_2$  exists as a bent molecule with a bond angle of  $134^\circ 15'$  and a bond length of  $1.1994\text{\AA}$  (Ref 4:252). Douglas and Huber (Ref 5:79) determined that  $\text{NO}_2$  in the  ${}^2\text{B}_1$  excited state has a linear or nearly linear bond angle of approximately  $180^\circ$ . In equilibrium



At pressures less than 10 Torr, less than 1% of  $N_2O_4$  exists in equilibrium with  $NO_2$ . Hence the  $N_2O_4$  concentration is neglected in this experimental effort since  $NO_2$  is maintained at approximately 19 mTorr.

$NO_2$  was chosen to be studied because it is one of the combustion species, it is an atmospheric pollutant and it possesses a wide absorption band ( $3200\text{\AA}$  to  $10,000\text{\AA}$  (Ref 5:74)) encompassing the visible region. Thus the  $NO_2$  absorption spectrum is readily accessible to tuneable dye lasers for fluorescence analysis and is easily studied in the laboratory.

$NO_2$  has been the subject of intensive analysis by several investigators for another important reason: fluorescence studies indicate that the  $NO_2$  radiative lifetime ( $T_r$ ) is more than two orders of magnitude in excess of that found using the integrated absorption coefficient lifetime (Ref 6:355). Douglas (Ref 7:1014) has analyzed the anomalously long  $NO_2$  radiative lifetime and concludes that four mechanisms may be responsible for this phenomena:

- (a) Interelectronic level mixing
- (b) Vibrational level mixing (upper level with lower level).
- (c) Frequency effect of excited versus fluorescence radiation
- (d) Transition moment variation of high vibrational levels

According to Douglas, the dominant long life producing mechanism is, the fact that interelectronic level mixing with the ground state produces a large number of weak lines, which tend to increase the radiative lifetime.

NO<sub>2</sub> has defied analysis since 1834 when Brewster (Ref 8:519) first observed its visible spectrum and also since 1929 when Baxter (Ref 9:3920) reported the first studies of the NO<sub>2</sub> radiative lifetime ( $T_r = 1\mu s$ ) by actual observation of fluorescence quenching by a foreign gas. The radiative lifetime has been analyzed using several experimental methods and values of  $T_r$  ranging from 44 $\mu s$  to 200 $\mu s$  have been determined.

More recently Monts, et al (Ref 10:37) have reported that

. . . the NO<sub>2</sub> visible spectrum has too many rotational lines associated with too many vibrational bands because there are four electronic states that may directly or indirectly, interact . . . .

Gillispie, et al (Ref 11:3425) calculated potential energy curves for the four electronic states lying in the 2 - 4 eV region, as shown in Fig. 1. The electronic states are the <sup>2</sup>A<sub>1</sub>, <sup>2</sup>B<sub>1</sub>, <sup>2</sup>B<sub>2</sub> and <sup>2</sup>A<sub>2</sub> states. The <sup>2</sup>A<sub>1</sub> state is the ground state and the ground state to first excited state interaction is assumed to be <sup>2</sup>B<sub>1</sub> ← <sup>2</sup>A<sub>1</sub> (Ref 12:459). Thus using an incident excitation wavelength ( $\lambda_E$ ) of 4368 $\text{\AA}$  or 2.84eV, this experimental effort is exciting NO<sub>2</sub> into either the <sup>2</sup>B<sub>1</sub>, <sup>2</sup>B<sub>2</sub> or the <sup>2</sup>A<sub>2</sub> excited state and the fluorescence studied will be from the continuum emission (Ref 13:817).

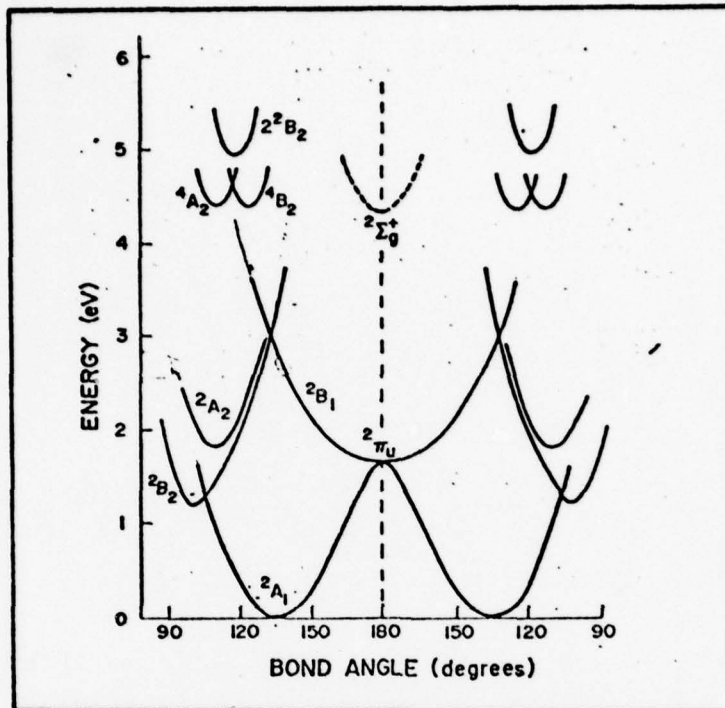


Fig. 1. NO<sub>2</sub> Potential Energy Curves

In the next section of this thesis, various laser diagnostic techniques will be briefly reviewed. The section will be followed by Chapter III, which introduces fluorescence theory and applications to combustion. Chapter IV describes the experimental procedures which includes gas handling, background counting and problem areas. Chapter V is the results and analysis section which compares the results of this effort with those of another investigator. Also discussed are error analysis and experimental results. Chapter VI gives a list of conclusions and recommendations.

## II. Diagnostic Techniques

This section discusses various laser diagnostic techniques which are presently being used to analyze the combustion process. The diagnostic techniques discussed are: (1) Doppler velocimetry, (2) Raman scattering, (3) Coherent-Anti-Stokes Raman Scattering (CARS) and (4) laser-induced fluorescence.

### Doppler Velocimetry

Laser velocimetry employs the Doppler effect (frequency shift) produced by the light scattered from particles. The velocity detection scheme collects the scattered and the unscattered beam and by mixing both beams, an optimum signal is derived which is proportional to the velocity of the particles (Ref 14:297). The method currently being used measures the time a particle takes to traverse a fringe pattern in the medium of interest.

### Raman Scattering

Raman scattering is the result of an inelastic collision between an incident photon and a molecule. This process (Raman effect) can take place for any wavelength of incident radiation. This energy exchange imparts to the scattered photon a different wavelength than its incident wavelength. Hence if the incident photon possesses energy  $h\nu$  where  $h$  is Planck's constant and  $\nu$  is the frequency, the scattered

photon may possess energy  $h\nu - \Delta E$  or  $h\nu + \Delta E$ . The energy difference  $\Delta E$  is the upper state energy  $E'$  minus the lower state energy  $E''$  or  $\Delta E = E' - E''$ .

The scattered photon having energy  $h\nu - \Delta E$  is known as Stokes radiation (scattered wavelength higher than incident wavelength). The scattered photon having energy  $h\nu + \Delta E$  is known as anti-Stokes radiation (scattered wavelength shorter than incident wavelength). If  $\Delta E = 0$ , then the scattered photon has experienced an elastic collision and the incident wavelength equals the scattered wavelength. This process is known as Rayleigh scattering (Ref 15:85) and is shown in Fig. 2. Rayleigh scattering produces a more intense signal than Raman scattering, however since the incident wavelength equals the scattered wavelength, it is not species specific. Raman scattering is species specific and proportional to species concentration but the signal is weak and difficult to detect.

#### Coherent-Anti-Stokes Raman Scattering (CARS)

Coherent-Anti-Stokes Raman Scattering (CARS) is a non-linear optical mixing process requiring two lasers, at different wavelengths ( $\lambda_1$  and  $\lambda_2$ ) such that  $(\lambda_1 - \lambda_2)$  corresponds to a molecular vibrational energy spacing (Ref 16:17). The CARS process is shown in Fig. 3. The radiation spectrum produced by the focusing action of two laser wavelengths is the anti-Stokes component of the molecule. The CARS experimental configuration is complex and extremely sensitive to

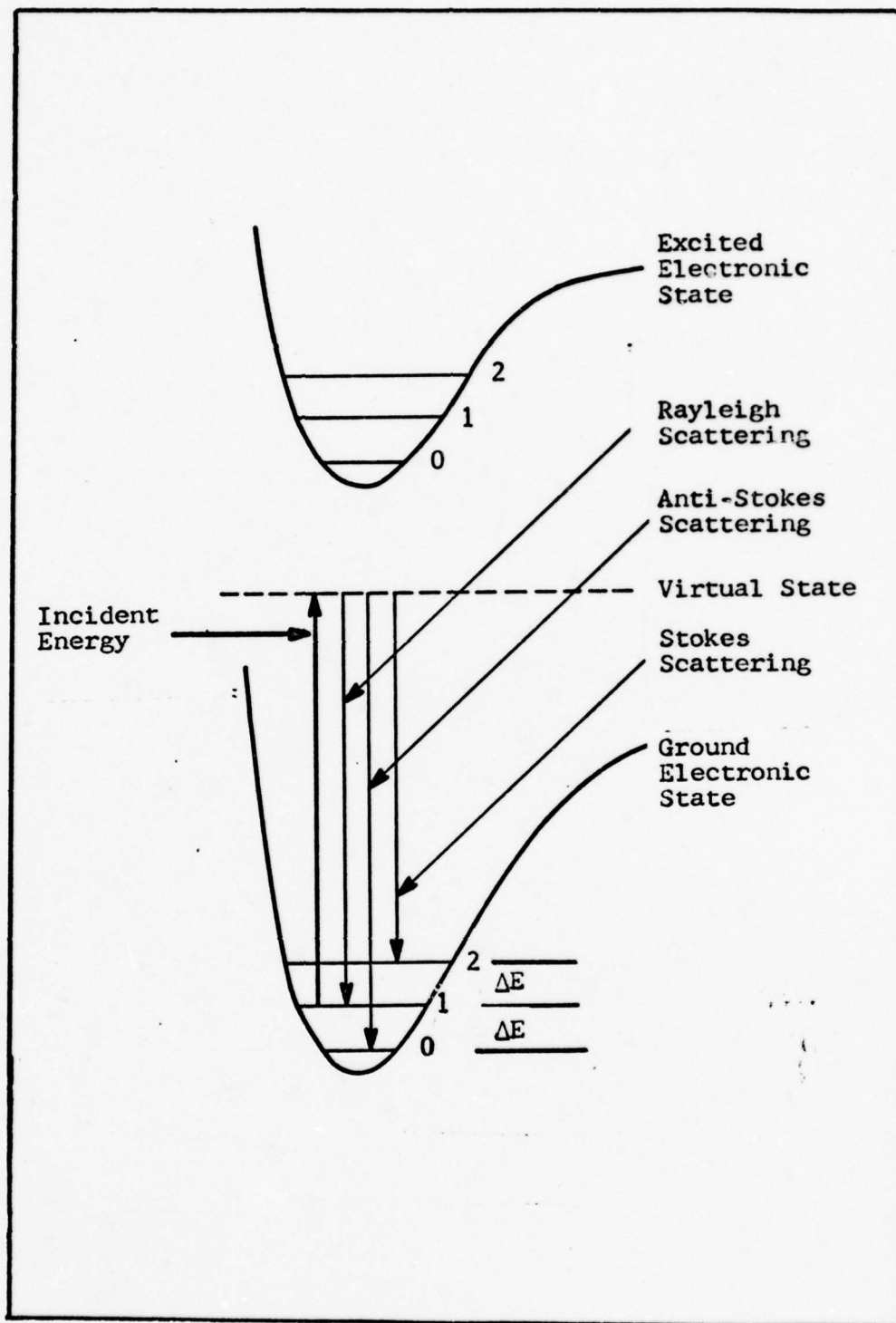


Fig. 2. Raman Scattering Process

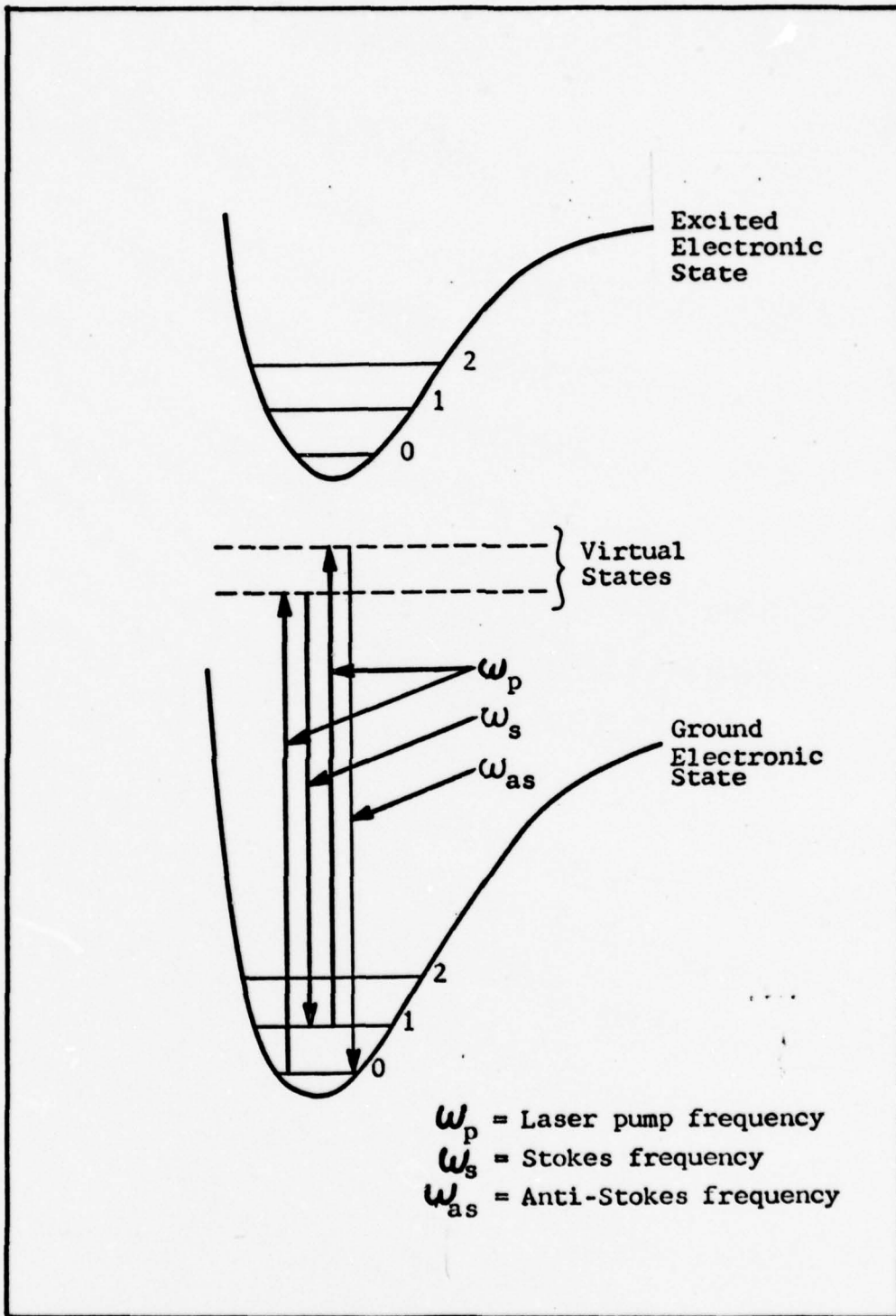


Fig. 3. CARS Sequence

optical alignment, however it offers some distinct advantages:

- (a) All of the radiation spectrum can be collected in real time.
- (b) Spatially resolved measurements of species concentrations and temperature are possible.
- (c) The anti-Stokes signal is very intense.
- (d) In comparison to the Raman signal, the CARS signal-to-noise ratio is several orders of magnitude stronger.

Roh (Ref 16:21) has investigated the CARS process using a single mode ruby laser and a ruby pumped dye laser.

#### Laser-Induced Fluorescence

Laser-induced fluorescence is an effective combustion diagnostic technique for studying energy transfer processes of molecules (Ref 17:1286). Its usage is due to the advance of tuneable dye lasers which can provide high intensity and narrow line widths for selective excitation of molecular absorption levels. Fluorescence requires that the incident wavelength energy possess exact coincidence with the energy difference between the ground state and an excited electronic state of the molecule of interest. This excited state can relax to a lower vibrational level within the excited state, or to the original ground vibrational level or to another ground vibration level after a finite resident time (mean-time) of the molecule (Fig. 4). Relaxation to a ground state level is accompanied by the emission of radiation which is normally Stokes shifted. Although fluorescence like the

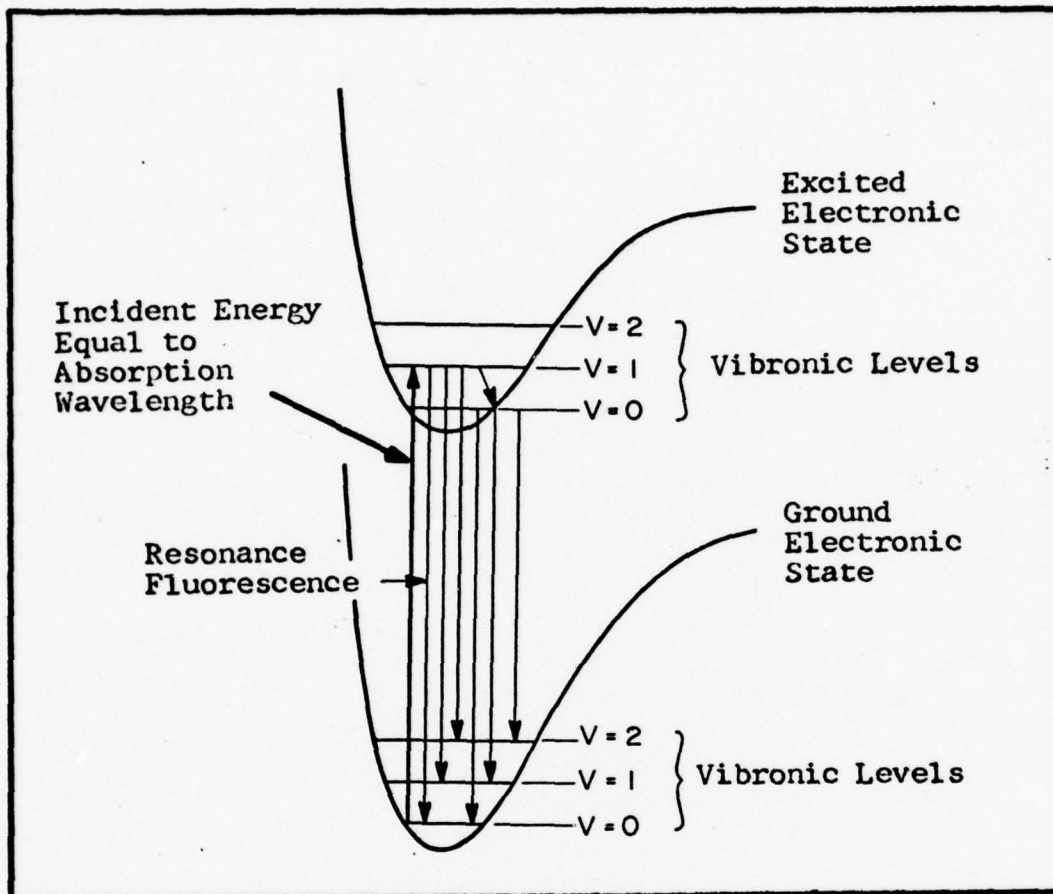


Fig. 4. Fluorescence Scattering

Raman phenomena is an optical process they are uniquely different. While Raman scattering can occur for any incident wavelength, fluorescence only occurs at the absorption wavelengths of the molecule (Ref 15:86). The resulting fluorescence emission can be several orders of magnitude more intense than either Raman or CARS. The fluorescence emission wavelength can equal the incident excitation wavelength (resonance fluorescence) or the emission wavelength can be different from the excitation wavelength (non-resonance

fluorescence), see Fig. 4. The fluorescence process has several advantages:

- (a) Fluorescence emission is characteristic of molecular structure, hence identification of a particular molecule is possible.
- (b) Fluorescence emission is characteristic of the relative population of molecular energy levels hence temperature values can be established.
- (c) Fluorescence emission is linearly dependent on species concentrations.
- (d) Fluorescence emission is usually much stronger than the Raman scattering signal or the CARS signal.

The simplest measure of species concentration arises from fluorescence intensity measurements made under collision free conditions; i.e., intensity being directly proportional to molecular density. The main disadvantage to direct measurement of species concentration is collisional non-radiative relaxation from the vibrationally excited level of the molecule of interest. This non-radiative relaxation is known as quenching and is of considerable significance in the combustion process because of the large number of species present. Quenching results from collisions between excited and unexcited molecules of the same species (self quenching), between excited molecules and foreign molecules, from dissociation and from intramolecular energy transfer. To quantitatively account for all of the quenching parameters, the following information must be available:

- (a) Collisional cross-section of each species
- (b) Concentration of each species
- (c) Rate of self quenching, dissociation and intramolecular energy transfer
- (d) Temperature dependence of the above rates
- (e) Partial pressures of each species present

This is a formidable task. However, if the absorption transition of the molecule of interest is fully saturated over the absorption wavelength (Ref 18:9), then quenching effects can be neglected. Saturation may not be possible due to the large values of incident laser energy required. Alternately, the quenching parameters can be controlled by experimental configuration. The determination of quenching rates and quenching cross-sections will be the subject of this report.

### III. Theory

This section begins with a problem statement, followed by a discussion of the relationship between theory and experiment. Also discussed are diffusion parameters, photon counting statistics and the application of saturation conditions to combustion.

#### Statement of the Problem

The problem is to calculate the quenching rate constants and corresponding cross-sections for each of several gases (Ar, He, N<sub>2</sub>) from the measured effective lifetime of a laser excited level of NO<sub>2</sub>. The experimental configuration is arranged such that NO<sub>2</sub>, at a constant low (mTorr) pressure is combined with each foreign gas (Ar, He, N<sub>2</sub>) at pressures ranging from 1 to 5 Torr which insures that the measured lifetime is due to only foreign gas quenching. A selected excitation wavelength, assumed constant and in the NO<sub>2</sub> visible absorption region irradiates the gas mixture and raises the NO<sub>2</sub> to an excited electronic state (NO<sub>2</sub><sup>\*</sup>). The density of the NO<sub>2</sub><sup>\*</sup> molecules will decay to lower states due to collisional deactivation and radiative transitions with an effective decay time T<sub>eff</sub>. If the measured fluorescent radiation is emitted from the original excited level only, the observed fluorescence radiation will decay exponentially and the NO<sub>2</sub> effective lifetime (T<sub>eff</sub>) will vary directly as

a function of the foreign gas pressure and the radiative lifetime ( $T_r$ ). Since the foreign gases used do not possess an absorption spectrum in the excitation wavelength ( $4368\text{\AA}$ ), only  $\text{NO}_2$  is raised to an excited state  $\text{NO}_2^*$ .

To theoretically determine the number density of the excited state  $N_j^*$  requires the solution of a rate equation which includes the processes of radiative absorption, spontaneous and stimulated emission, collisional deactivation and diffusion as illustrated in Eq (1). This rate equation can be written as

$$\frac{dN_j^*}{dt} = B_{ij}N_i\rho - \left[ \sum_i A_{ji} + B_{ji}\rho + \sum_i n_m K_{qi}(T) \right] N_j^* - Z_{jj}N_j^{*2} + D_f \nabla^2 N_j^* \quad (1)$$

where

$\rho$  = incident laser intensity in watts/  
cm x steradian

$N_j^*$  =  $\text{NO}_2^*$  number density of the  $j$ th vibrational level

$B_{ij}$  = Einstein B coefficient for isotropic absorption

$B_{ji}$  = Einstein B coefficient for stimulated emission

$B_{ij}N_i\rho$  = molecular excitation written as an absorption term

$B_{ij}g_i = B_{ji}g_j$  are related by their respective degeneracies

$\sum_i A_{ji} N_j^*$  = spontaneous emission rate from the jth excited level ( $N_j^*$ )

$B_{ji} N_j^* \rho$  = stimulated emission rate from the jth excited level ( $N_j^*$ )

$\sum_i n_m K_{qi}(T)$  = collective quenching of foreign gas molecules and  $n_m$  is the number density of the foreign gas molecular species and  $K_{qi}(T)$  is equal to the quenching rate constant of the foreign gas molecular species as a function of Temperature

$Z_{jj} N_j^*$  = self-collision or self-quenching rate ( $Z_{jj}$ ) of the excited jth level ( $N_j^*$ )

$D_f \nabla^2 N_j^*$  = diffusion rate of jth excited level where  $D_f$  is the diffusion coefficient

The self-collision rate can be ignored since calculations revealed that the low experimental pressure (mTorr) of the species to be excited ( $\text{NO}_2$ ) experiences negligible collisions. The diffusion rate can also be neglected at the specified pressures because the collision frequency per foreign gas allowed the  $\text{NO}_2^*$  to be collected by the experimental optics design.

If the self-collision rate plus diffusion rate is neglected, the rate equation becomes

$$\frac{dN_j^*}{dt} = B_{ij} \rho N_i - \left[ \sum_i A_{ji} + B_{ji} \rho + \sum_i n_m K_{qi}(T) \right] N_j^* \quad (2)$$

However, after the laser pulse, the absorption term ( $B_{ij} \rho N_i$ ) and the stimulated emission rate ( $B_{ji} \rho N_j^*$ ) becomes zero and

$$\frac{dN_j^*}{dt} = - \left[ \sum_i A_{ji} + \sum_i n_m K_{qi}(T) \right] N_j^* \quad (3)$$

with a solution

$$N_j^* = N_0 e^{-(t/T_{\text{eff}})} \quad (4)$$

where  $N_0$  is the number density of the excited species at  $t = 0$  and

$$T_{\text{eff}}^{-1} = \sum_i A_{ji} + n_m \sum_i K_{qi}(T) \quad (5)$$

The quantity  $\sum_i A_{ji}$  is equal to the inverse of the radiative lifetime  $(T_r)^{-1}$  in seconds of the excited species and in the absence of quenching,  $T_{\text{eff}}$  becomes the radiative lifetime  $(T_r)$ .

Eq (5) is a familiar straight line function,  $y = mx + b$  where  $y$  is equal to  $T_{\text{eff}}^{-1}$ ,  $b$  is equal to  $T_r^{-1}$ , the slope ( $m$ ) is equal to the quenching rate constant  $\sum_i K_{qi}(T)$  and  $x$  is equal to the total number density  $n_m$ , which is related to pressure through the ideal gas law;  $n_m = P_m(KT)^{-1}$  where  $n_m$  is the number density of the foreign gas species in molecules/cm<sup>3</sup>,  $P_m$  is the foreign gas pressure in dynes/cm<sup>2</sup>, and  $KT$  is the product of Boltzmann's Constant (ergs/°K) and Temperature (°K).

If  $T_{\text{eff}}^{-1}$  is plotted versus total number density ( $n_m$ ) or total pressure ( $P_m$ ) then extrapolation to the ordinate ( $y$ ) should yield the radiative lifetime  $T_r$ . However, this

would be a difficult task since this experimental effort uses large pressures (1 - 5 Torr) and the extrapolation to the ordinate would incur serious errors for any incremental change in slope. If the pressures of the foreign gas and  $\text{NO}_2$  were reduced to low (mTorr) values, then the sample tube size (Ref 17:1292) and the effects of diffusion would cause major difficulties. Hence the experimental calculation of  $T_r$  is a formidable problem which will not be investigated in this effort.

#### Rate Equation Relationship to Experiment

The experimental procedure allows for the control of  $\text{NO}_2$  gas pressure (approximately 19 mTorr) and foreign gas pressure (1 - 5 Torr) as well as a high probability of sufficient photons and photon detection rate (photons/pulse). The experimental procedure also allows for the electronic control of the Start-Stop ( $\Delta t$ ) interval between the end of the laser pulse and emission of a fluorescent photon. In order to find the foreign gas (m) quenching rate, Eq (3) will be further developed.

From the relationship

$$\frac{dN_j^*}{dt} = - \left[ \sum_i A_{ji} + n_m \sum_i K_{qi}(T) \right] N_j^* \quad (3)$$

and the fact that the  $\text{NO}_2$  number density is much less than the total number density ( $n_m$ ) or  $n_m \gg N_j^*$ , the factor  $N_j^*/T_r$  is neglected since  $N_j^*/T_r \ll N_j^* n_m K_q(T)$  in this

experiment. Neglecting  $N_j^* T_r^{-1}$  introduces an approximate 2% error, since  $T_r$  is between 44 $\mu$ s and 200 $\mu$ s (Refs 19:1694; 20:524; 21:3457; 22:4100) and the value of  $T_{\text{eff}}$  is of the order of 1 $\mu$ s. Neglecting  $\sum_i A_{ji}$  in Eq (3), leads to

$$T_{\text{eff}}^{-1} = n_m \sum_i K_{qi}(T) \quad (6)$$

and if  $T_{\text{eff}}$  is known, the slope of the curve  $T_{\text{eff}}^{-1}$  versus total number density ( $n_m$ ) is  $\sum_i K_{qi}(T)$  for the foreign gas.

This experimental effort is arranged such that  $T_{\text{eff}}$  is directly obtained from a least squares fit of the exponential decay curve relating the total number of counts (photons) to the  $\Delta t$  time interval. See Appendix C for a graphical interpretation of the actual decay curves as a function of foreign gas pressure and the least squares fit of the raw data. Appendix D contains the least squares computer program used to calculate  $T_{\text{eff}}$ .

Obtaining  $K_{qi}(T)$  directly also allows for the determination of the collisional cross-section  $\sigma_{ji}(T)$  of the molecular species. The collisional cross-section is found from the relation:

$$\sum_i n_m K_{qi}(T) = \sum_i n_m \bar{v}_r(T) \sigma_{ji}(T) \quad (7)$$

where  $\bar{v}_r$  is the average relative velocity of the molecular species and is equal to  $[8KT/\pi u]^{\frac{1}{2}}$ ;  $u$  being the reduced mass of the colliding species.

Since  $\sum_i K_{qi}(T)$  is the slope of the line  $T_{\text{eff}}^{-1}$  versus  $n_m$  then  $\sum_i K_{qi}(T)$  can be written as

$$\sum_i K_{qi}(T) = \frac{\Delta T_{\text{eff}}^{-1}}{\Delta n} \quad (8)$$

and considering the ideal gas law at constant temperature (T), then the change in number density is

$$\Delta n = \frac{\Delta P}{KT} \quad (9)$$

and

$$\sum_i K_{qi}(T) = \frac{\Delta T_{\text{eff}}^{-1}}{\Delta P} (KT) \quad (10)$$

However,  $\Delta P$  was measured in Torr for this experiment, hence multiplying by the correct conversion constant C will convert Torr to dynes/cm<sup>2</sup>. Therefore assuming no NO<sub>2</sub> losses, the equation for the analysis of  $\sum_i K_{qi}(T)$  is

$$\sum_i K_{qi}(T) = C \frac{\Delta T_{\text{eff}}^{-1}}{\Delta P} (KT) \quad (11)$$

where

$$C(\text{Torr}) = 7.53 \times 10^{-4} (\text{dynes/cm}^2)^{-1} \quad (12)$$

which was found using the conversion

$$1 \text{ Torr} = 1 \text{ mm Hg} = .1 \text{ cm Hg} \quad (13)$$

and  $P = \rho gh$  where  $\rho$  is the mass density of Hg in  $\text{gm/s}^2$  at  $20^\circ\text{C}$  (Ref 23:F-5),  $g$  is the acceleration due to gravity in  $\text{cm/s}^2$  at sea level and  $45^\circ$  latitude (Ref 23:A-10) and  $h$  is the height of the Hg column in cm.

If the product  $C(KT)$  is calculated for a Temperature of  $296.66^\circ\text{K} \pm 1.0^\circ\text{K}$  error (experimental value) then the quenching rate equation becomes

$$K_{\text{qm}}(T) = 3.083 \times 10^{-17} \frac{\Delta T_{\text{eff}}^{-1}}{\Delta P} \text{ cm}^3/(\text{molecules sec}) \quad (14)$$

The values found for  $K_{\text{qm}}(T)$  of Ar, He, and  $\text{N}_2$  are shown in Table I, page 48.

The equation used to find the collisional cross-section  $\sigma_{\text{qm}}$  is

$$\sigma_{ij}(T) = \sigma_{\text{qm}} = \frac{K_{\text{qm}}(T)}{\bar{v}_{\text{rm}}} \quad (15)$$

The values found  $\sigma_{\text{qm}}$  for Ar, He and  $\text{N}_2$  are also shown in Table I, page 48.

#### Diffusion Considerations

The experimental optical configuration was analyzed in order to insure that all photons from  $\text{NO}_2^*$  are collected. The distance travelled in three lifetimes is chosen as the maximum distance that  $\text{NO}_2^*$  may travel before leaving the focal volume. Therefore it is necessary to compare the solid angle ( $\Omega_1$ ) determined by the optics and the photomultiplier on the optical axis with the  $\Omega_2$  obtained using

the maximum allowed off axis distance. The optical diagram shown in Fig. 5 details the actual analysis and the collection solid angle  $\Omega_2$ .

The change in solid angle from the on axis position ( $\Omega_1 = .0287$  str) to the maximum off axis position ( $\Omega_2 = .0289$  str) is not appreciable when considered over the distance  $\sqrt{3}T_{\text{eff}}$  (.61 mm) plus the focused laser beam radius (.1 mm).

In order to insure that the solid angle remains essentially constant, a minimum foreign gas pressure of 1 Torr was used. A pressure of 1 Torr with a mean free path (L) of approximately .1 mm allows for a sufficient number of collisions within the  $\sqrt{3}T_{\text{eff}}$  diameter. A foreign gas pressure lower than 1 Torr would increase the  $T_{\text{eff}}$  and foreign gas L thus reducing the number of collisions and allowing  $\text{NO}_2^*$  to deexcite outside the region where  $\Omega_2$  is essentially constant.

#### Photon Counting Statistics

The photon per pulse rate was kept at  $\leq .15$  during the experiment. This was accomplished by insertion of neutral density filters in the dye laser beam path, prior to sample tube entry (See Chapter IV, Fig. 7, p. 34). The value of .15 photons per pulse was found by employing a probability relationship developed by Wharton (Ref 3:19). The relation determines the probability of producing a photon in the time

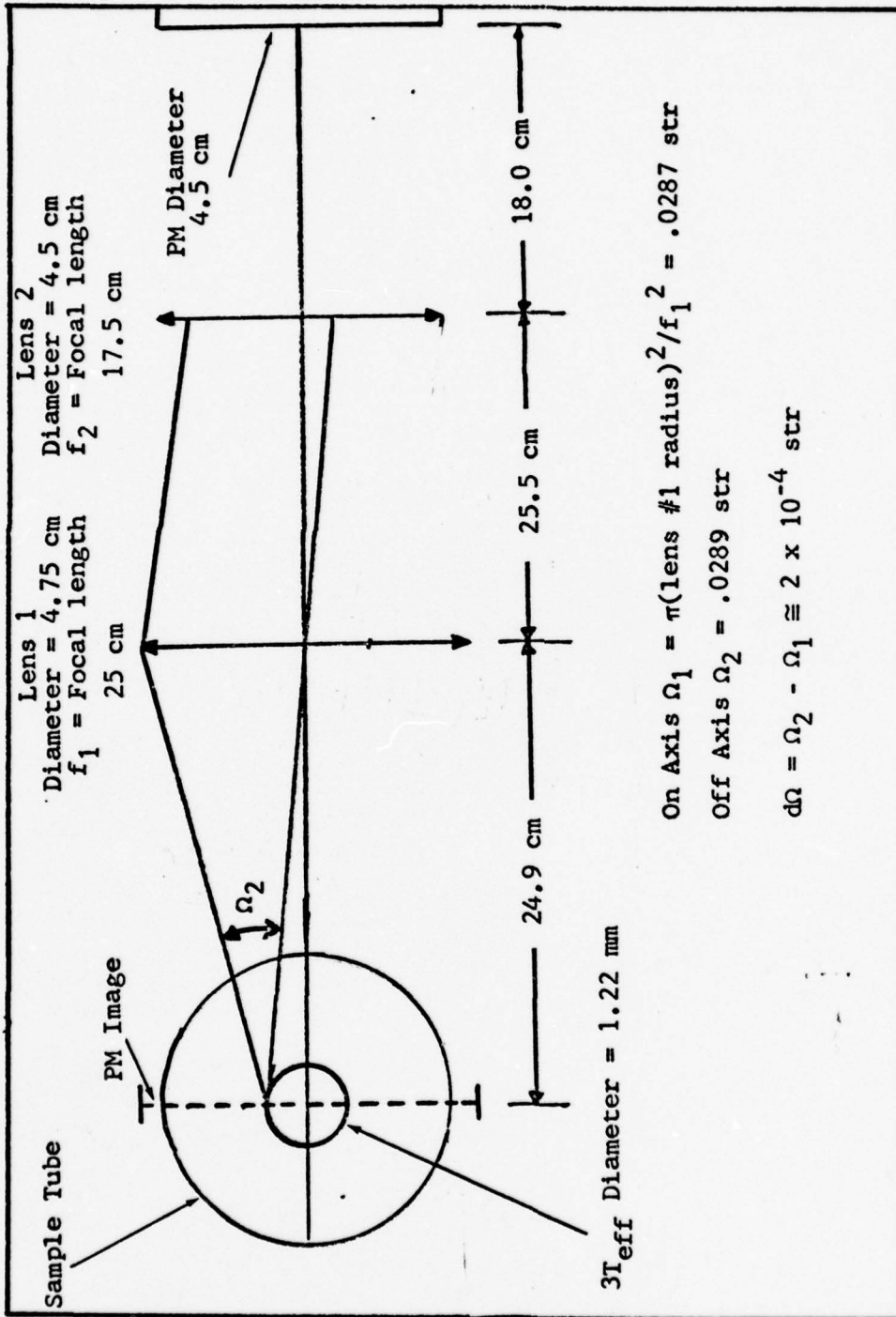


Fig. 5. Collection Optics Solid Angle

interval  $t$  to  $t + \Delta t$ . The relationship as derived in Appendix E is

$$P_p = P_c N_o \Delta t T_{eff}^{-1} [\exp(-t/T_{eff})] \\ [1 - N_o P_c (1 - \exp(-t/T_{eff}))] \quad (16)$$

where

$P_p$  = the probability of detecting a photon in the interval  $t$  to  $t + \Delta t$ .

$P_c$  = the probability that a photon will be detected in the interval  $t$  to  $t + \Delta t$

$N_o$  = the initial number of excited molecules at  $t = 0$

$\Delta t$  = the Start-Stop interval produced by the TPHC

$T_{eff}$  = effective lifetime as previously described

Expanding Eq (16) results in

$$P_p = A [(1 - N_o P_c) \exp(-t/T_{eff}) + N_o P_c \exp(-t/.5T_{eff})] \quad (17)$$

where

$$A = P_c N_o \Delta t T_{eff}^{-1} \quad (18)$$

Since  $N_o P_c$  is the counting rate (photons/pulse) as determined from the experimental configuration, then by insuring that  $(1 - N_o P_c) \gg N_o P_c$ , we can attain the desired result

$$P_p = P_c N_o \Delta t T_{eff}^{-1} \exp(-t/T_{eff}) \quad (19)$$

The value of  $P_c N_0$  equal to .15 was chosen as the value that produced minimum errors in satisfying Eq (16). This value was strictly adhered to during this experimental effort by the use of neutral density filters.

#### Applications to Combustion

The effects of quenching corrections in fluorescence diagnostics is of major importance in analyzing the combustion process. The quenching corrections can either be characterized or eliminated from consideration by showing that the fluorescence intensity is independent of quenching. If quenching corrections can be eliminated then direct calculation of species concentration is possible if full saturation of the absorbing transition is attained. Full saturation being defined as the condition when the rate of stimulated emission of radiation is much stronger than the combined rates for electronic quenching and radiative decay (Ref 18:10).

To illustrate the case for full saturation, a simple two-level model will be used as is shown in Fig. 6(b), where  $N_1$  and  $N_2$  are the number densities (molecules/cm<sup>3</sup>) of their respective levels and  $N_t = N_1 + N_2$ , the total number density.

Assuming that the incident intensity  $I(\nu)$  is constant and very broad in comparison to the absorption line (Fig. 6(a)), then the rate of change of level 2 with respect to time is

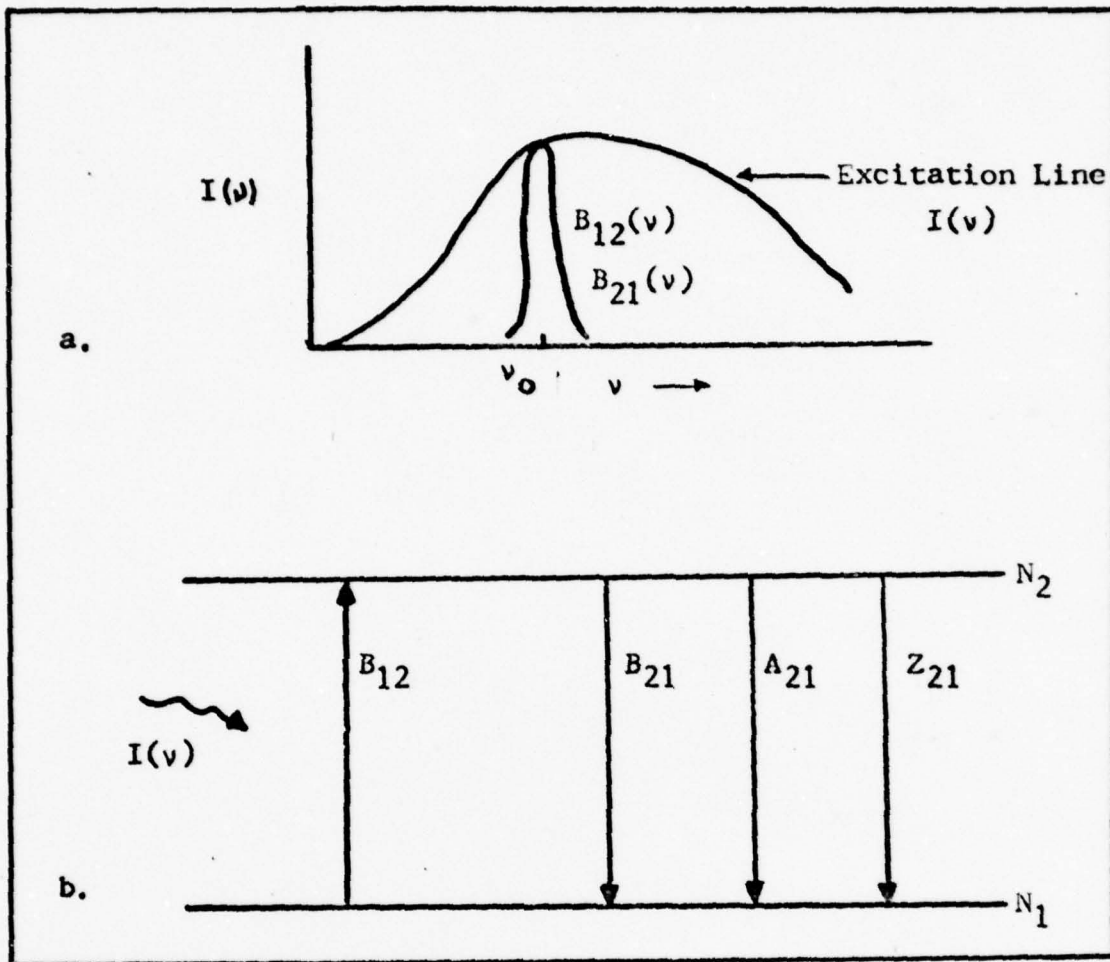


Fig. 6. Two-Level Model

$$\frac{dN_2}{dt} = N_1 \int B_{12}(\nu) I(\nu) d\nu - A_{21} N_2 - N_2 \int B_{21}(\nu) I(\nu) d\nu - N_2 Z_{21} \quad (20)$$

If  $I(\nu)$  is assumed constant over the range  $B_{21}(\nu)$  and  $B_{12}(\nu)$ , Eq (20) becomes

$$\frac{dN_2}{dt} = N_1 I(\nu) B_{12} - A_{21} N_2 - N_2 I(\nu) B_{21} - N_2 Z_{21} \quad (21)$$

where  $B_{12}$ ,  $A_{21}$ ,  $B_{21}$  and  $Z_{21}$  are the integrated absorption coefficient, the integrated spontaneous emission coefficient, the integrated stimulated emission coefficient and the quenching rate of the respective upper (2) and lower (1) levels.

The steady state condition ( $dN_2/dt = 0$ ) yields

$$\frac{N_1}{N_2} = \frac{A_{21} + I(\nu)B_{21} + Z_{21}}{I(\nu)B_{12}} \quad (22)$$

or upon rearranging terms and substituting  $N_t = N_1 + N_2$ , we have

$$\frac{N_2}{N_t} = \frac{B_{12}I(\nu)}{[B_{21}I(\nu) + B_{12}I(\nu) + A_{21} + Z_{21}]} \quad (23)$$

and if we consider the case when  $I(\nu)$  is very large, i.e., saturation conditions, then

$$\left. \frac{N_2}{N_t} \right|_{\text{saturation}} = \frac{B_{12}}{B_{12} + B_{21}} = \frac{1}{1 + (g_1/g_2)} \quad (24)$$

where  $g_1$  and  $g_2$  are the degeneracies of their respective levels. Hence

$$\left. \frac{N_2}{N_t} = \frac{N_2}{N_t} \right|_{\text{saturation}} \left\{ \frac{I(\nu)(B_{21} + B_{12})}{[B_{21}I(\nu) + B_{12}I(\nu) + A_{21} + Z_{21}]} \right\} \quad (25)$$

and letting

$$R = \left[ \frac{B_{21} + B_{12}}{A_{21} + Z_{21}} \right] I(\nu) \quad (26)$$

we have

$$N_2 = \left[ \frac{N_t}{1 + (\mathcal{E}_1/\mathcal{E}_2)} \right] \left[ \frac{R}{1 + R} \right] \quad (\text{Ref } 24:3) \quad (27)$$

Considering an actual experimental case where the decay from level 2 to level 1 is measured, we have that the fluorescence intensity  $I_f$  is proportional to the spontaneous transition probability  $A_{21}$  and to  $N_2$  or

$$I_f = h\nu A_{21} V(\Omega/4\pi)N_2 \quad (28)$$

where  $h\nu$  is the fluorescent radiation energy,  $V$  is the observation volume and  $\Omega/4\pi$  is the solid angle of the collection optics or detector. We can now use Eq (27) to rewrite Eq (28), thus

$$I_f = h\nu A_{21} V(\Omega/4\pi) \frac{N_t}{1 + (\mathcal{E}_1/\mathcal{E}_2)} \left[ 1 - \frac{1}{R} + \dots \dots \dots \right] \quad (29)$$

after expansion of Eq (27) for the case when absorption and stimulated emission are much larger than spontaneous emission and quenching or  $R > 1$ . When  $1/R$  is small, the relationship in Eq (29) allows us to solve for  $N_t$  without knowing  $Z_{21}$ . This is the desired result from saturation analysis, since  $Z_{21}$  is generally unknown in a combustion medium. It is interesting to note that to fully saturate the  $\text{NO}_2$  absorption transition is extremely difficult, since  $\text{NO}_2$  displays collisional relaxation among rotational levels (Ref 25:78).

Daily (Ref 26:569) has investigated fluorescence techniques using full saturation conditions, where the molecular absorption linewidth exceeds the incident spectral linewidth. He proposed a two-level and a three-level model. The two-level model results are similar to the results obtained from Eq (21). The three-level model shows that fluorescence power is also completely independent of incident laser intensity and quenching. The requirement for full saturation of the absorption transition is combined with a requirement to observe fluorescence, simultaneously, at two wavelengths. This model increases the complexity of the saturation procedure.

Piepeier (Ref 27:433) has presented a comprehensive three-level analytical discussion of saturated fluorescence which shows the cross-relation terms that occurs between level 3 and level 1. His proposal requires that the spectral width of the incident laser wavelength be much less than the molecular absorption linewidth.

Since the molecular absorption linewidth is directly related to either collisional broadening (homogeneous) or Doppler broadening (inhomogeneous), then the Peipeier approach must consider three possible cases for full saturation:

- (a) The lineshape is homogeneous (high pressure, low temperature).
- (b) The lineshape is inhomogeneous (low pressure, high temperature).

- (c) The lineshape is broadened by a combination of (a) and (b).

Case (a) would require the most intense incident laser spectral intensity due to the energy required to saturate a homogeneously broadened lineshape.

Baranovski, and McDonald (Ref 28:3300) produced a theoretical model for species measurements considering a partial saturation condition using an incident laser intensity width that exceeded the molecular absorption linewidth. Their two-level model result for fluorescence intensity is:

$$I_f = C[A_{21}N_1B_{12}/(Z_2 + A_{21})/(I(\nu) + B_{12} + B_{21})] \quad (30)$$

which after a Taylor expansion illustrates the importance of quenching when full saturation is not achieved.

Although the theoretical models described illustrate that the full saturation condition is possible, present research indicates that the high rate of quenching that accompanies the combustion process is a major obstacle in actual achievement of the full saturation condition. It should also be noted that a two-level model is not applicable to all species concentration cases, hence three-level models and cross-relaxation between the levels must be considered. Also the model in question must consider the laser spectral width plus the inhomogeneous and homogeneous absorption width (Ref 25:90).

#### IV. Procedure

The experimental procedure section explains the manner in which the data was collected. The equipment used to collect the data is detailed in Appendix A. This section is divided into the following areas: (1) Experimental Method, (2) Gas Handling, (3) Dye Laser, (4) Background Counting, and (5) Problem Areas.

##### Experimental Method

The equipment schematic is as shown in Fig. 7. The PIN diode, which is protected from overloading with a neutral density filter, detects the laser pulse. The PIN diode output becomes an input to the first discriminator (ungated). This discriminator produces three outputs:

- (1) An input to the linear gate and stretcher which provides an output signal that is an input to the multiscaler. This linear gate and stretcher is operated in the ungated mode.
- (2) An input to a delay box whose output provides an input (Start) pulse to the TPC. The delay box provides the desired ns delay which starts the timing in the area of the exponential curve to be investigated (See Fig. 8).
- (3) An input to the pulse generator whose output provides a gating pulse to the second discriminator (gated mode). This input to the #2 discriminator opens the gate that allows

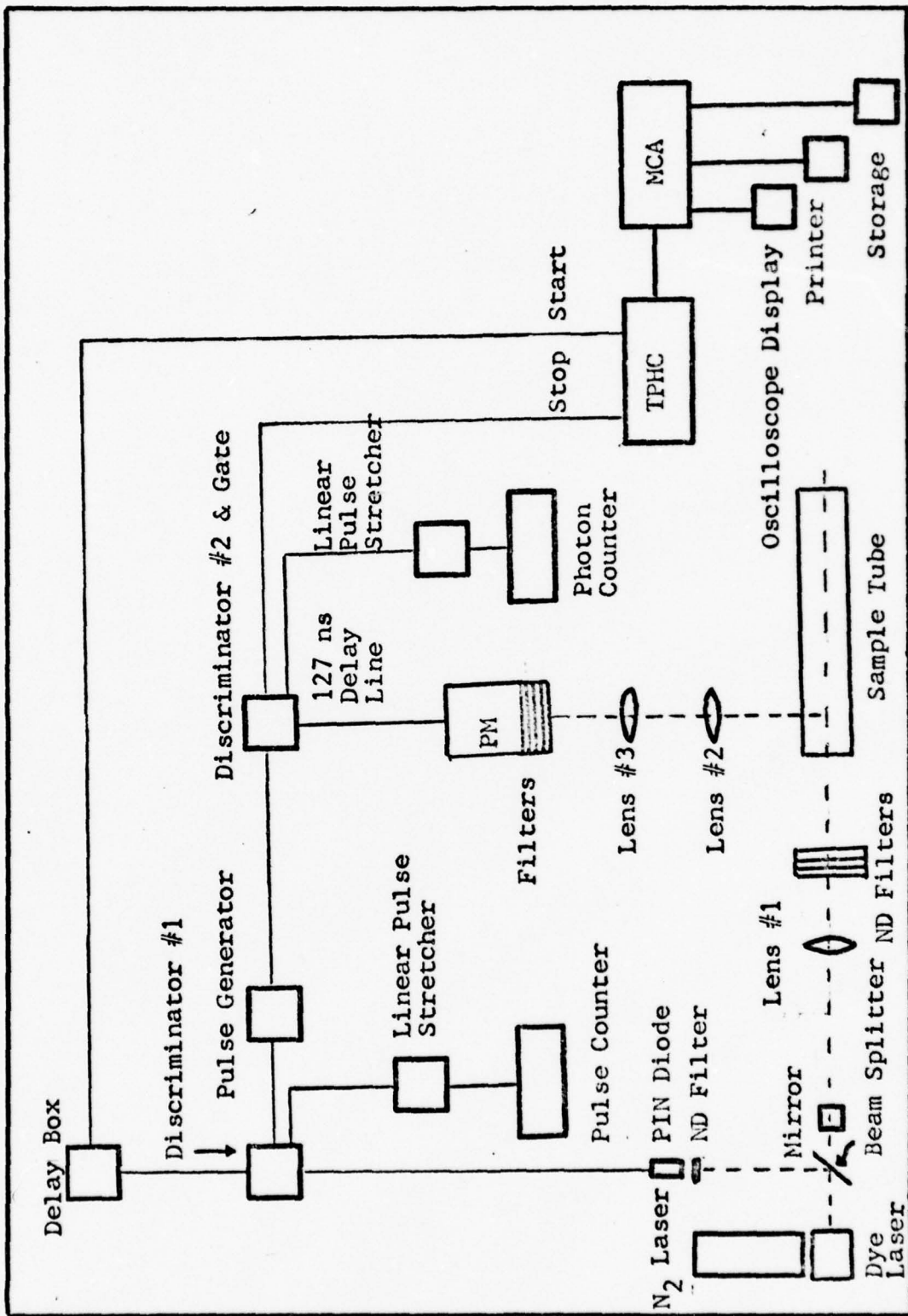


Fig. 7. Electronics Schematic

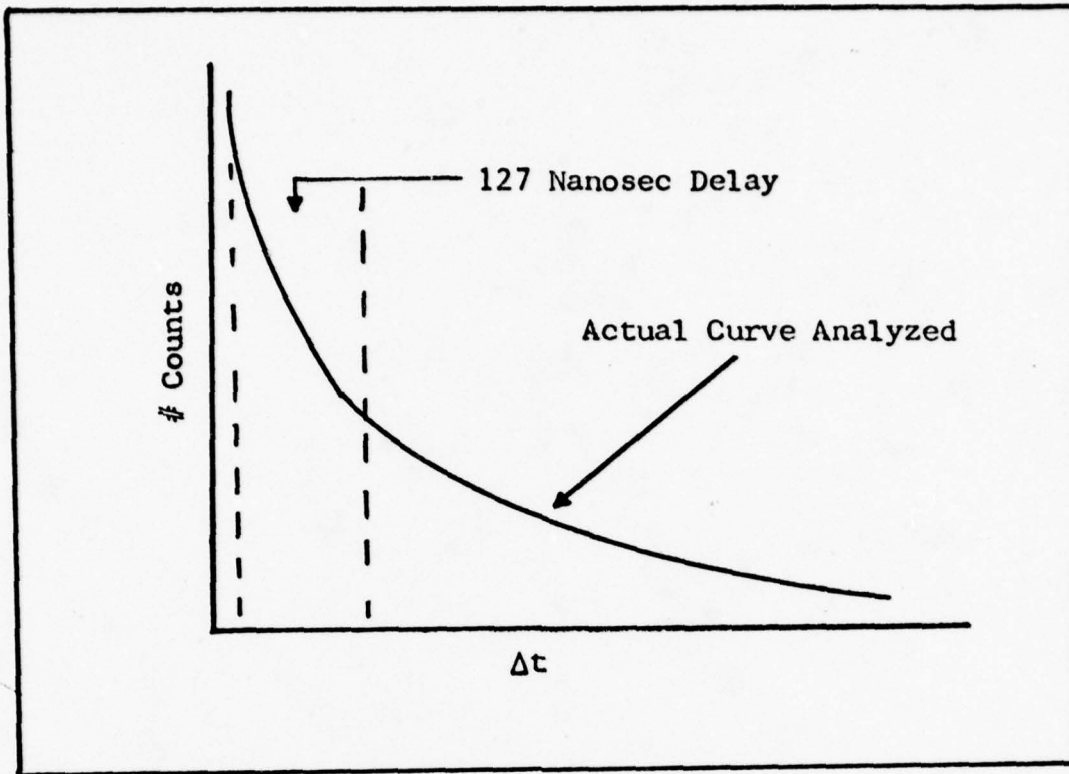


Fig. 8. Delay of Exponential Decay Curve

photomultiplier data to flow as one output from the second discriminator.

Prior to entering the sample test tube, the laser pulse is directed through neutral density filters in order to insure that the number of photons per pulse is reduced to much less than one. This is done so that the statistics of single photon counting as noted by Eq (19) is maintained. The addition of neutral density filters is accomplished by observing the photon per pulse count rate (between 1000 and 3000 pulses) and adjusting this rate, by trial and error insertion of filters until the desired rate (approximately .15 photons per pulse or less) is maintained. The strength of neutral density filters used varied with the laser pulse

power and the fluorescence intensity produced by the various  $\text{NO}_2$  plus foreign gas mixtures.

The fluorescence signal undergoes broadband detection ( $5430 \pm 15\text{\AA}$ ) by the colored glass plus interference filters and is sensed by the photomultiplier tube whose output is used as an input to a delay box (replaced by 82 feet of electrical wire) that provides an input to the second discriminator which is gated and produces two outputs:

- (1) An input to the linear pulse stretcher (gated) whose output provides an input to the multiscaler. This multiscaler determines the number of photomultiplier counts (photons) per laser pulse which flow during the gating interval.
- (2) An input (Stop) signal to the TPHC. The TPHC produces an output signal whose amplitude is proportional to the relative time difference between the Stop and Start signals.

The TPHC output is used as an input to the multichannel analyzer (MCA). The MCA input is distributed to one of the selected memory channels (256 channels were used in this effort). The MCA accumulates data (TPHC signals) over a period of time. The accumulation time for data collection is arbitrary. However, in this experiment the data accumulation time was between three and four hours in order to obtain a useful statistical curve. During the initial portion of data accumulation, the MCA oscilloscope is monitored in order to observe the exponential curve. If the decay curve does not cover the full range of the abscissa (as displayed), then the TPHC width (microsec) is adjusted

accordingly, the data erased and accumulation restarted. The TPHC adjustment varied with the pressure of the foreign gas as is shown in Tables IV, V and VI of Appendix B.

After data collection, a photograph of the statistical curve is produced and the MCA results are also printed on paper tape. The printed data is analyzed in order to eliminate the anomalous counts near the initial and final points of the exponential decay curve. The acceptable data points are then transferred to computer cards for a computer (Control Data 6600) run of a least squares fit of the  $\ln$  data as a function of time (See Appendix D). The result of the computer analysis is an effective lifetime ( $T_{\text{eff}}$ ). The effective lifetime of the exponential curve is calculated from the relation  $T_{\text{eff}} = (t_2 - t_1) / \ln(N_1/N_2)$  where  $N_1$  is the number of counts measured at time  $t_1$  and  $N_2$  is the number of counts measured at  $t_2$ . One data point is recorded for each foreign gas pressure, these points (5 per foreign gas) are then plotted using  $1/T_{\text{eff}}(\mu\text{s}^{-1})$  versus pressure (Torr). A least squares fit is then applied to the five data points and the slope of the resulting line is directly proportional to the foreign gas quenching rate. This procedure is repeated for several foreign gases and the quenching rate data is analyzed and compared as described in the results and analysis section of this report.

#### Gas Handling

After each daily set of data runs, the gas system is evacuated (overnight) by the Turbo Molecular Pump. Initial

evacuation requires that valves 2, 3, 4, 5, 11, 12, 14, and 15 (See Fig. 9) be fully opened (Valve 13 is always closed since the Vac Sorb Pump is not used in this effort). During and after evacuation, system pressure is monitored by the ionization gauges down to  $10^{-7}$  Torr. Overnight outgassing (baking) is accomplished by wrapping the sample tube with heat tape and then applying 110 volts (controlled by Staco variacs) to the tape. The temperature reached is greater than  $100^{\circ}\text{C}$  which aids the outgassing procedure. During outgassing the Turbo Molecular pump continues to evacuate the system.

After overnight pumpdown and outgassing (when required), the digital pressure meter is manually zeroed and  $\text{NO}_2$  is introduced (See Fig. 9). Prior to  $\text{NO}_2$  introduction, valves 1, 2, 5, 6, 7, 11, 12, 14, and 15 are closed. (Valves 3 and 4 are always left open for convenience.)  $\text{NO}_2$  is initially trapped between valves 1 and 2 by momentarily opening and closing valve 1. Valves 2 and 5 are then opened and valve 11 is used to control the  $\text{NO}_2$  pressure flow into the sample tube. The exact  $\text{NO}_2$  pressure (approximately 19 milli Torr) is monitored by the Baratron and visual observation of the digital pressure display is maintained while slowly opening and closing valve 11. After accumulating the desired  $\text{NO}_2$  pressure, valves 2, 5, and 15 are opened in order to evacuate residual  $\text{NO}_2$  in the lines.

Introduction of the foreign gas is accomplished by closing valves 5, 6, 7, 8, 9, 10, 11, 12, 14, and 15.

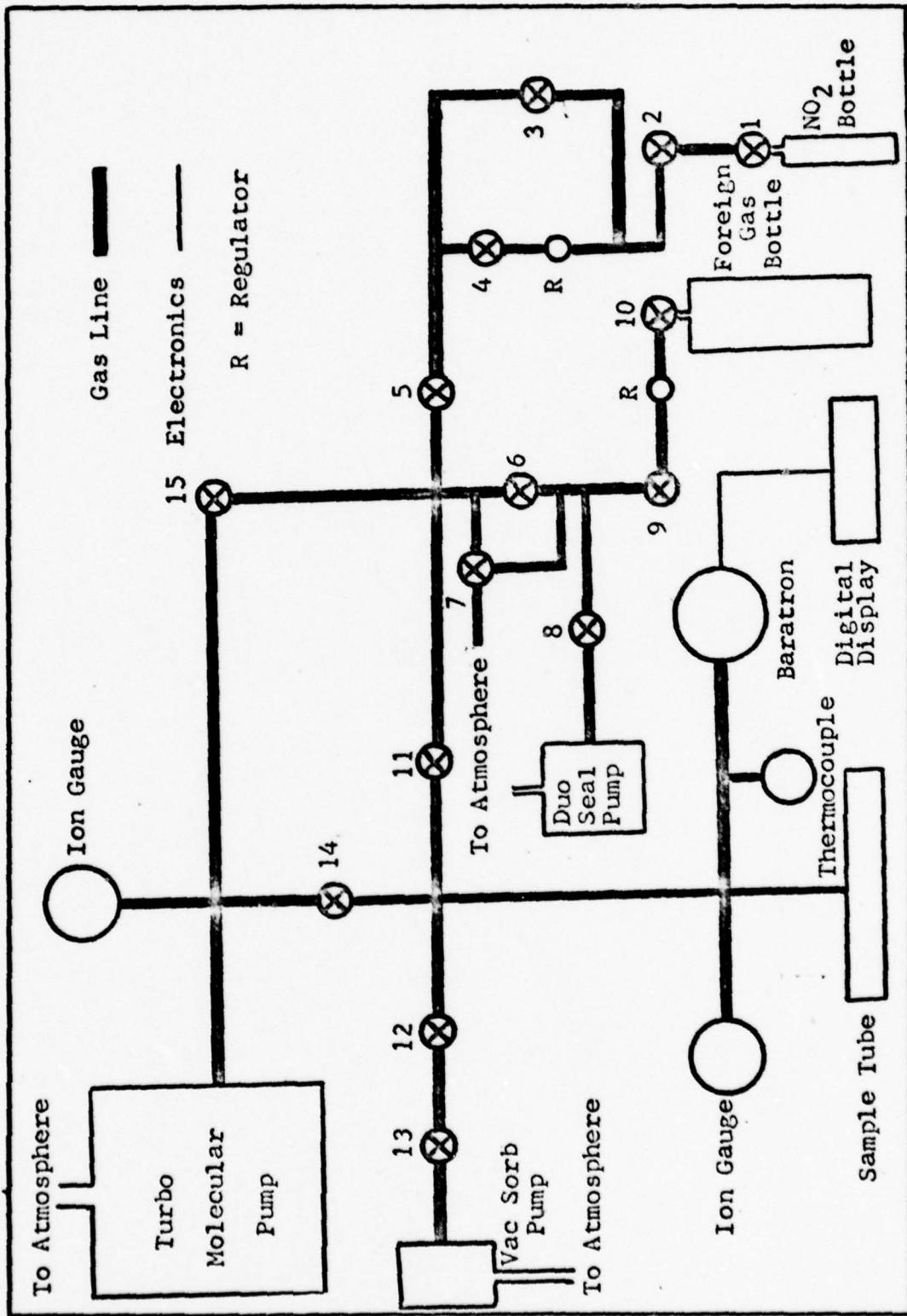


Fig. 9. Gas Handling Schematic

Valve 10 is then opened and closed. This allows the cylinder gas pressure to be trapped between the cylinder and regulator. This pressure is then manually reduced to approximately 5 psi by turning the vacuum regulator and allowing the gas to be trapped between the regulator and valve 9. Valve 9 is then opened and closed to trap the foreign gas between valves 6, 7, 8, and 9. Valve 8 is then opened and the lines are evacuated by the Duo Seal Pump and then valve 8 is closed. This evacuation procedure is accomplished several times. After line evacuation, the foreign gas is again trapped and allowed to enter the sample tube by opening and closing either valve 6 or 7 and controlling the gas flow to the sample tube with valve 11. Visual observation of the foreign gas pressure is via the digital meter, but on a different scale since the foreign gas pressure is in the Torr range and the  $\text{NO}_2$  pressure is in the millitorr range.

After the sample test tube area is loaded with the desired mixture of  $\text{NO}_2$  plus foreign gas, valves 2, 5, and 15 are opened to allow the remaining portion of the system to be continuously evacuated by the Turbo Molecular Pump.

#### Dye Laser

The output of the dye laser was set at  $4368\text{\AA}$  by mechanically rotating the dye laser grating. The output power is maximized using the Astrodata Nanovoltmeter and Eppley thermopile. The maximum output power was found to occur at  $4368\text{\AA}$ . The  $4368\text{\AA}$  wavelength was identified

using the Jarrell-Ash monochromator. The maximum power output occurring at  $4368\text{\AA}$  is in close agreement with the Coumarin 440 results found by Wharton (Ref 3:28). During the experiment, the Coumarin 440 dye was changed at regular intervals (approximately every 7 hours of laser operational time). The dye laser output was maintained between 70 and 120 micro joules/pulse throughout the experiment.

#### Background Counting

Prior to introducing any gas in the system, the dye laser output ( $4368\text{\AA}$ ) is beam split and directed to the PIN diode and the sample tube and windows. A count of the number of scattered plus background photons per pulse is then obtained from the counter displays. The laser output is then totally blocked from the sample tube and a count of the number of background counts (photons) per laser pulse is obtained. The number of scattered photons per laser pulse is the difference between the number of counts per pulse with the laser unblocked and the number of counts per pulse with the laser blocked. The scattered photons are significantly reduced by laser beam alignment through the sample tube and by elimination of reflecting materials around the sample tube. Experimental scatter was kept to  $\leq 10\%$  of the count rate with the foreign gases in the tube.

The experimental background count averaged out to approximately 8 photons/1000 pulses. Considering a three-hour data run ( $4.32 \times 10^5$  pulses) at a rate of 0.15 photons/pulse, the background counts amounted to 5% of the collected

data. This possible error source was made insignificant by the manual removal of anomalous counts near the initial and final portions of the data.

### Problem Areas

#### 1. Background Counting

The location of the laboratory (inside an open hangar bay) did not allow for complete isolation of scattered exterior natural (solar) or artificial (overhead) lights. This created some difficulty with background count elimination, unless data collection was integrated over more than three hours or accomplished during the late evening hours.

#### 2. Delay Box Noise

As is shown in Fig. 7, the delay box prior to the photomultiplier tube produced excessive noise which randomly increased the count rates until the delay box was eliminated. The delay box was replaced with a cable whose length corresponded to an approximate delay of 1.55 nanosec per foot (82 feet of cable was used in order to produce 127 ns delay). The cable eliminated the excessive noise.

#### 3. UV 1000 Laser

##### (a) Dye Laser

The dye laser was difficult to align after the telescope was removed for realignment of the laser cavity and reinserted. The maximum output power was obtained after the dye laser flow lines were manually elevated. This may have

been due to a misalignment of the fluorescence window with the nitrogen ( $N_2$ ) laser output. An approximate  $3\frac{1}{2}$ -inch elevation of the flow lines was accomplished by placing a square aluminum block between the dye laser cannister and the fluorescence window. This configuration continued throughout the experiment.

(b)  $N_2$  Laser

The  $N_2$  laser was responsible for the majority of the problems that beset the experiment. The problems were thyatron arcing, vacuum pump malfunction, and cavity (discharge channel) breakdown. Each problem will be separately discussed.

b1. Thyatron Arcing

During the first week of data collection, excessive arcing was observed to be coming from the output end of the  $N_2$  laser. This was followed by an excessive reduction in the dye laser power and noticeable vibration. An investigation of the  $N_2$  laser components revealed the thyatron problem. The thyatron was repaired locally and the arcing eliminated.

b2. Vacuum Pump Breakdown

During the second week of data collection the Alcatel Model 1050 nitrogen vacuum pump completely malfunctioned. This vacuum pump was initially replaced by one Duo Seal Model 3000 vacuum pump. However, the Duo Seal pump experienced overheat problems within less than one hour of continuous operation. A second Duo Seal Model 3000 vacuum

pump was connected in parallel to the first pump. In this configuration, one pump was allowed to operate for approximately one hour, then shutdown and simultaneous with shutdown, the second pump was started. Considering data collection, this configuration proved to be awkward but effective. During the fifth week of data collection, the Alcatel pump was repaired and reconnected to the N<sub>2</sub> laser. During the sixth week of data collection, the newly repaired Alcatel pump was observed to be smoking near the exhaust ports. A thorough check of the pump revealed no damage or breakdown of components. The probable cause of the pumping problem was due to excessive overworking of the components at 40 pps and/or a low oil supply. This high pulse rate should be avoided in further experiments. No further vacuum pump problems were experienced.

### b3. N<sub>2</sub> Cavity Breakdown

During the fourth week of data collection and while in the standby (ready) mode, a loud vibrating noise was heard to come from the laser area. Prompt main power shutdown was followed by visible smoke and the acrid odor of burnt components. Investigation revealed that a massive electrical discharge (unknown origin) caused the two protective 1000 ohm resistors to rupture and the optical elements of the discharge channel (transmission and 100% mirror) to be severely damaged (burned circular spot on each element). Also noted, was damage (charred spots to

the discharge channel electrodes and end connectors (phenolic strips) to the optical element plates. Investigation revealed that six coaxial cables were oxidized at the connecting ends to the cavity. This oxidation problem was reduced by cleaning the oxidized ends with common emory paper. Since the discharge channel was damaged beyond repair, a new one was purchased from the Molelectron Corporation (Sunnyvale, California). An alpha emitting pre-ionizer was also purchased from Molelectron in order to improve initial  $N_2$  lasing action. Prior to the  $N_2$  discharge channel breakdown, some noise was introduced into the collected data as is evidenced by Fig. 10. Fig. 10a shows an  $NO_2$  (19.58 mT) plus  $N_2$  (5.08 Torr) mixture that is hampered by noise. Fig. 10b shows an identical  $NO_2$  plus  $N_2$  mixture taken after the new discharge channel was installed. The amount of noise due to the delay box and  $N_2$  laser collected along with experimental data prior to the  $N_2$  laser breakdown is unknown.

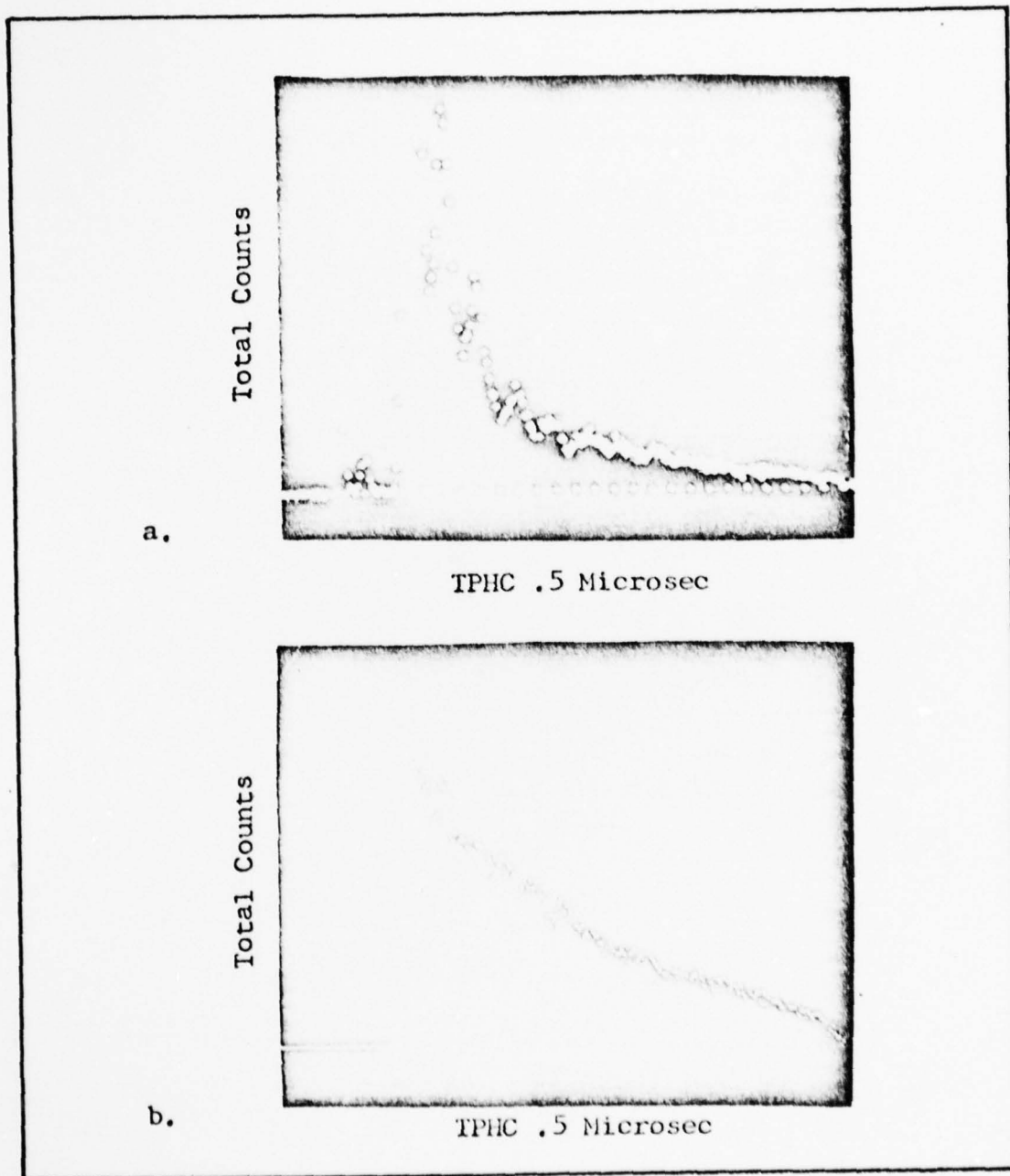


Fig. 10. Noise Comparison at 5 Torr of  $N_2$

## V. Results and Analysis

The results and analysis section presents the calculation of quenching rate constants and quenching cross-sections, error analysis and a discussion of the overall results.

### Calculation of Quenching Rate Constants and Cross-Sections

The quenching rate constants,  $K_q(T)$ , and quenching cross-sections,  $\sigma_q(T)$  for the foreign gas M, were calculated using the equations derived in Chapter III. The equations used are

$$\sum_i K_{qi}(T) = C(KT) \Delta T_{\text{eff}}^{-1} / \Delta P \quad \text{cm}^3(\text{molecules sec})^{-1} \quad (11)$$

where  $C(KT) = 3.083 \times 10^{-17}$  and  $\Delta T_{\text{eff}}^{-1} / \Delta P =$  regression curve slope in  $(\mu\text{s Torr})^{-1}$  and

$$\sigma_{qm}(T) = K_{qm}(T) / \bar{v}_r \quad \text{cm}^2 \text{ molecules}^{-1} \quad (15)$$

The results are shown in Table I and are compared with those of Kaufman, et al (Ref 29:720). It should be noted that the quenching cross-sections found by the Kaufman investigation are related to this work thusly:

$$\begin{array}{ccc} \sigma_{qm}(T) & \rightleftharpoons & \pi \sigma_q^2 \\ \text{(this work)} & & \text{(Kaufman)} \end{array}$$

Table I

Quenching Rate Constants, Cross-Sections and Exponential Lifetimes

$\lambda_E = 4368\text{\AA}$	<u>This Effort</u>	<u>Ref 29</u>
	$\lambda_F = 5430\text{\AA}$	$\lambda_E = 4358\text{\AA}$
Foreign Gas	$K_q(T)$	$K_q$
	$10^{-11} \text{ cm}^3 (\text{molecules x sec})^{-1}$	$10^{-11} \text{ cm}^3 (\text{molecules x sec})^{-1}$
Ar	2.81	2.1
He	2.04	2.0
N <sub>2</sub>	3.92	3.1

<u>This Effort</u>	<u>Ref 29</u>
$\sigma_q(T)$	$\frac{\pi\sigma_q^2}{2}$
$10^{-16} \text{ cm}^2 (\text{molecules})^{-1}$	$10^{-16} \text{ cm}^2 (\text{molecules})^{-1}$
Ar 5.19	3.80
He 1.56	1.60
N <sub>2</sub> 6.55	5.00

<u>Foreign Gas</u>	<u>Ref 29</u>
Ar	Experimental Lifetime (T')
	32.88 $\mu$ s

The  $\sigma_q^2$  value is a radius and hence  $\pi\sigma_q^2$  is a cross-sectional area which is identical to the calculation of the  $\sigma_{qm}$  of this work.

The Kaufman investigation required an  $\text{NO}_2$  radiative lifetime ( $T_r$ ) in order to calculate the quenching rate constant  $K_q(T)$ . The  $T_r$  used by Kaufman was  $44\mu\text{s}$  as found by Neuberger and Duncan (Ref 19:1693) and also verified by Douglas (Ref 7:1007). In order to compare the Kaufman data further, a relationship was established to determine a  $T_r'$  (experimental radiative lifetime) for the data in this experimental effort. Only the Ar fluorescence wavelength ( $\lambda_F$ ) was compared since the  $\lambda_F$  for He and  $\text{N}_2$  was not available from the Kaufman data. The relationship is as follows:

$$K_q(T) = \frac{T_r K_q K(T)}{T_r'} \quad (31)$$

where

$$T_r = 44\mu\text{s} \text{ (Kaufman data)}$$

$$K_q K(T) = \text{Ar quenching rate constants (Kaufman data)}$$

$$K_q(T) = \text{Ar quenching rate constants (this experimental effort)}$$

$$T_r' = \text{experimental radiative lifetime}$$

In order to determine the fluorescence wavelength ( $\lambda$ ) of the Kaufman data for Ar, a plot (Fig. 11) of the Ar quenching constant versus  $\lambda$  indicated that for the  $4368\text{\AA}$

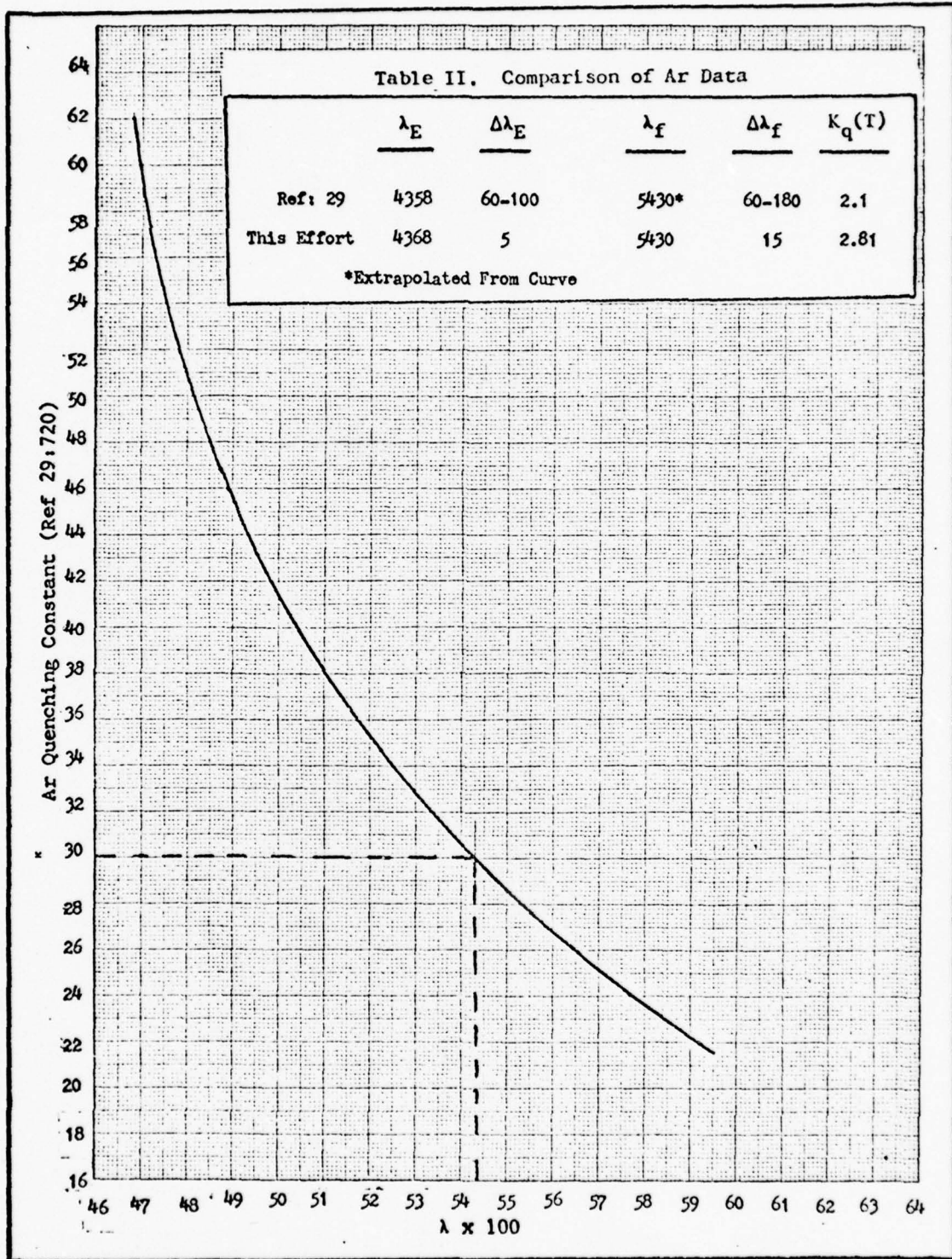


Fig. 11. Quenching Constant Plot of Ref 29:720

excitation, the  $\lambda_F$  coincided with  $5430\text{\AA}$  of this effort. This value for  $\lambda_F$  (Kaufman) was considered only as a coincidence. Table II illustrates a comparison of various parameters between this effort and the Kaufman effort.

### Error Analysis

To consider the statistical and systematic errors of the collected data, Eq (11) will be analyzed. Recall

$$\sum_i K_{qi} = C(KT) \Delta T_{\text{eff}}^{-1} / \Delta P \quad (11)$$

which can be written as

$$K_q = C KT m \quad (32)$$

where

$$m = \Delta T_{\text{eff}}^{-1} (\Delta P)^{-1} \quad (\text{slope})$$

Then the change in  $K_q$  is  $\Delta K_q$  written as

$$\Delta K_q = CmK \Delta T + CKT \Delta m \quad (33)$$

and the ratio of  $\Delta K_q$  to  $K_q$  is

$$\frac{\Delta K_q}{K_q} = \frac{\Delta T}{T} + \frac{\Delta m}{m} \quad (34)$$

Since Eq (34) contains all of the variable experimental parameters, each part will be individually error analyzed. Thus beginning with Temperature,

$$\Delta T/T = \pm \Delta T_s/T \text{ (statistical)} \pm \Delta T_i/T \text{ (instrument)} \quad (35)$$

- (a) The statistical error was found from the daily temperature variation ( $2^\circ\text{C/day}$ ) and is correct to within 1%

hence

$$\frac{\Delta T}{T} = \pm 0.01 \quad (36)$$

- (b) For this experimental effort the instrument error of the Moeller thermometer is assumed to be negligible ( $\approx .1/296.6$ ) and is discarded.

The errors associated with  $\Delta m$  requires a close look at the second term in Eq (34)

$$\Delta m = \Delta[\Delta T_{\text{eff}}^{-1}/\Delta P] \quad (37)$$

hence  $\Delta P$  and  $\Delta T_{\text{eff}}^{-1}$  will be individually analyzed. It should be noted that the  $\Delta P$  and the  $\Delta T_{\text{eff}}^{-1}$  that will be discussed are directly related to the instruments producing them and not the slope that is used to calculate  $K_q(T)$ . Considering the pressure term first, we will write  $\Delta P$  as  $\Delta p$

$$\Delta p = nK\Delta T + \Delta nKT \quad (38)$$

and assuming no change in temperature and no change in total number density during data collection, then the error in pressure is due solely to instrument considerations.

Therefore,

$$\Delta p = \pm \Delta p \text{ (statistical)} \pm \Delta p \text{ (instrument)} \quad (39)$$

- (a) The statistical error in the pressure meter was assumed to be zero as the Baratron reading remained constant during all data collection periods.
- (b) The instrument error was determined from a calibration chart supplied by the MKS Instruments laboratory. Using the ideal gas law, the calibrations were determined as actual d.c. voltage outputs at various STD pressures (mm H<sub>g</sub>). The average error in the 1 - 5 Torr range is  $1.64 \times 10^{-3}$  Torr with a standard deviation of  $1.13 \times 10^{-3}$  Torr. This error is neglected for this effort, since it amounts to less than 1%. Hence, the errors in pressure are assumed to be zero.

The largest error associated with the quenching rate constant  $K_q(T)$ , comes from the deviations in  $\Delta T_{\text{eff}}$ . The errors in  $T_{\text{eff}}$  presents the most interesting analysis due to the myriad of electronic equipment, for which no corrections were made, required to produce  $T_{\text{eff}}$  plus the fact that  $T_{\text{eff}}$  is related to each individual data point and the overall calculation of  $K_q(T)$ . Hence

$$\Delta T_{\text{eff}} = \pm \Delta T_{\text{eff}} (\text{statistical}) \pm \Delta T_{\text{eff}} (\text{instrument}) \quad (40)$$

The statistical error in  $\Delta T_{\text{eff}}$  is directly related to the error in slope per foreign gas pressure. This error in slope is graphically illustrated in Appendix C for each data point, as the maximum limits of the  $n \pm 2\sqrt{n}(\sigma = \pm n$  where  $\sigma$  is the standard deviation), (Ref 30:54)) values. The error in  $T_{\text{eff}}$  per foreign gas was manually determined by

placing a straight edge along the line that intercepted the  $+2\sqrt{n}(\Delta)$  and the  $-2\sqrt{n}(\square)$  on each side of the least square fit line. This method of determining the maximum deviation in slope has in itself errors which are unknown. The results are shown as error bars in Figs. 12, 13, and 14. The variable errors for each  $T_{\text{eff}}$  made it difficult to obtain an overall error for each  $K_q(T)$ . However, a relative error was determined as is shown in Table III by placing a straight edge along the line intercepting the maximum error bars on either side of the least square fit for each foreign gas.

Table III  
Relative Error in  $K_q(T)$

Foreign Gas	Relative Error in $K_q(T)$
Ar	+0.27, -0.08
He	+0.17, -0.26
N <sub>2</sub>	+0.03, -0.13

The final area considered is the error associated with photon counting and the probability of photon detection in the interval  $t$  to  $t + \Delta t$ . Using Eq (19) with  $P_c N_o \Delta t T_{\text{eff}}$  equal to  $P_o$  and  $T_{\text{eff}}$  equal to  $\tau$  for convenience, we have

$$P = P_o e^{-t/\tau} [1 - N_o P_c (1 - e^{-t/\tau})] \quad (41)$$

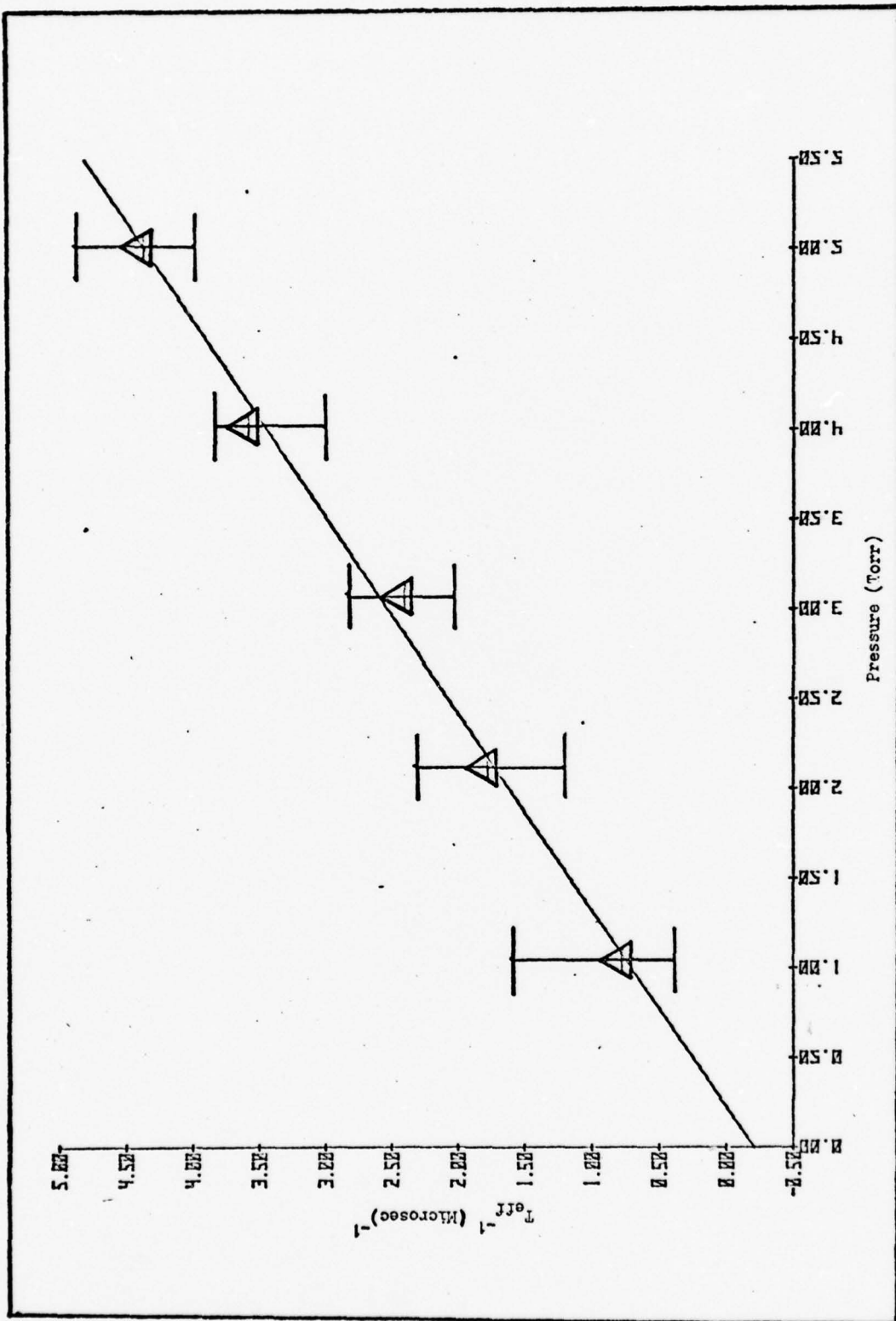


Fig. 12. Argon Deviations in  $T_{eff}$

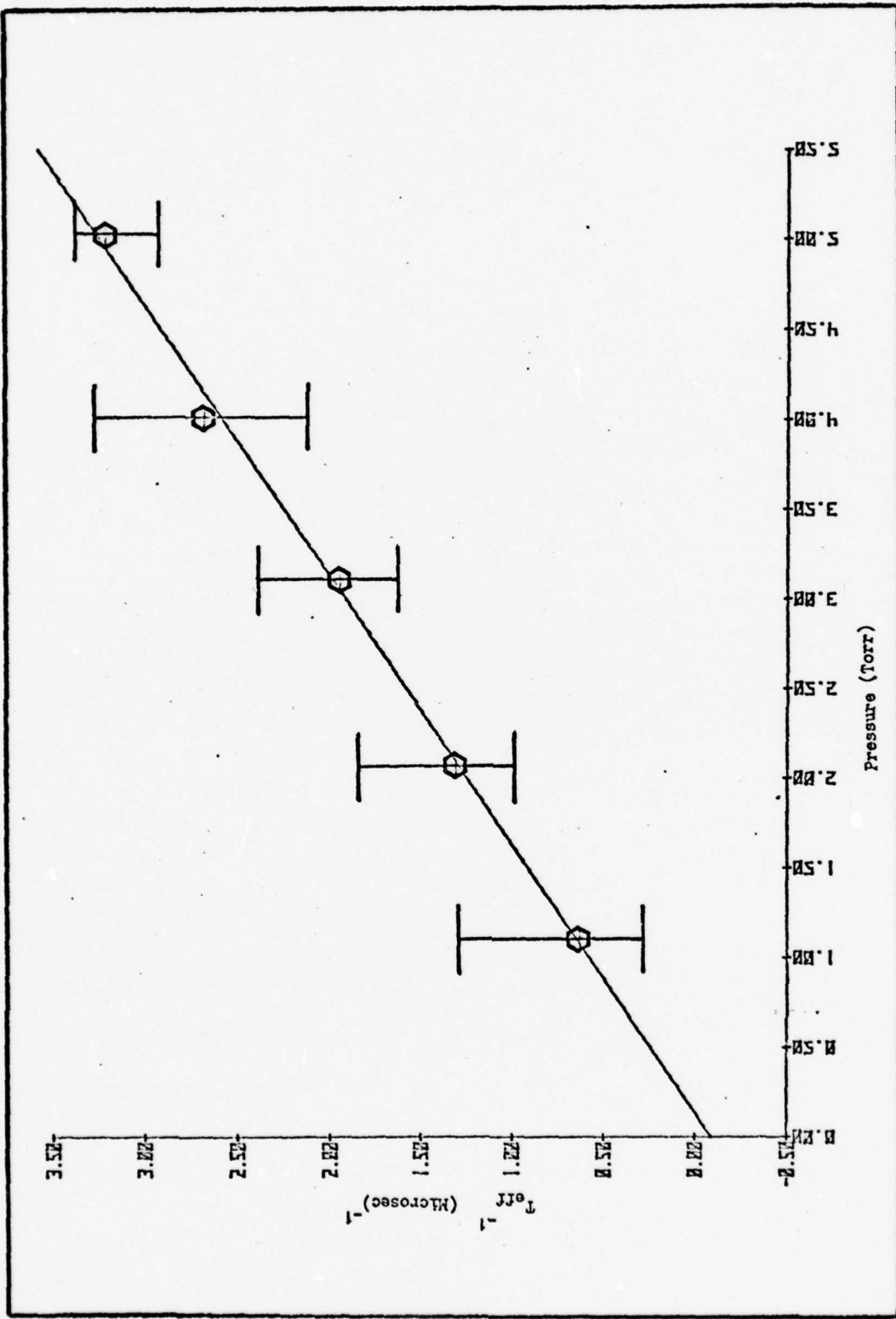


Fig. 13. Helium Deviations in  $T_{\text{eff}}$

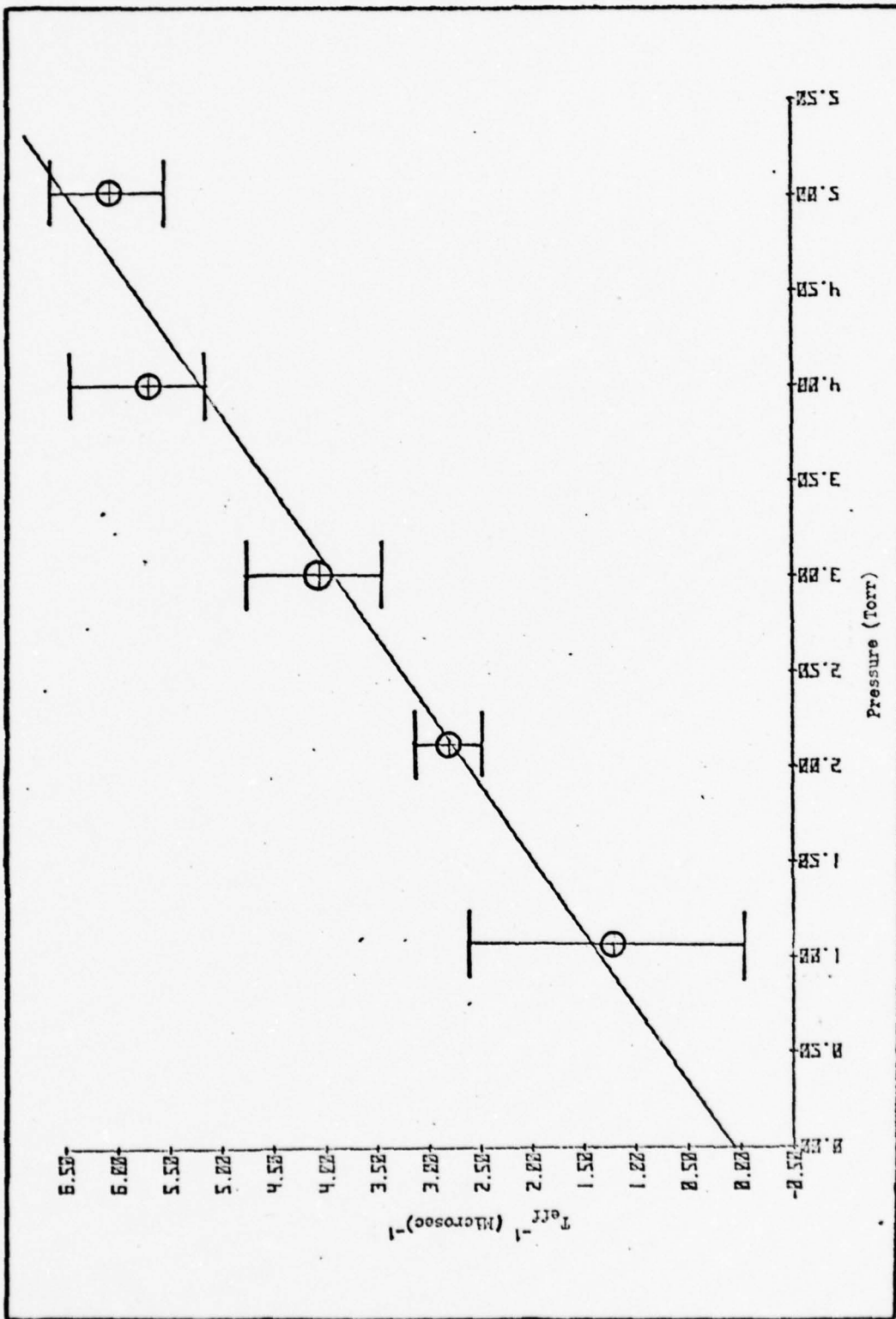


Fig. 14. Nitrogen Deviations in  $T_{eff}$

and

$$P = P_0 \quad \text{when } t = 0 \quad (42)$$

and as an approximation

$$P = P_0 e^{-t/\tau} \quad \text{when } N_0 P_c (1 - e^{-t/\tau}) \ll 1 \quad (43)$$

Since Eq (43) is only an approximation, the calculated  $\tau$  will be in error, this value of  $\tau$  will be represented by  $\tau_1$ . Hence

$$\ln P/P_0 = -t/\tau_1 \quad (44)$$

and

$$\tau_1 = t \ln P_0/P \quad (45)$$

However, if we now consider the experimental values of  $N_0 P_c$  equal to .15 and  $t$  equal to the maximum of  $3T_{\text{eff}}$ , Eq (41) becomes

$$P = P_0 e^{-t/\tau} [1 - .15(.95)] \quad (46)$$

and

$$\ln P/.86 P_0 = -t/\tau \quad (47)$$

or

$$\tau = t [\ln .86 P_0/P] \quad (48)$$

Then the change in  $\tau$  is  $\Delta\tau$  or

$$\Delta\tau = \tau_1 - \tau \quad (49)$$

which is

$$\Delta\tau = t [\ln P_o/P - \ln .86 P_o/P] \quad (50)$$

and the error in  $\tau$  is

$$\Delta\tau/\tau_1 = [(\ln P_o/P)^{-1} - (\ln .86 P_o/P)^{-1}] \ln P_o/P \quad (51)$$

which approximately reduces to

$$\% \text{ error} = [1 - n/(n + \ln .86)] 10^2 \quad (52)$$

Eq (52) is the % error in  $\tau$  where the substitution  $t = n\tau$  was used, where  $n$  is the number of  $T_{\text{eff}}$ 's considered. Thus for the experimental value of probability of photon detection of .15 photons/pulse and a maximum of  $3T_{\text{eff}}$  ( $n = 3$ ), the error is approximately 5%. If  $2T_{\text{eff}}$  and .15 photons/pulse are used, then the error increases to approximately 8%. Analysis of the raw data indicated that the least square fit curves were generated between  $2T_{\text{eff}}$  and  $3T_{\text{eff}}$  utilizing a photon/pulse rate  $\leq .15$ .

### Discussion

#### a. Experimental Results

Considering a first attempt at employing the data collection method developed by Wharton (Ref 3:38) plus the fact that only one data run per foreign gas per pressure was accomplished, the results are fair. The method employed to directly measure the quenching rate constant is effective but time consuming.

The overall quenching rate constants for Ar, He, and N<sub>2</sub> are in good agreement with the Kaufman (Ref 29:720) results. The quenching constant result for Ar is in very good agreement with the Kaufman data, while the He result is in excellent agreement. Prior to obtaining any data for this experiment, it was expected that the Ar and He results would agree closely with the Kaufman (Ref 29:720) data. This speculation was due to the fact that the 4368<sup>0</sup>Å incident energy is far below the atomic energy levels of either Ar or He and thus only translational and no vibrational interaction was expected.

The high quenching rate constant obtained for N<sub>2</sub> was expected, since NO<sub>2</sub><sup>\*</sup> and the N<sub>2</sub> ground state vibrational levels should interact due to their common energy level configuration. Although the N<sub>2</sub> quenching rate constant for this effort was larger than the Kaufman results, the overall result is termed as a fair comparison.

In comparison to the Kaufman quenching cross-sections, the values of  $\sigma_q(T)$  for this effort were higher. The variation in  $\sigma_q(T)$  with temperature was not observed since the sample tube temperature remained constant.

The value of  $T_r'$  for Ar obtained by comparison with Kaufman was in excellent agreement with the 44 $\mu$ s value used by Kaufman. No  $T_r'$  values for He or N<sub>2</sub> were calculated since the fluorescence detection wavelength was not available from the Kaufman data.

All of the collected data displayed a possible biexponential curve that was most prominent near the initial portion of the decay. This phenomena may be due to noise or to two  $\text{NO}_2$  lifetimes. The most significant experimental error, neglecting electronic errors, was due to the measurement of  $T_{\text{eff}}$ .

b. General Results

Overall, the  $\text{N}_2$  and dye laser operated satisfactorily, with the exception of the problems discussed earlier. Some problems were expected, since all of the data was collected at 40pps. This high pulse rate possibly contributed to the  $\text{N}_2$  and Alcatell pump breakdown. The Coumarin 440 dye decreased its output power after approximately 7 hours of uninterrupted lasing time. The dye laser output ( $4368\text{\AA}$ ) was periodically checked with the Jarrell-Ash monochromator and the dye laser grating required no adjustment. Subsequent to installation of the new  $\text{N}_2$  discharge channel, the dye laser beam, observed after mirror reflection, exhibited excessive fluorescence surrounding the actual lasing area. This visual observation showed that the fluorescence area was 2 cm in diameter and the lasing area was 1.2 cm in diameter and removed from the center of the beam. Dye laser realignment attempts did not improve the situation.

The gas handling system was excellent in delivering and evacuating  $\text{NO}_2$  plus foreign gas from the sample tube. The Baratron and ion gauges operated within their specified

ranges at all times. The gas ( $\text{NO}_2$  plus foreign gas) loading required extreme care in avoiding an overpressure in the sample tube. The loading of gas mixtures was time consuming but effective. The Turbo Molecular pump provided continuous evacuation (to  $10^{-7}$  Torr) throughout the experiment with no malfunctions.

Oscilloscope analysis of the electronic components was kept to a minimum (only the delay box was analyzed). The MCA continued to malfunction in every eighth channel as previously experienced by Wharton (Ref 3:45). This malfunction did not pose any problems to the experimental objectives.

## VI. Conclusions and Recommendations

### Conclusions

The following conclusions summarize this experimental effort:

1. The experimental method can be used to calculate quenching rate constants from measured data in the 1-5 Torr pressure range for  $\text{NO}_2$  and foreign gases.

2. The method of single photon counting is time consuming and requires elaborate electronic instrumentation. However, the advantage of this method over the Kaufman method is that this effort calculates a quenching rate constant directly.

3. The errors introduced by accumulating data over a two-day period and integrating the results is unknown.

4. The appearance of detectable counts near the initial (rise) area of the individual curves may be due to noise and the laser pulse (build up of excited states). This fact was evidenced by visual inspection of the rising portion of the curves as shown in Appendix C.

5. A significant portion of the data was collected in the presence of electrical noise produced by the delay box (following photomultiplier tube in Fig. 7 and the old  $\text{N}_2$  laser discharge channel.

6. Visual inspection of the initial portion of the least square fit curve of each foreign gas also indicates that the excited  $\text{NO}_2$  may possess two lifetimes; one short (ns range) and one long ( $\mu\text{s}$  range). The fast lifetime undergoes minimum collisional quenching while the long lifetime may be primarily due to quenching.

7. The placing of neutral density filters in the laser beam path is an effective control of the photon per pulse rate.

8. By insuring that the photon per pulse rate was  $\leq .15$ , the probability of photon detection within  $3 T_{\text{eff}}$  was adequate.

9. Broadband detection can be used to improve the collected signal strength.

10. The gas pressure measuring system was extremely effective down to  $10^{-7}$  Torr.

11. The error calculated for each quenching rate constant is a conservative estimate.

#### Recommendations

In order to improve or assist future experimental attempts to study similar areas, the following recommendations are made:

1. An aperture should be placed near the sample tube entry window in order to insure that only the lasing portion of the dye laser beam is transmitted through the tube.

2. The sample tube should be heated in order to experimentally determine the effect of temperature on quenching cross-sections  $\sigma_q(T)$ .

3. Quenching rate constants for Ar, He and  $N_2$  should be measured using a narrowband (monochromator) fluorescence detection scheme and the results compared to this effort.

4. The following sequence should be used if a future experiment is to be conducted with the objectives of this effort:

- (a) The background counts should be normalized to the data collection time.
- (b) The background plus signal counts collected as per this effort.
- (c) Find the difference between signal and background--this is the basic data.
- (d) Correct for multiple counts per pulse by utilizing Eq (16). The first approximation for  $T_{eff}$  as determined in this effort may be used to estimate the correction.
- (e) Correct the collected data for multiple counts and determine a new lifetime.

5. Extend this effort to examine the effect on quenching rate constants,  $K_q(T)$ , as the difference between excitation wavelength ( $\lambda_E$ ) and fluorescence wavelength increases, i.e., examine the stepwise vibrational deactivation of the excited electronic state of  $NO_2$ .

6. Examine the quenching rate constants,  $K_q(T)$ , of several other gases as per the Kaufman (Ref 29:720) effort and compare results.

7. A single lens arrangement to collect the emitted radiation from the sample tube should be used. The double lens arrangement used in this effort made it difficult to determine the collection solid angle.

8. Replace the electronic board required to allow data accumulation in every eighth channel of the MCA.

9. If possible, conduct the entire experiment in an area where the artificial and natural lighting effects can be controlled.

10. The possibility of two effective lifetimes should be investigated in a similar effort.

## Bibliography

1. American Physical Society (APS) Summer Study. The Role of Physics in Combustion. July 1974.
2. Marowsky, G. "Principle of Dye Laser Operation and Dye Laser Tuning Methods," Optica ACTA, 23: 855-873 (Nov 1976).
3. Wharton, John E. "Lifetime Measurements Using Fluorescence Emission." MS Thesis. Wright-Patterson AFB, Ohio: Air Force Institute of Technology, December 1977.
4. Hardwick, J. L. "Fluorescence from the  $^2B_1$  State of  $NO_2$  Excited at 4545Å," Journal of Molecular Spectroscopy, 66: 248-258 (1977).
5. Douglas, A. E. and K. P. Huber. "The Absorption Spectrum of  $NO_2$  in the 3700Å-4600Å Region," Canadian Journal of Physics, 43: 74-81 (January 1965).
6. Keyser, L. F. et al. "Kinetics and Mechanism of  $NO_2$  Fluorescence," Journal of Chemical Physics, 54: 355-363 (January 1971).
7. Douglas, A. E. "Anomalously Long Radiative Lifetimes of Molecular Excited States," Journal of Chemical Physics, 45: 1007-1015 (February 1966).
8. Brewster, W. P. et al. "Observations on the Lines of Solar Spectrum and Those Produced by the Earths Atmosphere and by the Action of Nitrous Acid Gas," Transactions of the Royal Society (Scotland), 519-525 (1834).
9. Baxter, W. P. "The Fluorescence of Nitrogen Dioxide," The Journal of American Chemical Society, 52: 3920-3927 (October 1930).
10. Monts, D. L. et al. Spectral Atlas of Nitrogen Dioxide 5530 to 6480Å. New York, New York: Academic Press, 1978.
11. Gillispie, Gregory D. and Ahsan V. Khan. "The Electronic Structure of Nitrogen Dioxide. I. Multiconfiguration Self-Consistent-Field Calculation of the Low Lying Electronic States," Journal of Chemical Physics, 63: 3425-3444 (October 1975).

12. Hardwick, J. L. and J. C. D. Brand. "The  $2B_1 \leftarrow 2A_1$  System of Nitrogen Dioxide," Chemical Physics Letters, 21: 458-461 (September 1973).
13. Butler, Shala, et al. "Some Observations on the Continuum Emission from  $NO_2$ ," Journal of Chemical Physics, 62: 815-820 (February 1975).
14. Squid Workshop. Combustion Measurements in Jet Propulsion Systems. Purdue University (22-23 May 1975).
15. Herzberg, Gerhard. Molecular Spectra and Molecular Structure (2nd ed.). Vol. I: Spectra of Diatomic Molecules. New York, New York: Van Nostrand Reinhold Company, 1950.
16. Roh, Won B. "Coherent Anti-Stokes Raman Scattering of Molecular Gases," Technical Report AFAPL-TR-77-47, August 1977.
17. Schwartz, Stephen E. and Harold S. Hohnston. "Kinetics of Nitrogen Dioxide Fluorescence," Journal of Chemical Physics, 51: 1286-1302 (August 1969).
18. Eckbreth, A.C. et al. Experimental Investigations of Saturated Laser Fluorescence and CARS Spectroscopic Techniques For Practical Combustion Diagnostics. EPA-68-02-2176. U.S. Environmental Protection Agency, Office of Research and Development, Triangle Park, North Carolina 27711, February 1978.
19. Neuberger, Dan and A. B. F. Duncan. "Fluorescence of Nitrogen Dioxide," Journal of Chemical Physics, 22: 1693-1696 (October 1954).
20. Keyser, L. F. et al. "Radiative Lifetime and Collisional Quenching of  $NO_2$  Fluorescence and Nature of the Air Afterglow," Chemical Physics Letters, 2: 523-525 (December 1968).
21. Uselman, W. M. and Edward K. C. Lee. "A Study of Electronically Excited  $NO_2$  in its First Predissociation Region: Fluorescence Emission Lifetimes and Electronic Quenching," Journal of Chemical Physics, 64: 3457-3462 (April 1976).
22. Donnelly, V. M. and F. Kaufman. "Fluorescence Lifetime Studies of  $NO_2$ . I. Excitation of the Perturbed  $2B_2$  State Near 600nm," Journal of Chemical Physics, 66: 4100-4110 (May 1977).
23. Handbook of Chemistry and Physics (47th edition), Cleveland, Ohio: Chemical Rubber Company, 1971.

24. Schreiber, Paul W. et al. "Application of Lasers to Combustion Diagnostics," Proceedings of Society for Photo-Optical Instrumentation Engineers (SPIE). 22nd Technical Symposium, San Diego, California, August 1978.
25. Eckbreth, A. C. et al. Review of Laser Raman and Fluorescence Techniques for Practical Combustion Diagnosis. Task I Report, EPA 68-02-2176, U.S. Environmental Protection Agency, Office of Research and Development, Triangle Park, North Carolina 27711, February 1977.
26. Daily, J. W. "Saturation Effects in Laser Induced Fluorescence Spectroscopy," Applied Optics, 16: 568-571 (March 1977).
27. Piepmeier, E. H. "Theory of Laser Saturated Atomic Resonance Fluorescence," Spectrochimica Acta, 27B: 431-444 (1972).
28. Baranovski, A. P. and J. R. McDonald. "An Application of Saturation Spectroscopy," Journal of Chemical Physics, 66: 3300-3301 (April 1977).
29. Kaufman, F. et al. "Quenching of NO<sub>2</sub> Fluorescence," Journal of Chemical Physics, 44: 718-723 (January 1966).
30. Price, William J. Nuclear Radiation Detection. New York, New York: McGraw-Hill Book Company, 1958.

## Appendix A

Appendix A lists the equipment used for this experiment. The equipment is discussed in the following order: (1) gas handling system, (2) laser, (3) optics, (4) electronics and (5) temperature.

### Gas Handling System

The gas handling system was designed to obtain low gas pressures ( $10^{-7}$  Torr) and a low leak-up rate (.19 mTorr/hour). It was also designed to allow the introduction and evacuation of  $\text{NO}_2$  only or  $\text{NO}_2$  plus a foreign gas. A Baratron pressure gauge allows the sample test tube pressure to be monitored during data collection, while the remainder of the system is continuously evacuated by a Turbo Molecular pump. A photograph of the gas handling system is shown in Fig. 15 and a schematic as shown in Fig. 7. All gases flow through 1/4-inch and/or 1/2-inch stainless steel tubing connected with Cajon, Varian and/or Swagelok fittings. The valves used to control the gas flow are Nupro valves with the exception of the  $\text{NO}_2$  bottle valve, which is a Whitey needle valve and the foreign gas cylinder valves, which are Kerotest valves. The foreign gas cylinders (size A, 22.8 x 139.7 cm) are directly connected to a Matheson Model 3500 pressure vacuum regulator which allows controlled handling of cylinder pressure in  $\text{Kg/cm}^2$  or  $\text{lb/in}^2$ . The



Fig. 15. Experimental Equipment

foreign gases are used without further purification and are supplied by Air Products (Middletown, Ohio) with the following grade specifications:

- (a) Helium (He), high purity grade; 99.995%--8240 liters/cylinder
- (b) Argon (Ar), ultra high purity grade; 99.998%--9543 liters/cylinder
- (c) Nitrogen (N<sub>2</sub>), ultra high purity grade; 99.998%--8495 liters/cylinder

The NO<sub>2</sub> sample is contained in a Whitey lecture cylinder of length 20 cm and 5 cm diameter. The NO<sub>2</sub> cylinder is also supplied by Air Products, is not further purified and is of (99.99%) purity grade.

Pressure in the gas system is monitored by two Granville Phillips Model 274 ionization gauges, one MKS Type 170 Baratron (capacitance manometer type for absolute pressure control) and one Granville-Phillips Model 260 thermocouple (See Fig. 9). The MKS Baratron is directly connected to a Hewlett-Packard Model 3480B digital pressure volt meter which displays absolute pressure as a DC voltage output (0-10V). The digital pressure volt-meter is manually zeroed on the face of the MKS Type 170M-6B Range Multiplier which is adjacent to a Type 170M-26B meter unit. The meter unit and the range multiplier are applicable to the Baratron readouts only. Ion gauge pressure is monitored by a Granville-Phillips Model 260 gauge controller which displays pressures as low as 10<sup>-9</sup> Torr and also serves the thermocouple. The thermocouple gauge is used to monitor the

pressure before starting the Turbo Molecular Pump. The ionization gauges are used to monitor system pressure only during non-data collection times; e.g., leak testing or system pump-down because it was discovered that the emitted radiation from the ionization gauges contributed to the background photons (counts) detected by the photomultiplier. Therefore, only the Baratron monitors the sample tube pressure during data collection.

The sample tube is T-shaped and is 30.9 cm long with a diameter of 4.7 cm. The T is also 30.9 cm long and is located at the center (15.45 cm) of the longitudinal axis of the tube and has a metal-to-glass seal. The sample tube and end windows are made of quartz. The fluorescence radiation is collected, in a direction perpendicular to the laser beam, from the excited molecules located near the longitudinal axis of the sample tube. This tube is housed in an insulative box (46 cm x 23 cm x 28 cm) with a flat black-coated interior (to eliminate laser beam scatter) and wiring for temperature control. This box has three ports for laser beam entry, exit and fluorescence viewing.

System evacuation is accomplished by a Welch (Model 3101) Turbo Molecular pump, (140 liters per second pumping speed), a Varian (Model 301) Vac-Sorb pump, and a Welch (Model 3000) Duo Seal pump. The Turbo Molecular pump can evacuate the total system or only the test tube area continuously. The Turbo Molecular pump is operated on a 24-hour basis during the experiment. All valves are open for system evacuation

after each data run and pumped down to  $10^{-5}$  Torr. The Duo Seal pump evacuates the foreign gas line by using valve 8 (Fig. 9). The foreign gas line is evacuated several times prior to each data collection run.

### Laser

Identically, as used by Wharton (Ref 3:27), a Molectron DL200 Tuneable Dye Laser pumped by a Molectron UV1000 Nitrogen ( $N_2$ ) Laser was used during the experiment. For this effort the  $N_2$  laser is pumped at 40 pulses per second and a pulse width of 10 nanosec. The dye laser was tuned to an excitation (output) wavelength of  $4368\text{\AA}$  using the diffraction grating. The dye used is an Exciton product known as Coumarin 440 (110 mg mixed with 125 cc of pesticide quality ethyl alcohol).

The output power of the laser is measured using an Astrodata Nanovoltmeter (Model TDA121) connected to an Eppley (Model 12026) thermopile. The power meter was calibrated using a known He Ne laser source.

### Optics

The optical elements used in the experiment are as shown in Fig. 16. The beam splitter reflects 50% of the dye laser energy to the PIN diode. The transmitted beam is focused by lens 1 (4.75 cm diameter) through neutral density filters to a point on the axis of the sample tube.

The fluorescence spectrum is focused first by lens 2 (4.5 cm diameter) and then lens 3 (4.75 cm diameter) onto

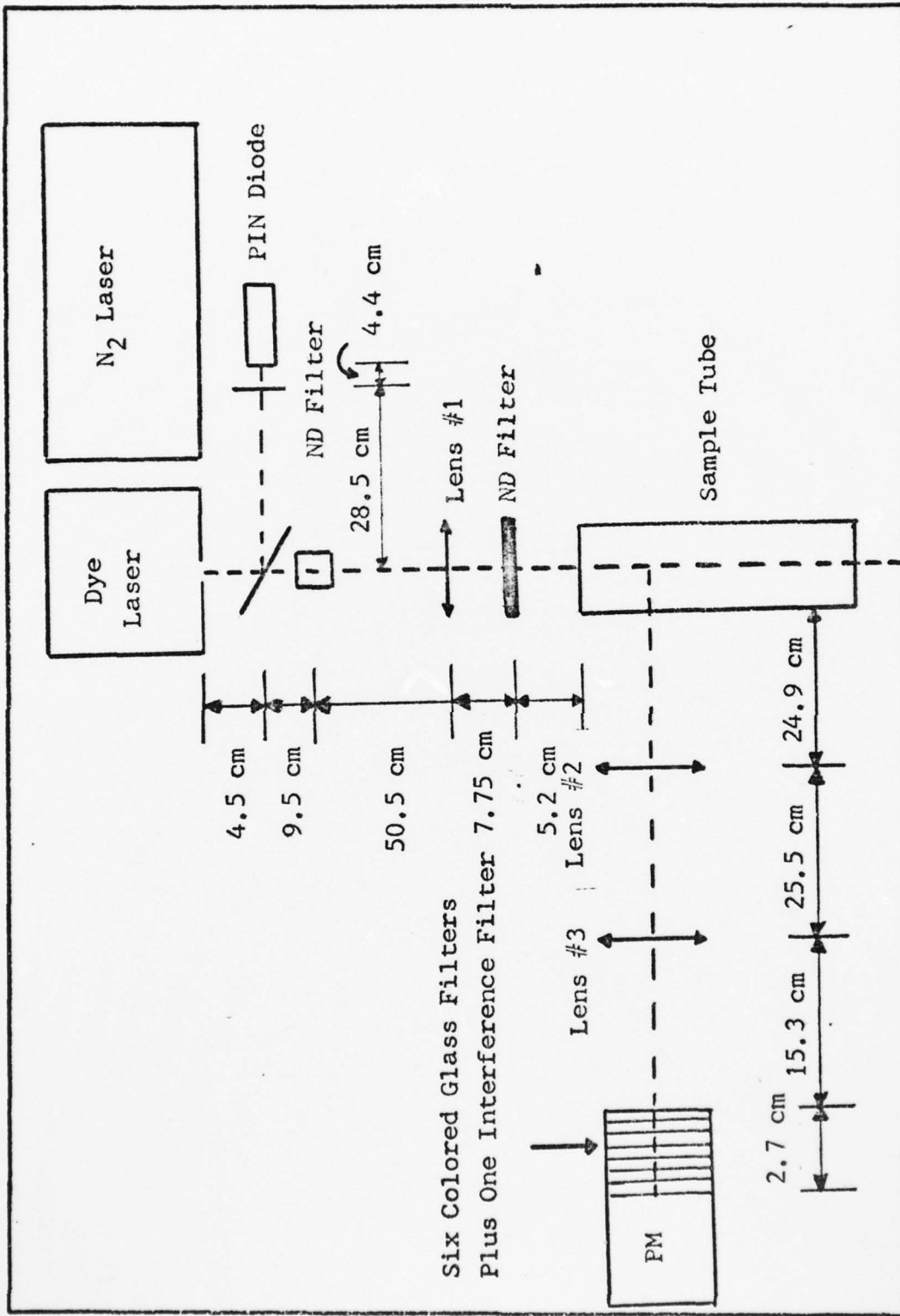


Fig. 16. Optics Schematic

the first of six consecutively stacked Corning colored-glass filters. The seventh optical element that follows the colored-glass filters is a Farrand interference filter. The transmission characteristics of the colored filters and the interference filter were measured using a Perkins-Elmer Model 350 spectrophotometer and the results are shown in Fig. 17. The spectrophotometer results clearly indicate that the 4368 $\text{\AA}$  laser pulse wavelength was effectively cutoff from detection. Following the interference filter is an Emitronics 9816B photomultiplier tube which is operated at 2000 volts. This is a 14 stage dynode chain with a response active in the 3000 $\text{\AA}$  to 8500 $\text{\AA}$  range. The photomultiplier absolute sensitivity was 54mA/watt and the corresponding quantum efficiency was 12% at the peak fluorescence wavelength of 5430 $\text{\AA}$ .

A Jarrell-Ash Model 82 monochromator is used to measure the wavelength of the dye laser. This spectrometer has a 52 mm x 52 mm grating of 1180 grooves/mm blazed for 4000 $\text{\AA}$ . The entrance and exit slit width is  $6.35 \times 10^{-2}$  mm.

### Electronics

The electrical equipment required for single photon counting is as shown in Fig. 7. The equipment configuration uses several of the same electronic components used by Wharton (Ref 3:39) in his second experimental method. The components and function of each is described as follows. The PIN diode is a Motorola MRD 500 (ultra high speed)

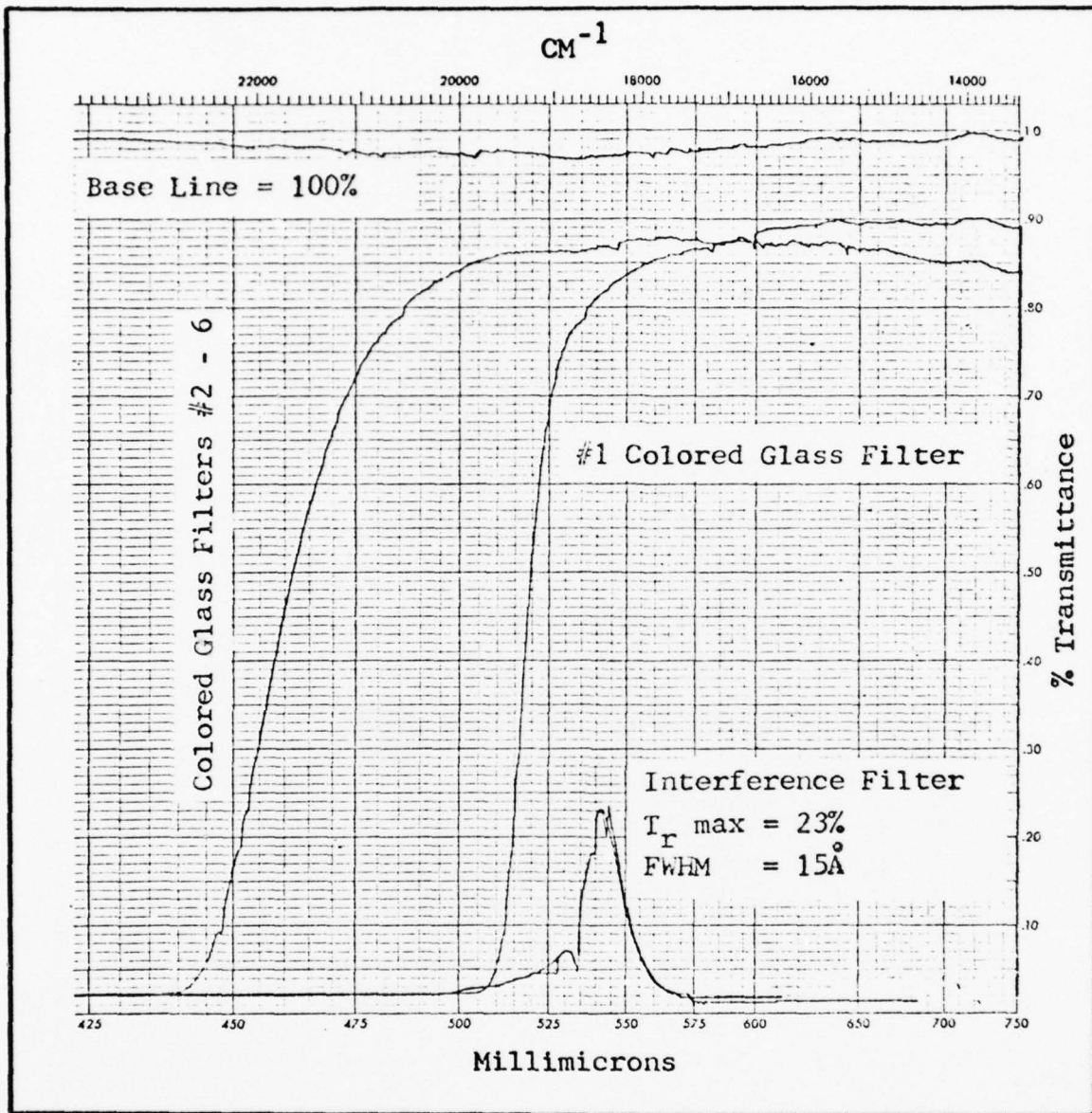


Fig. 17. Filter Transmission Characteristics

silicon photo diode with a convex lens design sensitive throughout the visible and near IR. The rise time is less than 1 nanosec and the radiation sensitivity is  $1.8 \text{ uA/mW/cm}^2$ .

The Dual Discriminator is an Ortec EG and G Model T105/N which can be operated in a gated (requires a positive 4 to 12

volt signal) or ungated mode. The function of the discriminator is to produce a reference output pulse (-800 mv) of controlled amplitude and width whenever the input pulse exceeds a preset threshold. This threshold is controlled with a potentiometer and the width is controlled via a variable external delay line. The Hewlett-Packard Model 8012B Pulse Generator Produces pulses whose amplitude, pulse width and pulse delay can be varied from 0.1 to 10 volts, 10 nanosec to 1 sec and 35 nanosec to 1 sec, respectively.

Delay signals required during the experiment are produced by two Ortec EG and G Model DB 463 Delay Boxes and by ordinary electrical wire cut to approximately 1.55 nanosec per foot. The Ortec Delay Boxes can produce delays of 0.5, 1, 2, 4, 8, 16, and 32 nanosec. The delay box prior to the photomultiplier tube provided excessive noise and was replaced by 82 feet of ordinary electrical wire.

Total counts (999,999 maximum) and frequency measurements (.1 Hz, 1 Hz and 100 Hz resolution) are made by the Fluke Model 1900A<sup>o</sup> Multicounter. The required input signal must be at least 20 ns long. The Ortec EG and G Model LG 105/N Linear Gate and Pulse Stretcher produces a maximum amplitude signal stretched by 3 $\mu$ s for the Multicounter. The LG 105/N operates in the ungated mode or in the gated mode (-800 mv gating signal required).

An Ortec EG and G Model 467 Time-to-Pulse Height Converter (TPHC) receives a Stop and Start input signal which is generated into an output pulse whose amplitude (10 volts

full range) is proportional to the difference in time between the Stop and the Start input signals. Preset panel switches allow selection of a .05 $\mu$ s, .1 $\mu$ s, .2 $\mu$ s, .4 $\mu$ s, or .8 $\mu$ s, with a x10, x100 and x1000 range multiplier controlling the minimum time required between an input Stop signal which follows an input Start signal. The TPHC can operate in an ungated mode or a gated mode (two volts gating signal required). A minimum of 24 ns is required for the TPHC to process a Stop signal after a Start signal is received (gated or ungated mode). A false signal, indicating an elapsed time of 24 ns, is produced if Stop signal is received prior to 24 ns.

Pulse height analysis is produced by a Hewlett-Packard Model 5400A Multi-Channel Analyzer (MCA). The MCA receives input signals, from the TPHC, whose amplitude is proportional to the difference between a Stop and a Start signal. This input (10 volts maximum) flows to one of the 1024 available memory channels for storage. After integrating several input pulses over a period of time, the MCA can display, print or store the data. A Model C-51 Oscilloscope camera (uses Poloroid Type 107 Poloroid film) is used for photographing the displayed data on the integral oscilloscope. Signal analysis of the electronic components is accomplished by a Tektronics Model 7904 Oscilloscope. This oscilloscope is equipped with a Hewlett-Packard Oscilloscope camera (uses Type 47 Poloroid film).

### Temperature

A Moeller Model 63C precision thermometer was used to measure the variation in room temperature during data collection. The thermometer is graduated in one-degree increments and can be read to within one-tenth of a degree.

## Appendix B

Appendix B contains the experimental data that has been computer (CDC 6600) processed.

### Raw Data

Tables IV, V and VI represent the overall results of Ar, He and N<sub>2</sub> respectively. Included in the overall results is the linear regression curve of each foreign gas. The regression curves were calculated from the  $Y = a + bx$  form, where  $a$  equals the  $Y$  - intercept in  $(\mu s)^{-1}$  and  $b$  equals the slope in  $(\text{Torr}, \mu s)^{-1}$ . Fig. 18 shows a composite graphical presentation of the linear regression curve fit for each foreign gas plus NO<sub>2</sub> mixture plotted as a straight line from the ordinate axis ( $Y$  - intercept). Superimposed on each calculated regression curve are the actual data points for each gas mixture. Appendix C shows the exponential decay curve and least squares fit for each data point taken at various pressures (1 - 5 Torr). The straight line fit of each data point indicates that the decay curve approximated an exponential. The calculated correlation coefficient for each regression curve ( $> .90$ ) showed a strong relationship between the variables  $T_{\text{eff}}^{-1}$  and combined pressure of NO<sub>2</sub> plus foreign gas.

The N<sub>2</sub> data at 1 Torr and 4 Torr was collected over two runs. The N<sub>2</sub> and NO<sub>2</sub> pressures were equal for each

separate run. The error introduced by this collection process is unknown.

Table IV  
Argon Data

NO <sub>2</sub> Pressure (mTorr)	Ar Pressure (Torr)	Argon		
		Integration Time (hrs)	TPHC (μs)	T <sub>eff</sub> (μs)
19.57	1.025	3.00	4	1.29213
19.71	2.098	3.00	4	0.56295
19.40	3.050	3.00	2	0.41566
19.70	4.000	3.00	2	0.27893
19.50	5.003	3.00	1	0.22880
$\bar{x} = 19.57$	$\bar{x} = 3.04$			
$\sigma = 0.13$	$\sigma = 1.56$			

Actual Plotted Data (Fig. 18)

T <sub>eff</sub> <sup>-1</sup> (μs) <sup>-1</sup>	NO <sub>2</sub> + Ar Pressure (Torr)
0.7740	1.044
1.7774	2.117
2.4058	3.069
3.5851	4.019
4.3706	5.022

- a. Argon Linear Regression Curve:  $Y = -.204 + .912x$   
 b. Correlation Coefficient: .99

Table V  
Helium Data

NO <sub>2</sub> Pressure (mTorr)	He Pressure (Torr)	Helium		
		Integration Time (hrs)	TPHC (μs)	T <sub>eff</sub> (μs)
19.16	1.086	4.00	4	1.57750
19.00	2.050	3.25	4	0.76306
19.40	3.000	3.17	2	0.51232
19.48	3.993	4.08	2	0.37165
19.40	5.010	3.42	1	0.30988
$\bar{x} = 19.29$	$\bar{x} = 3.03$			
$\sigma = 0.20$	$\sigma = 1.55$			

Actual Plotted Data (Fig. 18)

T <sub>eff</sub> <sup>-1</sup> (μs) <sup>-1</sup>	NO <sub>2</sub> + He Pressure (Torr)
0.6340	1.105
1.3106	2.069
1.9520	3.109
2.6907	4.012
3.2271	5.029

- a. Helium Linear Regression Curve:  $Y = -.083 + .662x$   
 b. Correlation Coefficient: .99

Table VI  
Nitrogen Data

<u>Nitrogen</u>				
NO <sub>2</sub> Pressure (mTorr)	N <sub>2</sub> Pressure (Torr)	Integration Time (hrs)	TPHC (μs)	T <sub>eff</sub> (μs)
20.00	1.048*	3.00	2	0.82111
19.68	2.108	3.58	2	0.35758
19.60	3.004	3.00	2	0.24786
19.51	4.001*	4.60	1	0.17592
19.40	5.020	5.00	.5	0.16549
$\bar{x} = 19.64$	$\bar{x} = 3.04$			
$\sigma = 0.23$	$\sigma = 1.56$			

Actual Plotted Data (Fig. 18)

T <sub>eff</sub> <sup>-1</sup> (μs) <sup>-1</sup>	NO <sub>2</sub> + N <sub>2</sub> Pressure (Torr)
1.2179	1.068
2.7966	2.127
4.0345	3.023
5.6844	4.020
6.0427	5.039

- a. Nitrogen Linear Regression Curve:  $Y = .067 + 1.273x$   
 b. Asterick (\*) indicates that data was integrated.  
 c. Correlation Coefficient: .96

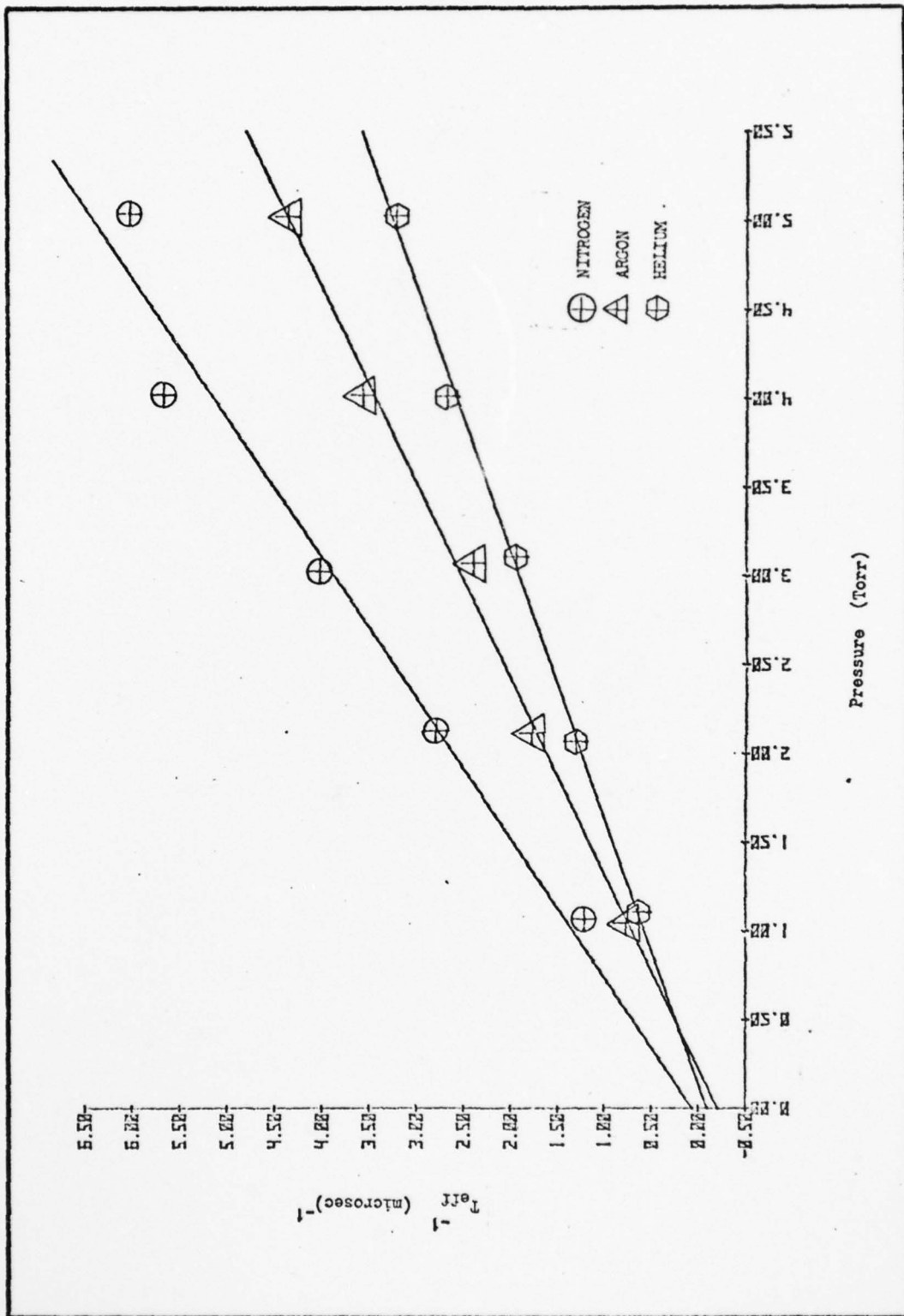


Fig. 18. Regression Curves of Foreign Gases

### Appendix C

Appendix C contains the individual results of the least squares fit analysis to the raw data (photograph in the inset of each figure). The plotted raw data (counts =  $n$ ) is indicated by an asterisk (\*) with a best fit line drawn through these points. The triangles ( $\Delta$ ) and the squares ( $\square$ ) indicate a plus and a minus, respectively, of two standard deviations ( $2\sigma$ ) from the counts. The deviations were calculated from the relation  $n \pm 2\sqrt{n}$ , where  $\sqrt{n}$  is equal to  $\sigma$  (Ref 30:54). Each photograph was obtained from the MCA and the plotted data was computer (CDC 6600) generated from the program shown in Appendix D.

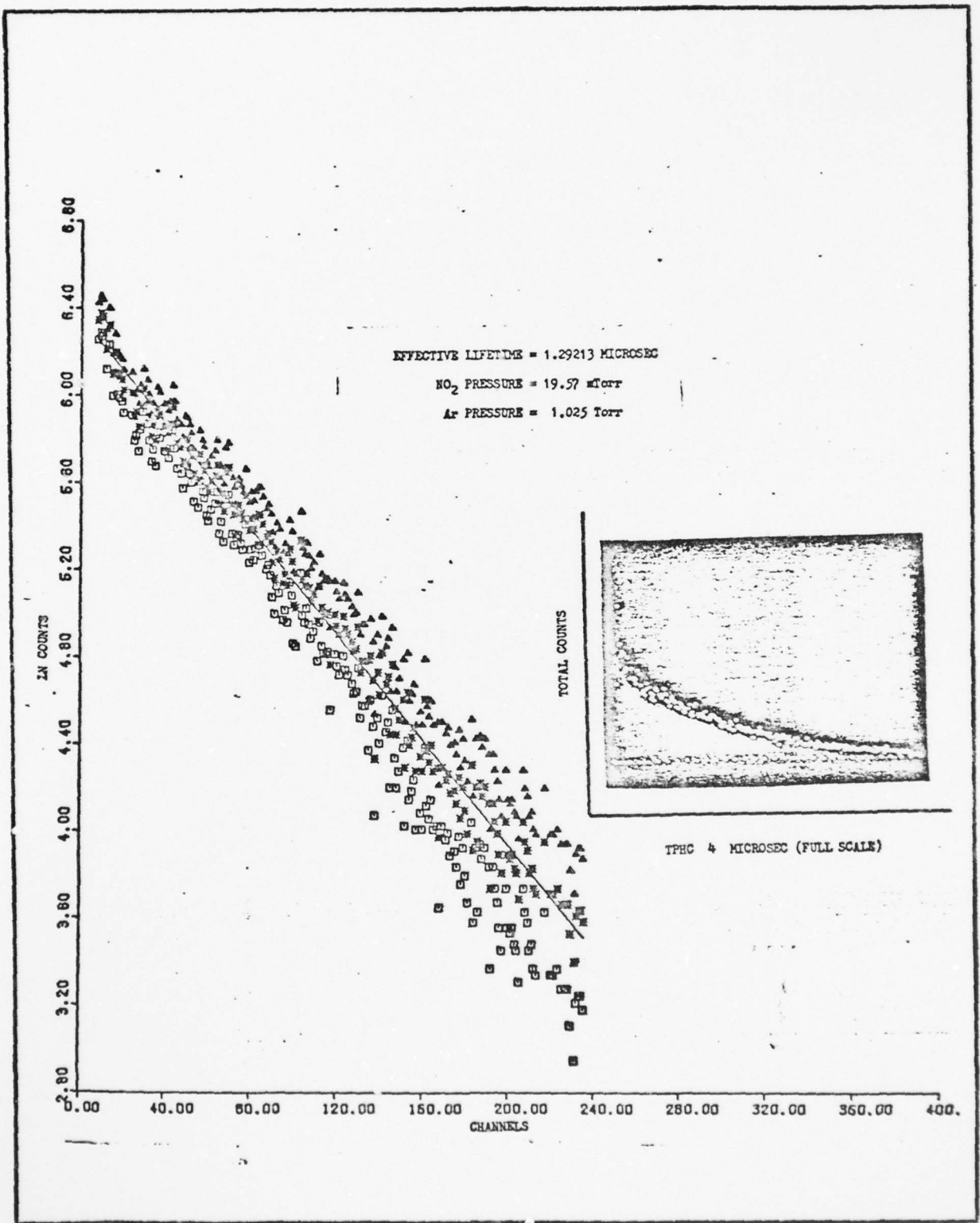


Fig. 19. Ar at 1 Torr

AD-A064 055

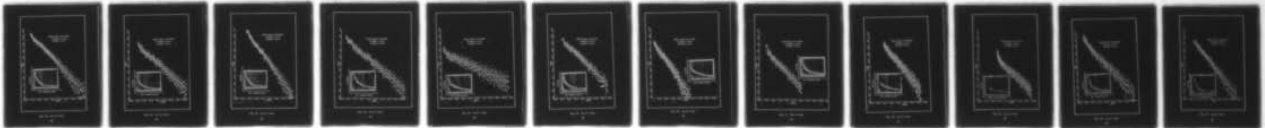
AIR FORCE INST OF TECH WRIGHT-PATTERSON AFB OHIO SCH--ETC F/G 7/2  
THE MEASUREMENT OF QUENCHING RATE CONSTANTS USING FLUORSCENCE E--ETC(U)  
DEC 78 F GARCIA

UNCLASSIFIED

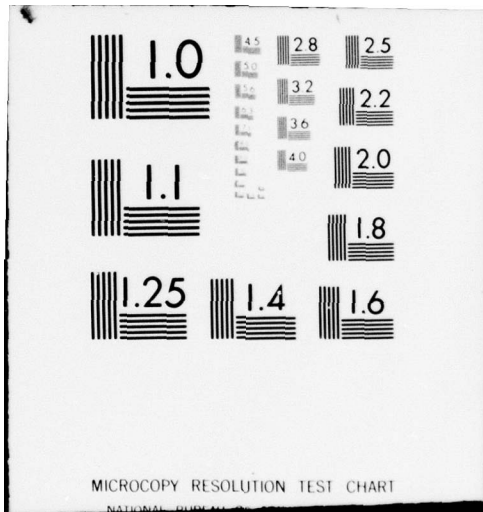
AFIT-6EP/PH/78-3

NL

2 of 2  
AD  
A064055



END  
DATE  
FILMED  
3-79  
DDC



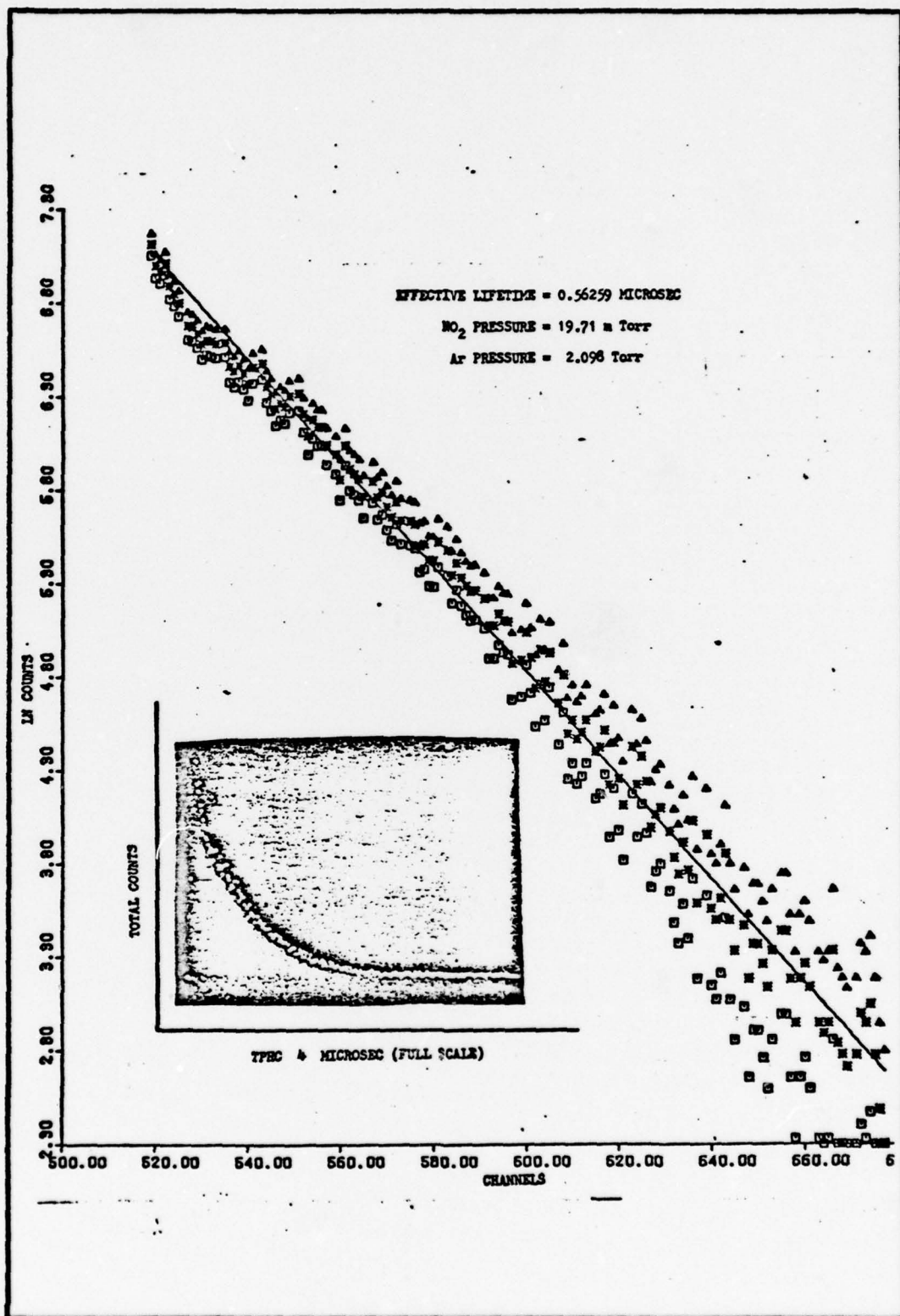


Fig. 20. Ar at 2 Torr

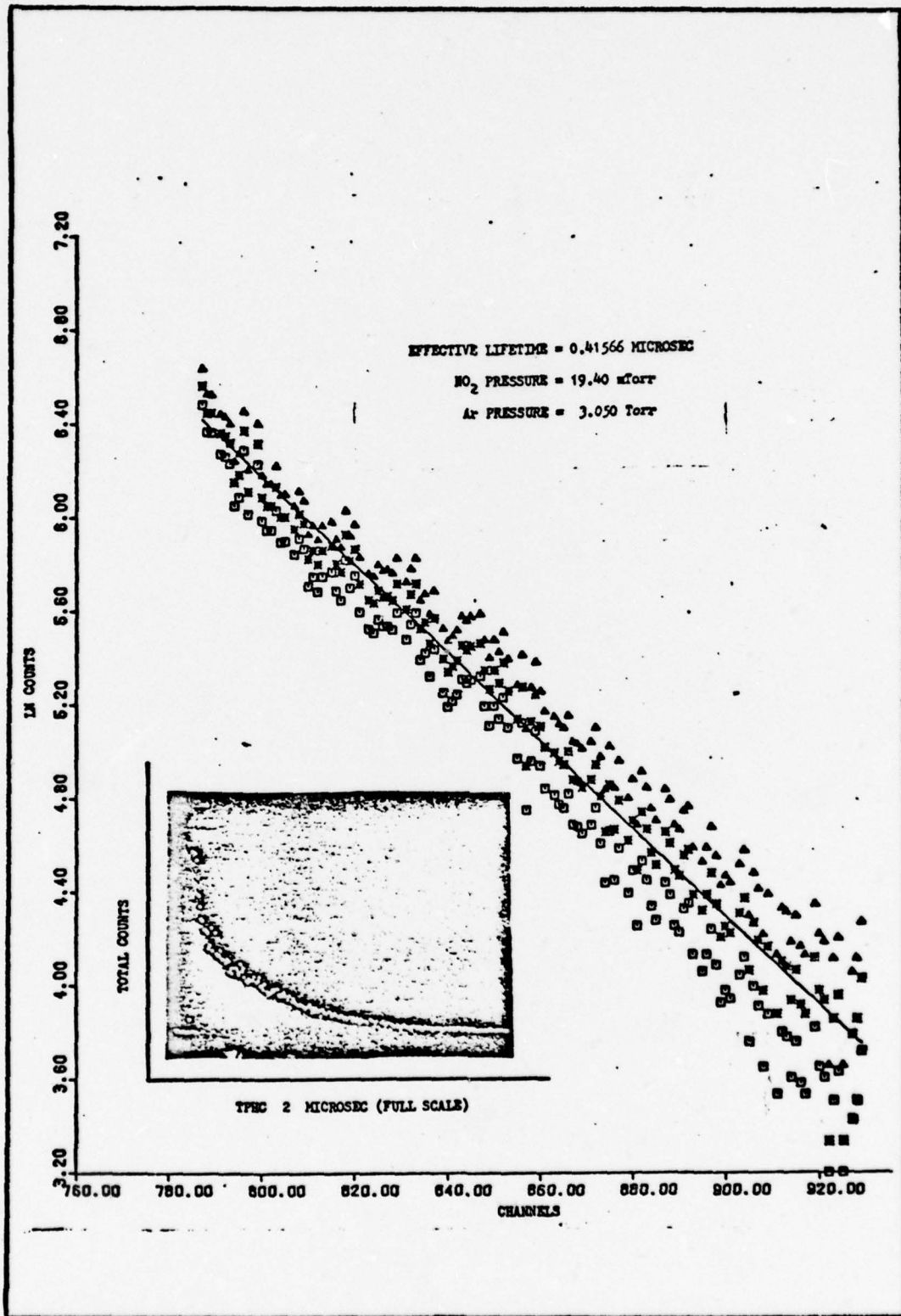


Fig. 21. Ar at 3 Torr

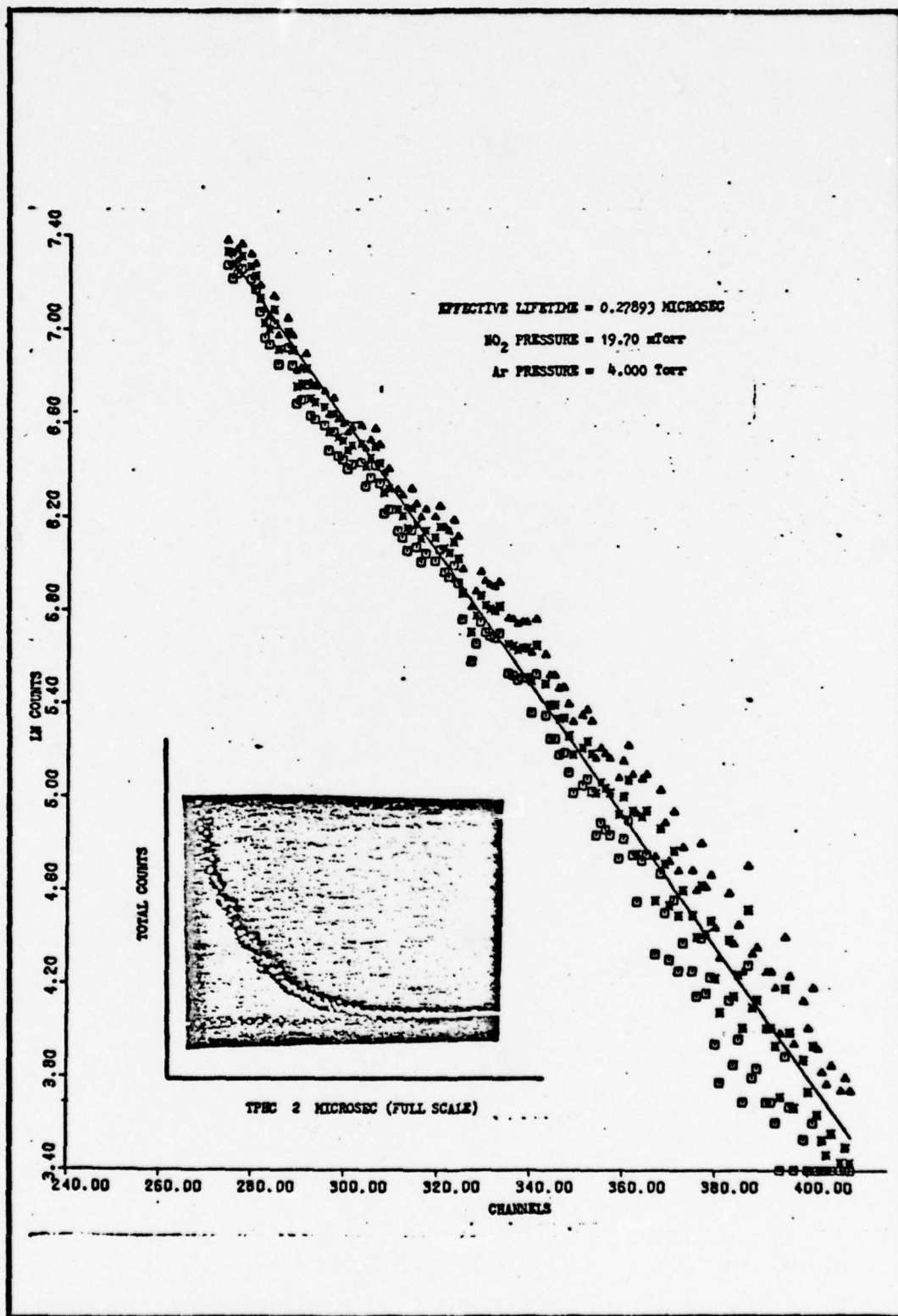


Fig. 22. Ar at 4 Torr

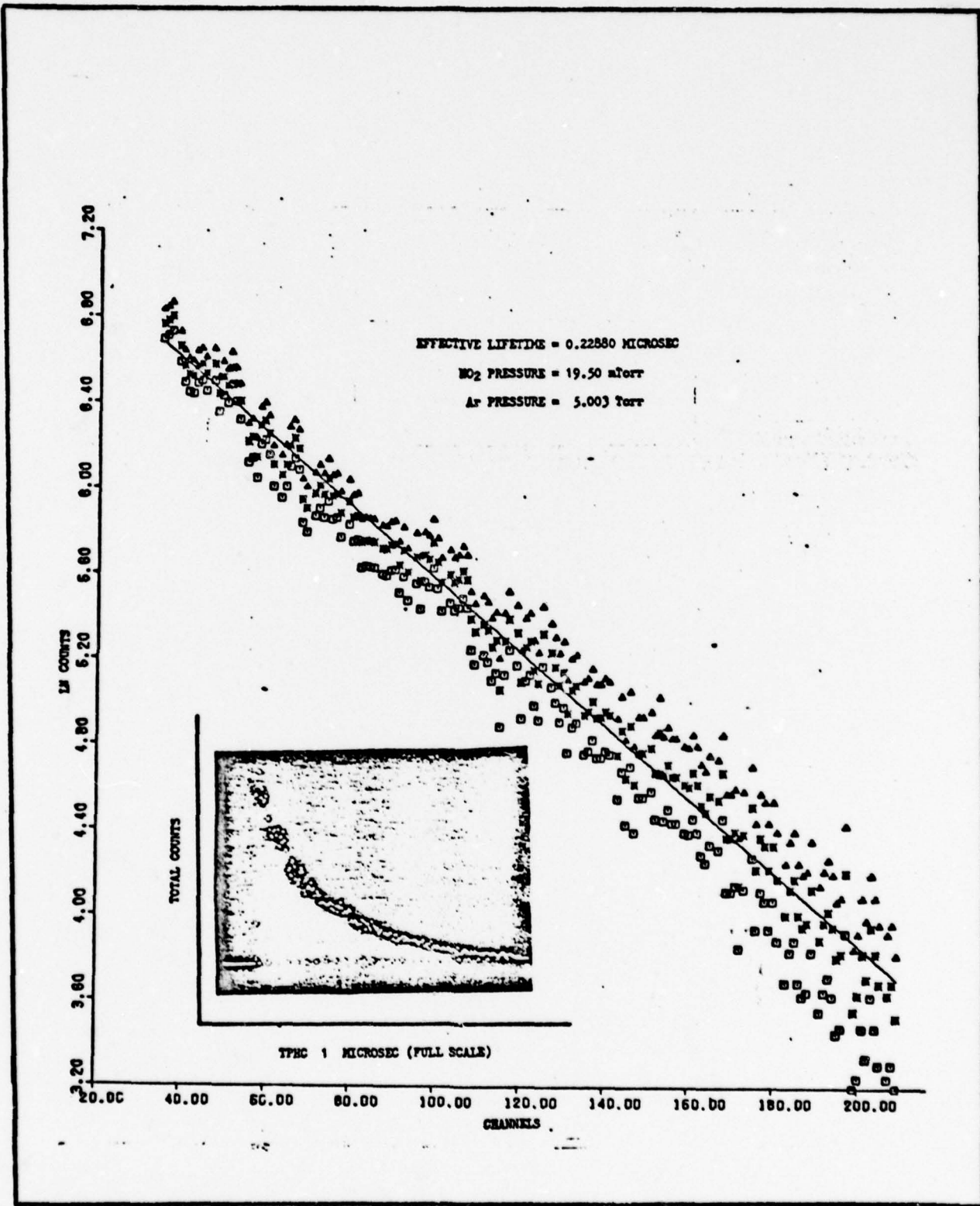


Fig. 23. Ar at 5 Torr

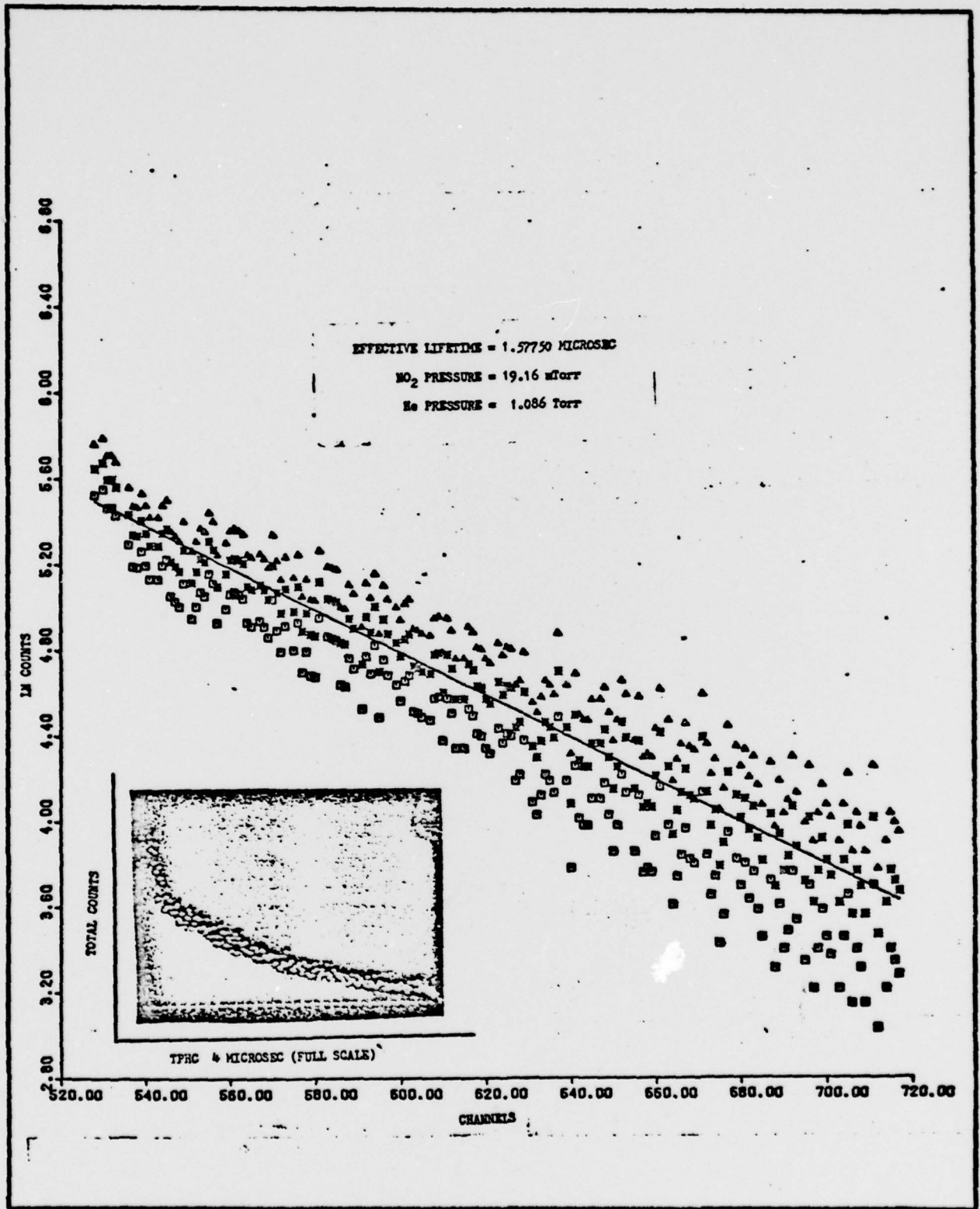


Fig. 24. He at 1 Torr

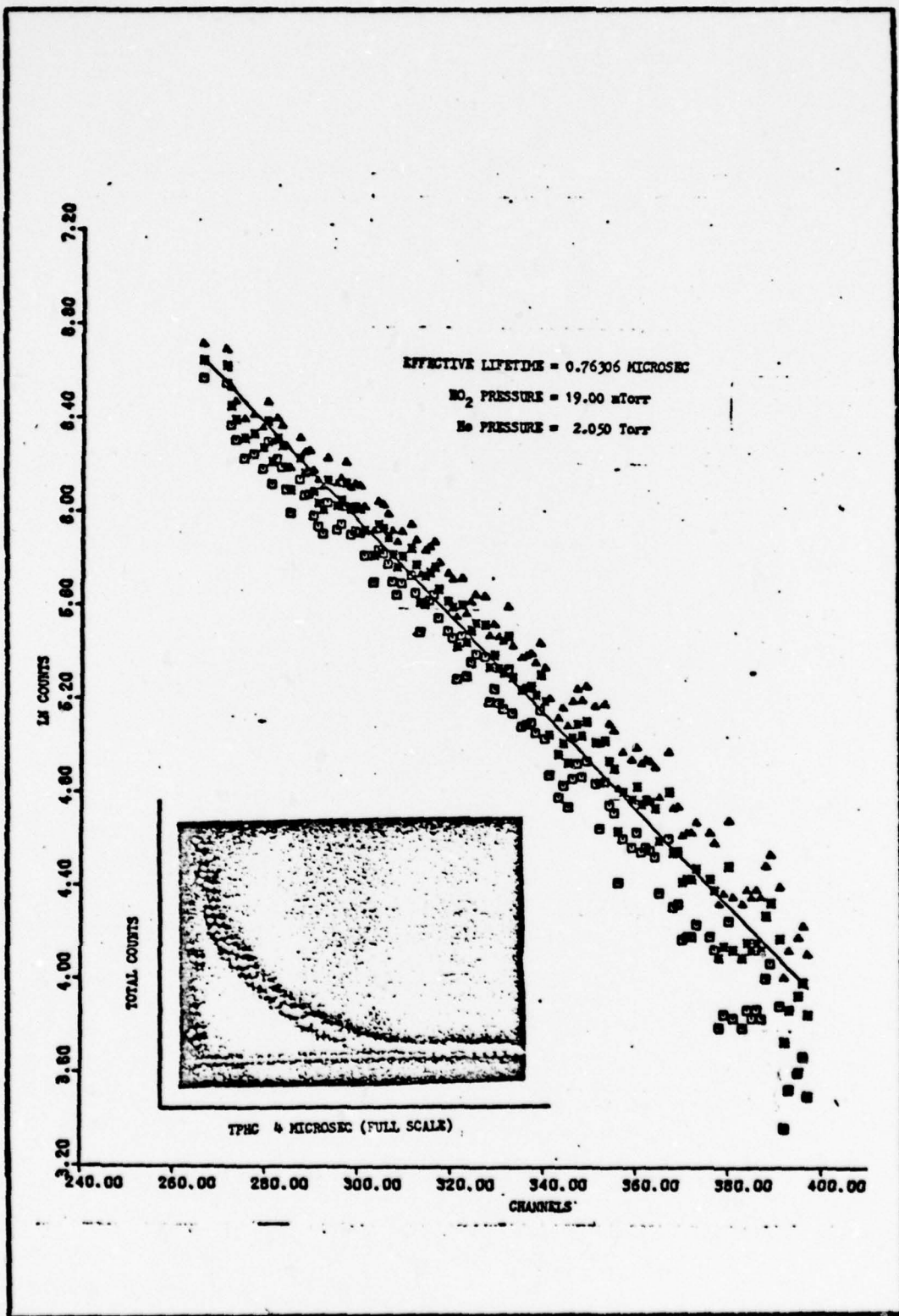


Fig. 25. He at 2 Torr

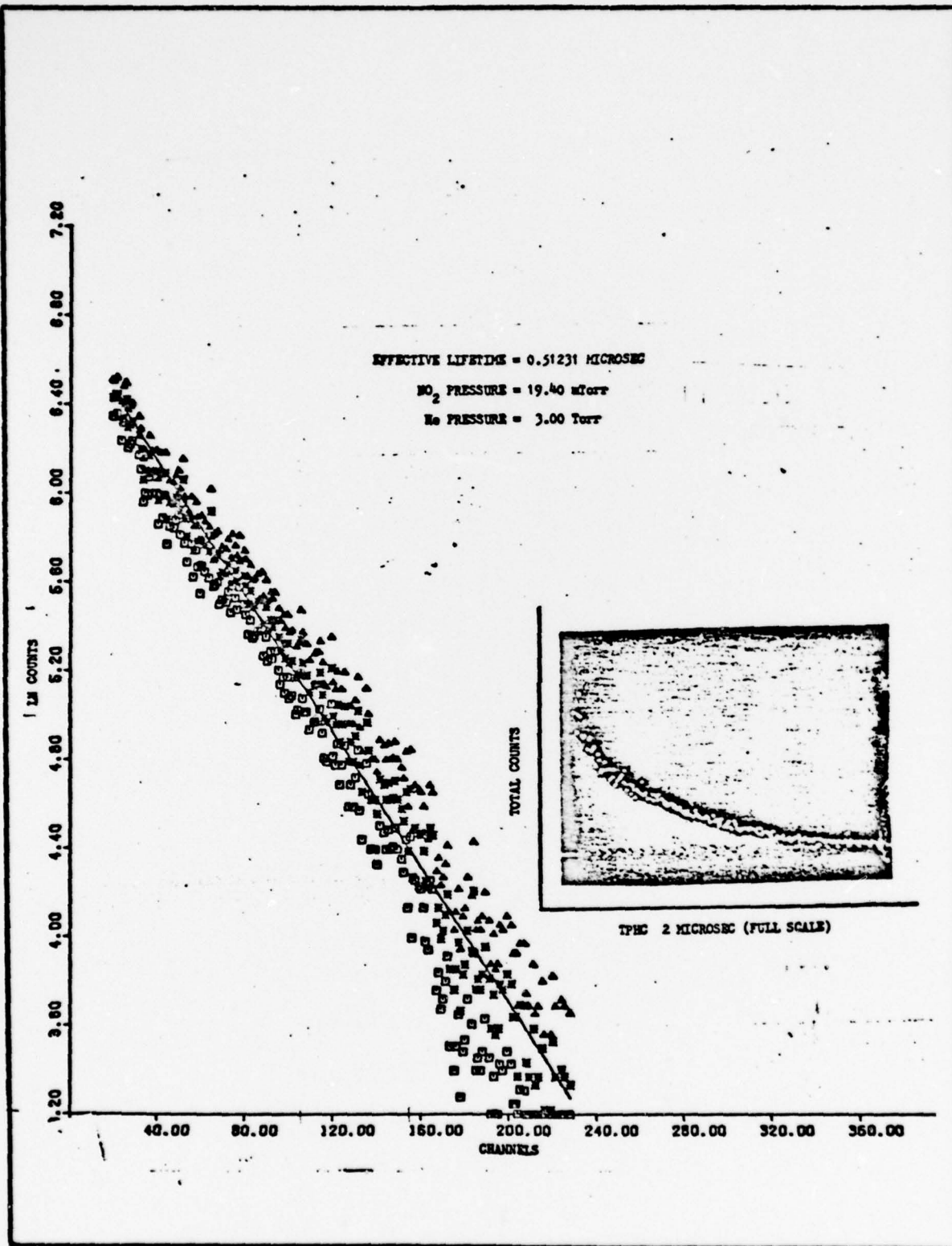


Fig. 26. He at 3 Torr

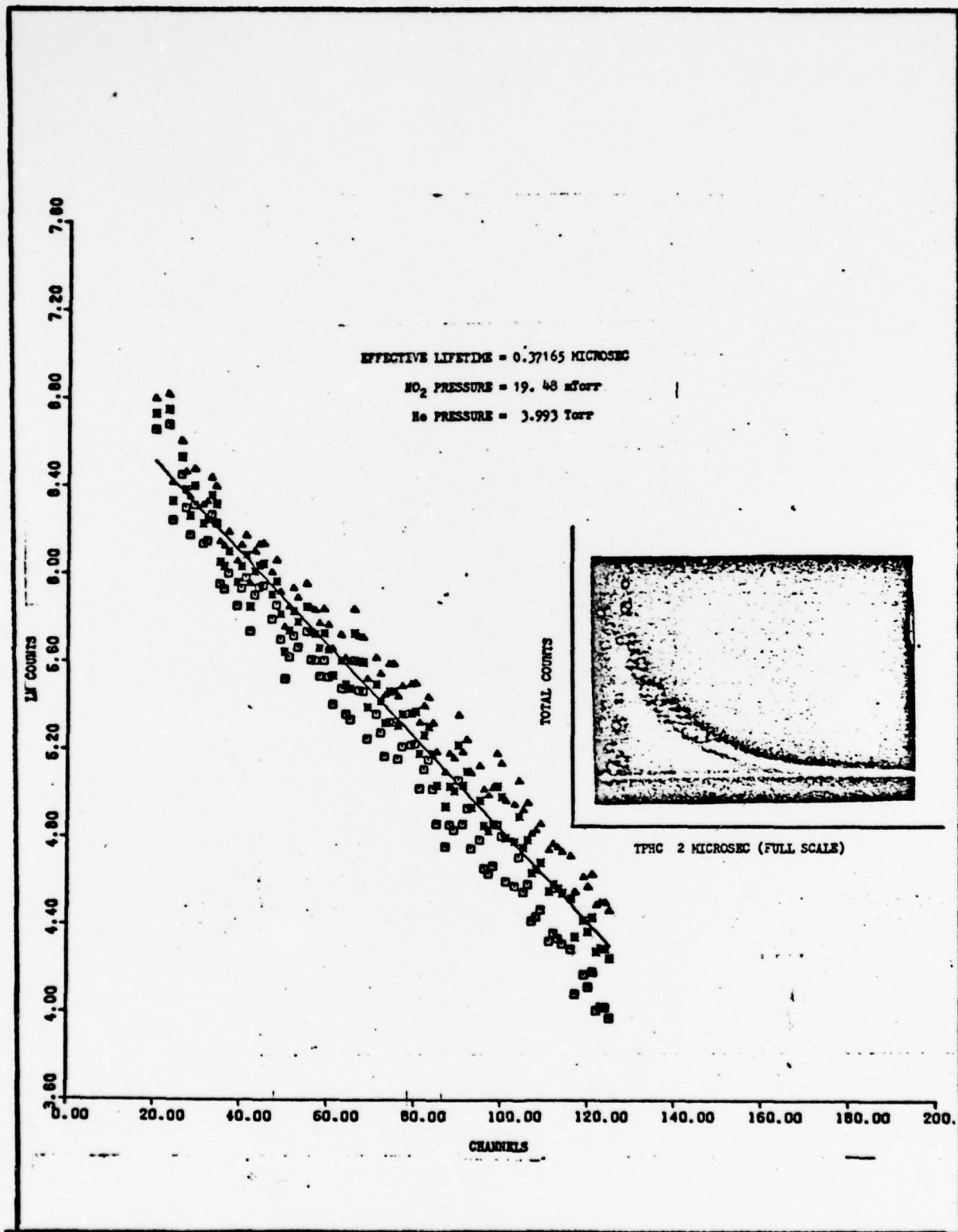


Fig. 27. He at 4 Torr

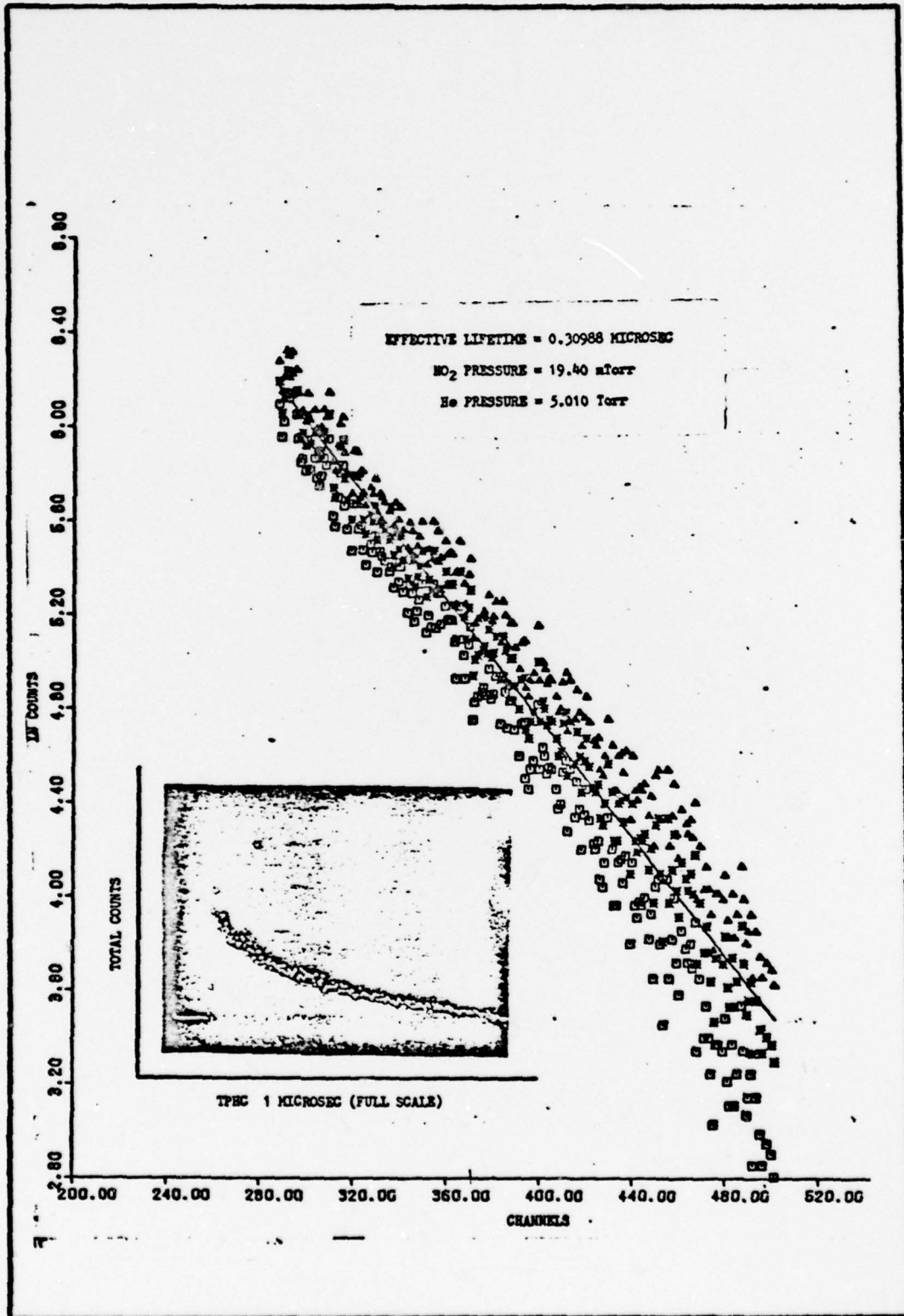


Fig. 28. He at 5 Torr

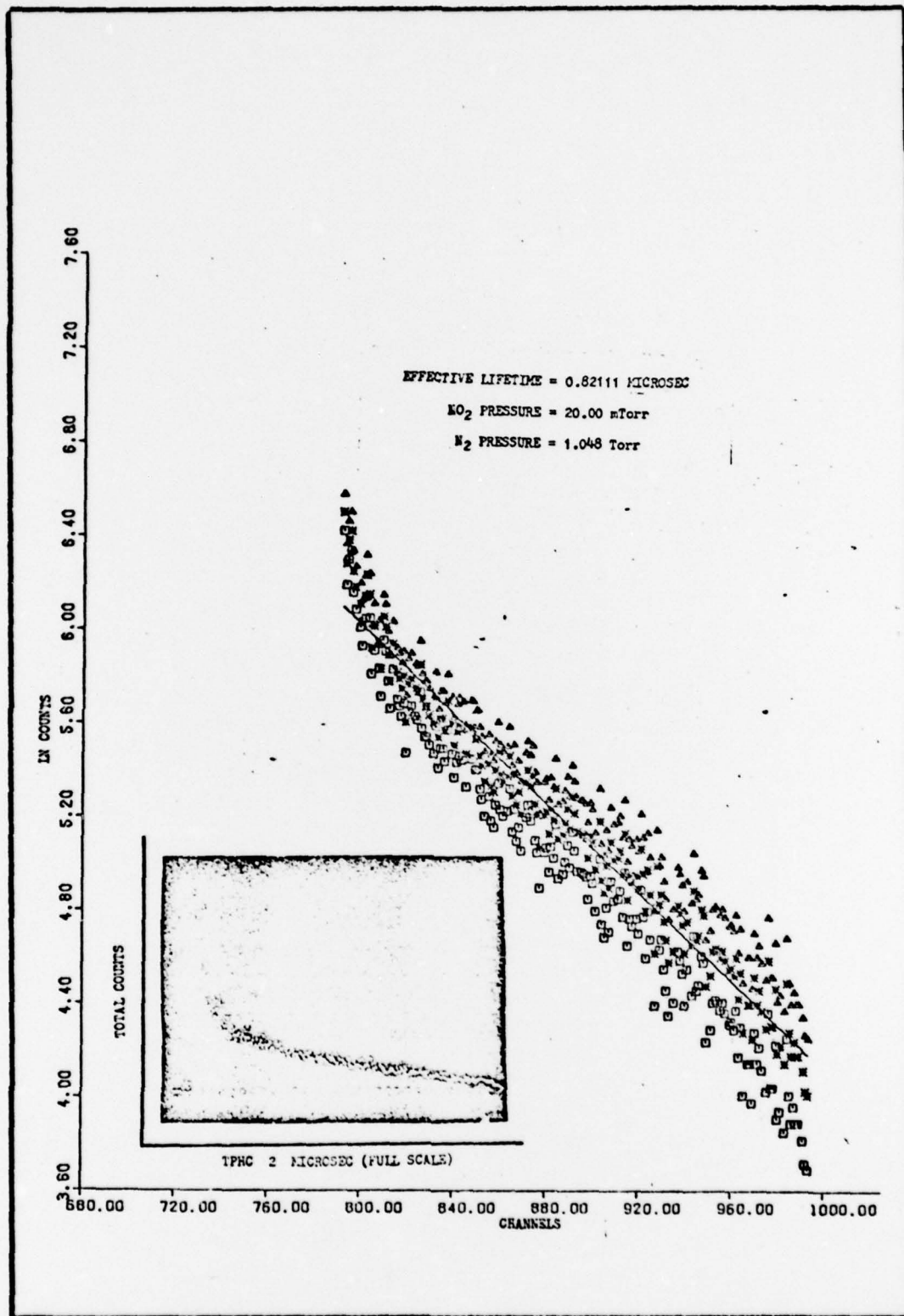


Fig. 29. N<sub>2</sub> at 1 Torr

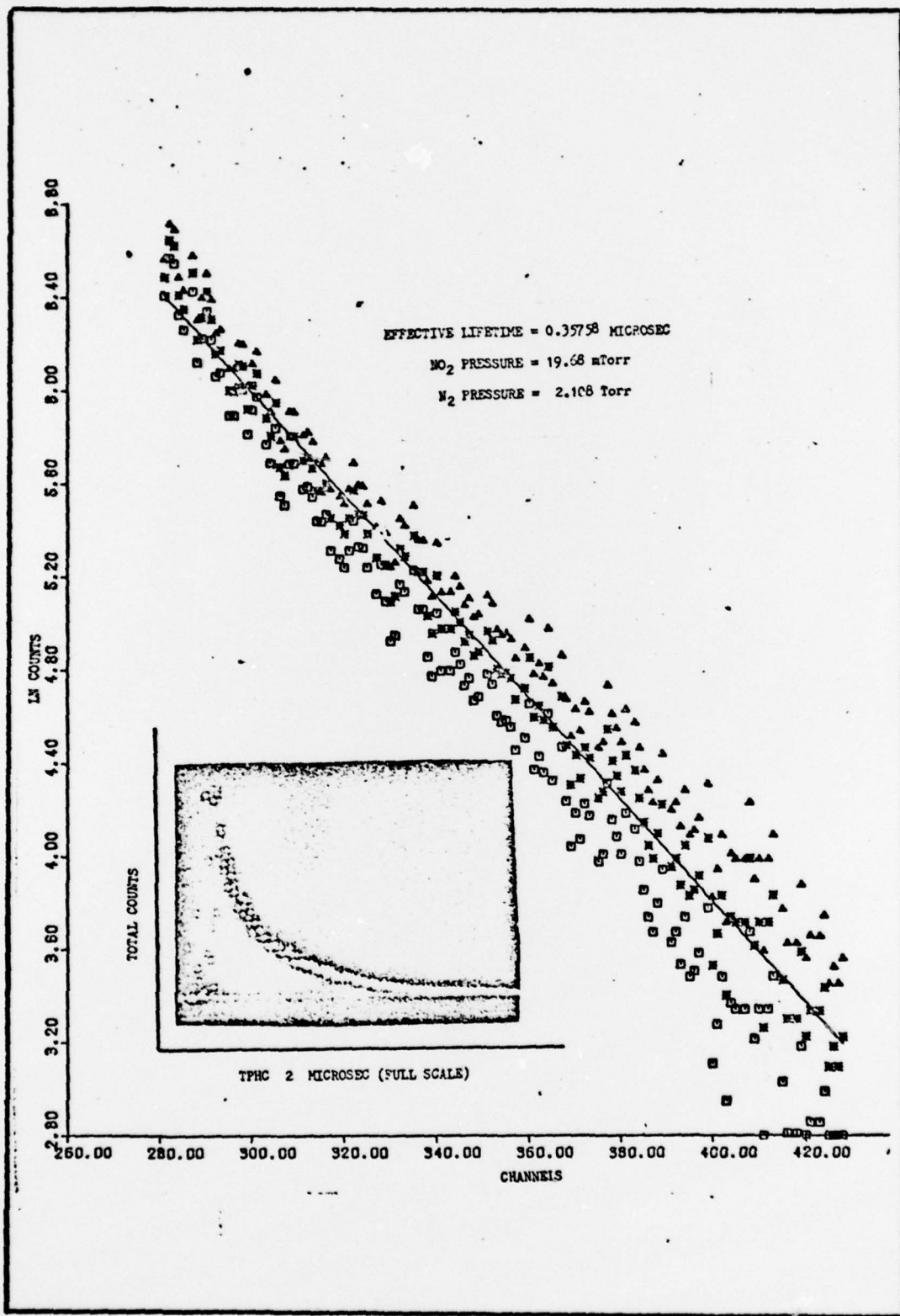


Fig. 30. N<sub>2</sub> at 2 Torr

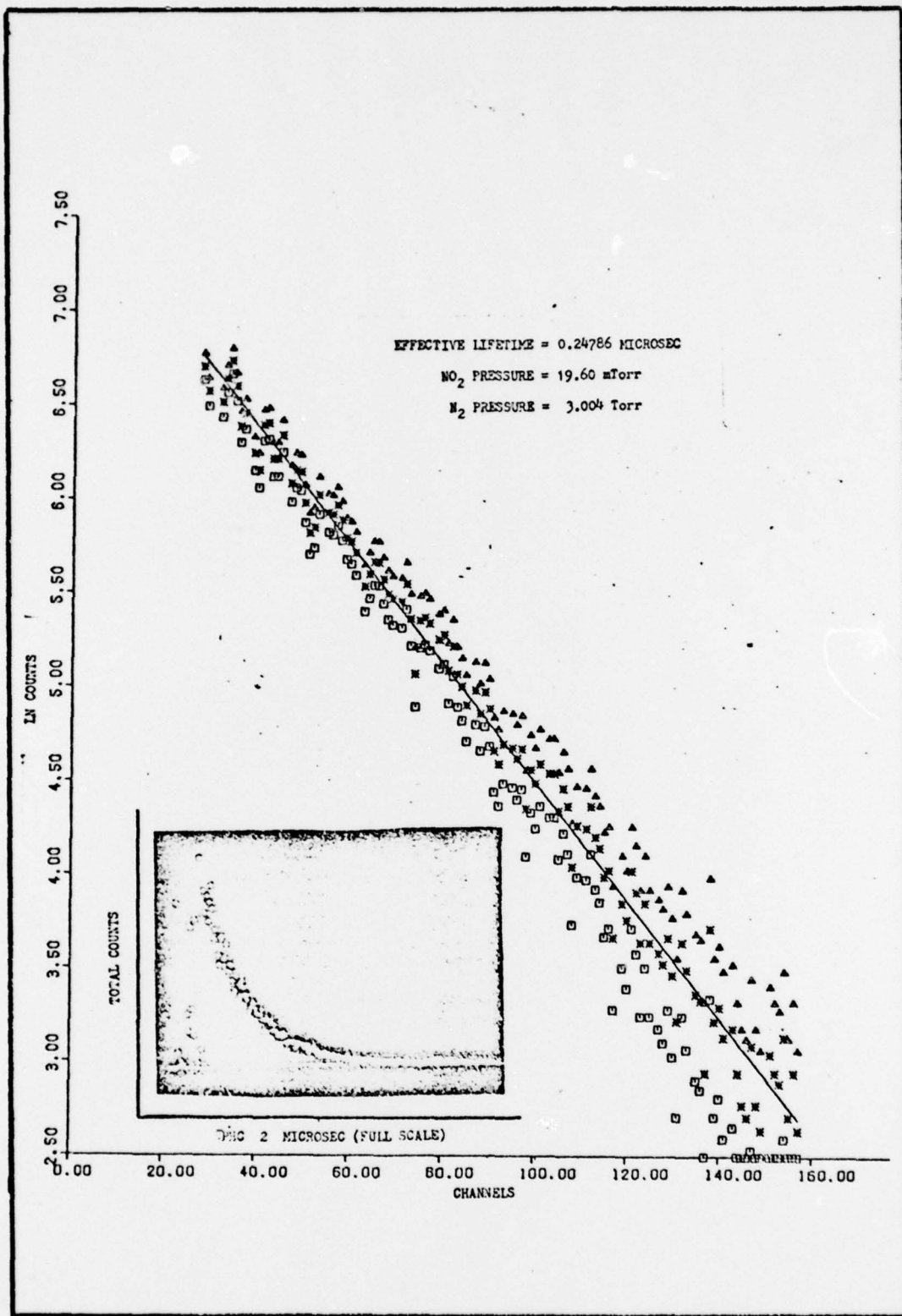


Fig. 31. N<sub>2</sub> at 3 Torr

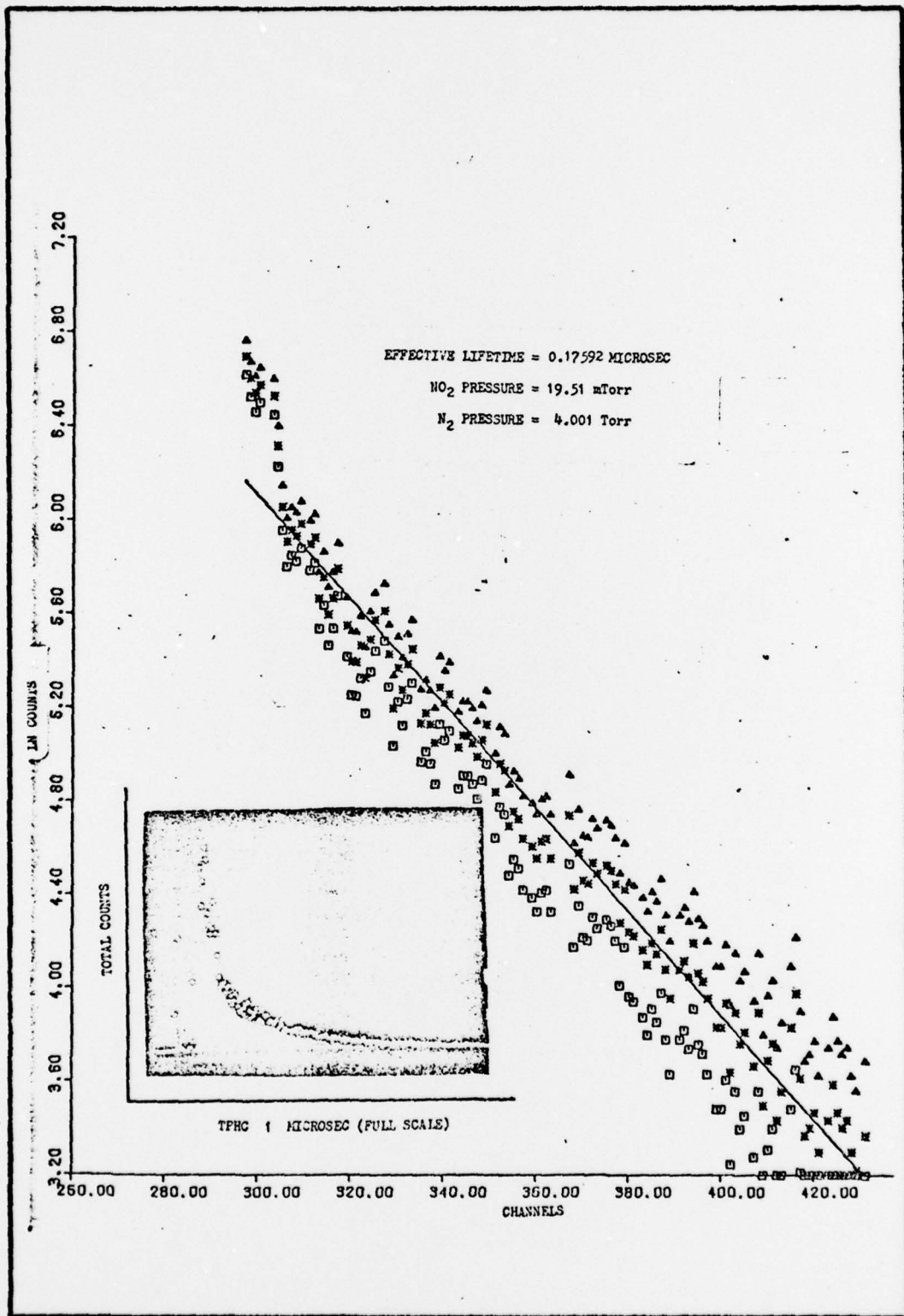


Fig. 32. N<sub>2</sub> at 4 Torr

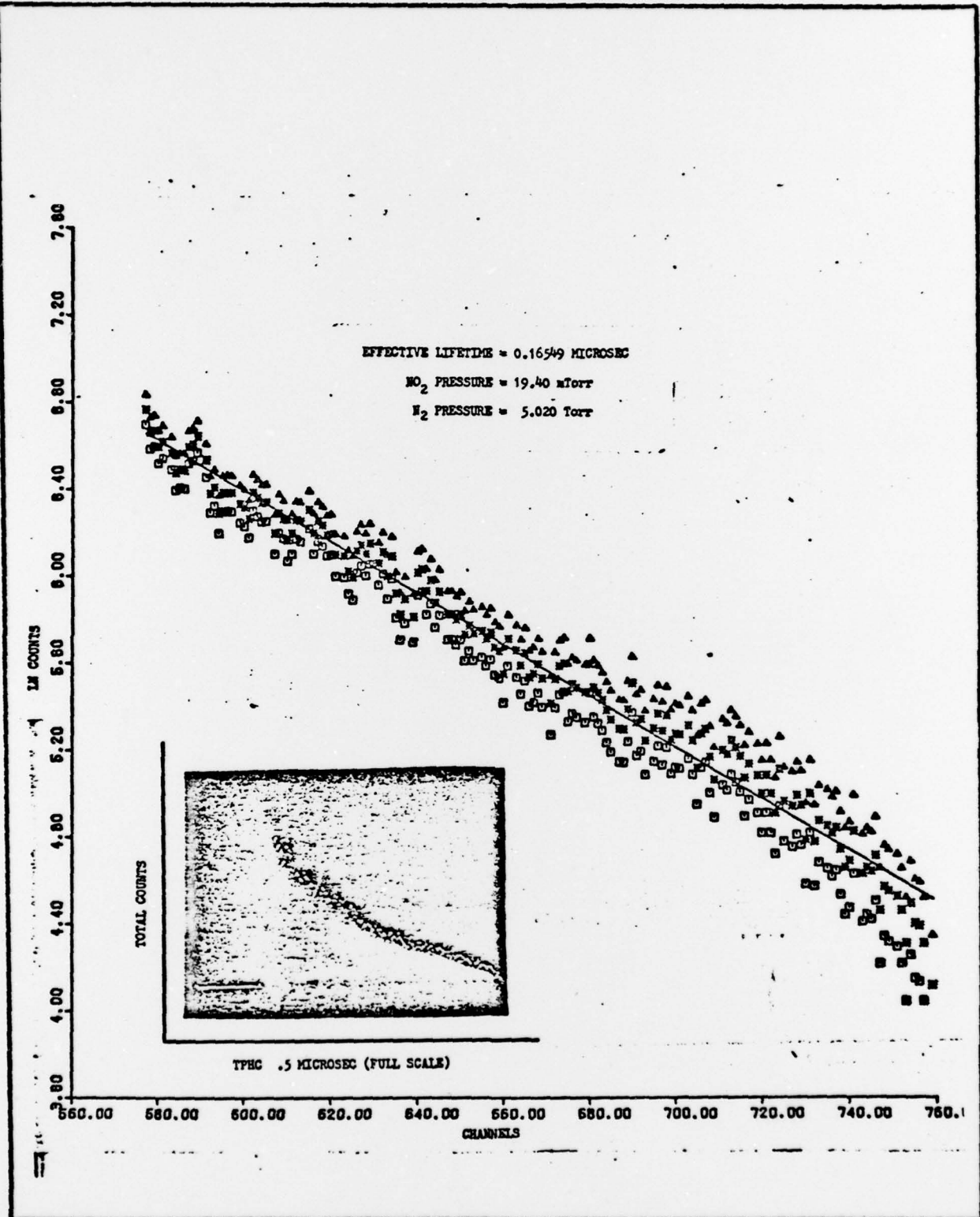


Fig. 33. N<sub>2</sub> at 5 Torr

Appendix D

Appendix D contains the computer program that was used to generate the effective lifetime ( $T_{eff}$ ) and the plots shown in Appendix C.

1 C THIS PROGRAM CALCULATES THE LEAST SQUARES FITTED VALUE OF THE EFFECTIVE

2 C LIFETIMES

3 PROGRAM MAIN (INPUT,OUTPUT,TAPES=INPUT,TAPES=OUTPUT)

4 DIMENSION X(300),Y(300),X(300),Y(300),M(300),C(2),WORK(7),

5 FLOT(300),F(300),G(300),G(300),G(300)

6 CALL PLCT (G,C,C,-3)

7 1 REFC(2) IRH,J

8 2 FORNAT(15,11)

9 10 WRITE(8,11) IN

10 11 FORNAT(15,11) IN

11 12 FORNAT(15,11) IN

12 13 FORNAT(15,11) IN

13 14 FORNAT(15,11) IN

14 15 FORNAT(15,11) IN

15 16 FORNAT(15,11) IN

16 17 FORNAT(15,11) IN

17 18 FORNAT(15,11) IN

18 19 FORNAT(15,11) IN

19 20 FORNAT(15,11) IN

20 21 FORNAT(15,11) IN

21 22 FORNAT(15,11) IN

22 23 FORNAT(15,11) IN

23 24 FORNAT(15,11) IN

24 25 FORNAT(15,11) IN

25 26 FORNAT(15,11) IN

26 27 FORNAT(15,11) IN

27 28 FORNAT(15,11) IN

28 29 FORNAT(15,11) IN

29 30 FORNAT(15,11) IN

30 31 FORNAT(15,11) IN

31 32 FORNAT(15,11) IN

32 33 FORNAT(15,11) IN

33 34 FORNAT(15,11) IN

34 35 FORNAT(15,11) IN

35 36 FORNAT(15,11) IN

36 37 FORNAT(15,11) IN

37 38 FORNAT(15,11) IN

38 39 FORNAT(15,11) IN

39 40 FORNAT(15,11) IN

40 41 FORNAT(15,11) IN

41 42 FORNAT(15,11) IN

42 43 FORNAT(15,11) IN

43 44 FORNAT(15,11) IN

44 45 FORNAT(15,11) IN

45 46 FORNAT(15,11) IN

46 47 FORNAT(15,11) IN

47 48 FORNAT(15,11) IN

48 49 FORNAT(15,11) IN

49 50 FORNAT(15,11) IN

50 51 FORNAT(15,11) IN

51 52 FORNAT(15,11) IN

52 53 FORNAT(15,11) IN

53 54 FORNAT(15,11) IN

54 55 FORNAT(15,11) IN

55 56 FORNAT(15,11) IN

56 57 FORNAT(15,11) IN

57 58 FORNAT(15,11) IN

58 59 FORNAT(15,11) IN

59 60 FORNAT(15,11) IN

60 61 FORNAT(15,11) IN

61 62 FORNAT(15,11) IN

62 63 FORNAT(15,11) IN

63 64 FORNAT(15,11) IN

64 65 FORNAT(15,11) IN

65 66 FORNAT(15,11) IN

66 67 FORNAT(15,11) IN

67 68 FORNAT(15,11) IN

68 69 FORNAT(15,11) IN

69 70 FORNAT(15,11) IN

70 71 FORNAT(15,11) IN

71 72 FORNAT(15,11) IN

Fig. 34. Effective Lifetime Computer Program Page 1

```

60      G(NP+1)=Y(NP+1)
        S(NP+2)=V(NP+2)
        Z(NP+3)=Y(NP+1)
        C(NP+2)=Y(NP+2)
        Y(NP+1)=Y(NP+1)
        Y(NP+2)=Y(NP+2)
        DO 100 I=2,NP
          IF(I).LT.YMIN) F(I)=YMIN
          IF(C(I).LT.YMIN) G(I)=YMIN
          IF(D(I).LT.YMIN) S(I)=YMIN
          IF(E(I).LT.YMAX) F(I)=YMAX
          IF(G(I).LT.YMAX) G(I)=YMAX
          IF(H(I).LT.YMAX) C(I)=YMAX
100      CONTINUE
        CALL AXIS (0,0,1500,AXIS,6,10,90, Y(NP+1), Y(NP+2))
        CALL AXIS (0,0,1500,AXIS,6,10,90, Y(NP+1), Y(NP+2))
        CALL LINE(X1,Y1,X2,Y2)
        CALL LINE(X1,Y1,X2,Y2)
        CALL LINE(X1,Y1,X2,Y2)
        CALL SYM30(3,0,0,0,21,9,LIFETIME=0,9)
        CALL NUMBER(9,0,0,5,90,0,0,21,TAU,0,16)
        CALL SYM30(3,0,0,0,21,9,MICROSEC,0,8)
        CALL PLOT(1)
30      WRITE (10,1) IER
31      FORMAT (2H, I4ERROR FLAG IS , I1)
40      WRITE (6,1) C(I), G(I)
41      FORMAT (6H C1 = , I5,13,5,6X,5H C2 = , I5,13,5)
50      WRITE (6,1) TAU
51      FORMAT (//22H EFFECTIVE LIFETIME IS = ,F10.5, 11H MICROSEC//)
52      WRITE (6,1) CF
53      FORMAT (//50HCF = ,F10.5)
        IF(I.EQ.0) GO TO 1
        STOP
        END

```

SYMBOLIC REFERENCE MAP (R=1)

ENTRY POINTS  
4135 MAIN

ADDRESS	SN	TYPE	RELOCATION	4773	CF	REAL
7251	C	REAL		5455	CNT	REAL
4770	GHS	REAL	ARRAY	4771	CSUM	REAL
4772	GTH	REAL	ARRAY	10422	F	REAL
4724	FOI	REAL	ARRAY	4772	FUCT	REAL
4723	FOI	REAL	ARRAY	4753	I	REAL
4722	IER	INTEGER		4762	IN	INTEGER
4723	IR4	INTEGER		4754	J	INTEGER
4724	K	INTEGER		5000	N	INTEGER
4725	N016	INTEGER		4751	NMAX	INTEGER
4727	N0	INTEGER		4766	SUM1	REAL

Fig. 35. Effective Lifetime Computer Program Page 2



### Appendix E

This appendix develops the basic derivation of the relationship that describes the probability of obtaining a photon in the interval  $t$  to  $t + \Delta t$ . The derivation was developed by Wharton (Ref 3:19) and used in a similar manner in his experimental effort.

The probability relationship begins by considering the fact that it is the timing equipment which detects the initial photon. Thus, if we let

$q$  = the probability that a molecule does not decay before some time  $t$ .

$p$  = the probability that a molecule will decay in the next time interval,  $t$  to  $t + \Delta t$ .

$P_c$  = the probability that a photon will be detected

$N_0$  = the initial number of excited molecules at time  $t = 0$ .

If we allow the initial number of molecules  $N_0$  to be unity, then the probability of detecting a photon in the interval  $t$  to  $t + \Delta t$  is

$$P = qpP_c N_0 \quad (53)$$

or

$$P = qpP_c$$

If  $N_0 = 2$ , then either the two molecules remain excited at time  $t$  or one molecule remains excited and the other has

decayed but not detected. The probability of detecting a photon in the interval  $t$  to  $t + \Delta t$  is

$$P = 2q^2 p P_c + 2q(1 - q)(1 - P_c) p P_c \quad (54)$$

If  $N_0 = 3$ , then three molecules can be excited, or two excited molecules can exist at time  $t$  with one molecule decayed but not detected. Alternately, at time  $t$  we can have one molecule excited with two molecules decayed and neither detected. The probability of detecting a photon in the interval  $t$  to  $t + \Delta t$  is

$$P = 3q^3 p P_c + 6q^2 p P_c (1 - q)(1 - P_c) + 3q p P_c (1 - q)^2 (1 - P_c)^2 \quad (55)$$

Considering the general case of  $N_0$  excited atoms, the probability of detecting a photon in the interval  $t$  to  $t + \Delta t$  is by induction

$$P = p P_c \left[ \sum_{m=1}^{N_0} \frac{m N_0!}{m! (N_0 - m)!} q^m [1 - q]^{(N_0 - m)} [1 - P_c]^{(N_0 - m)} \right] \quad (56)$$

which upon rewriting becomes

$$P = p P_c N_0 q [1 - P_c (1 - q)]^{(N_0 - 1)}$$

and using the substitutions  $p = \Delta t / \tau$  and  $q = \exp(-t/\tau)$

Eq (56) becomes

$$P = P_c N_0 \Delta t \tau^{-1} \exp(-t/\tau) \left[ 1 - P_c [1 - \exp(-t/\tau)] \right]^{(N_0 - 1)} \quad (57)$$

If we consider the case for large  $N_0$ , then  $N_0 - 1 = N_0$ ,  
and retaining only the first terms gives us

$$P = P_c N_0 \Delta t \tau^{-1} [\exp(-t/\tau)] [1 - N_0 P_c [1 - \exp(-t/\tau)]] \quad (58)$$

and finally if  $N_0 P_c \ll 1$  we achieve the desired result  
from Eq (58)

$$P = P_c N_0 \Delta t \tau^{-1} \exp(-t/\tau) \quad (59)$$

### Vita

Freddie Garcia, Jr. was born on January 12, 1941, in Tampa, Florida. He is the son of Mrs. Marina Garcia. He attended the University of South Florida (USF) at Tampa, Florida, after graduating from high school in 1960. In 1964 he received the degree of Bachelor of Science in Physics and entered the United States Air Force Officer Training School (OTS) at Lackland AFB, Texas. After OTS he was assigned to the 44th Strategic Missile Wing (SAC), Ellsworth AFB, South Dakota. In 1967 he entered Undergraduate Navigator Flying Training at Mather AFB, Sacramento, California. Upon graduation from navigator flying training he was assigned to the 362 Tactical Electronic Warfare Squadron (PACAF) Pleiku AB, Vietnam. After one year and more than 800 hours of combat flying time, he was assigned to 76th Military Airlift Squadron (MAC), Charleston, South Carolina. In 1970, he was assigned to the Royal Air Force (RAF) College of Air Warfare, Manby, Lincolnshire, England, as an allied exchange officer. While serving with the Royal Air Force, he graduated from the Number 4 General Duties Aerosystems Course and served as a flight and academic instructor at the RAF College of Air Warfare. In 1973 he was assigned to the Aviation Science Division of the Air Force Academy, Colorado Springs, Colorado, where he served as the Chief, Advanced Systems and Concepts Branch and served as a flight instructor. He is married to the former Renee Wilson and has two daughters--Nicole, age 7 years, and Yvette, age 4 years. Major Garcia began his tour at the Air Force Institute of Technology in June 1977.

Permanent address: 2604 North Habana  
Tampa, Florida 33607

REPORT DOCUMENTATION PAGE		READ INSTRUCTIONS BEFORE COMPLETING FORM
1. REPORT NUMBER GEP/PH/78-3	2. GOVT ACCESSION NO.	3. RECIPIENT'S CATALOG NUMBER
4. TITLE (and Subtitle) THE MEASUREMENT OF QUENCHING RATE CONSTANTS USING FLUORESCENCE EMISSION		5. TYPE OF REPORT & PERIOD COVERED MS Thesis
7. AUTHOR(s) Freddie Garcia, Jr. Major USAF		6. PERFORMING ORG. REPORT NUMBER
9. PERFORMING ORGANIZATION NAME AND ADDRESS Air Force Institute of Technology(ATC)AFIT/EN Wright-Patterson AFB, Ohio 45433		8. CONTRACT OR GRANT NUMBER(s)
11. CONTROLLING OFFICE NAME AND ADDRESS		10. PROGRAM ELEMENT, PROJECT, TASK AREA & WORK UNIT NUMBERS
14. MONITORING AGENCY NAME & ADDRESS(if different from Controlling Office) Air Force Aeropropulsion Laboratory (AFPL)		12. REPORT DATE December 1978
		13. NUMBER OF PAGES 119
		15. SECURITY CLASS. (of this report) Unclassified
		15a. DECLASSIFICATION/DOWNGRADING SCHEDULE
16. DISTRIBUTION STATEMENT (of this Report)  Approved for public release; distribution unlimited		
17. DISTRIBUTION STATEMENT (of the abstract entered in Block 20, if different from Report)		
18. SUPPLEMENTARY NOTES Approved for public release; IAW AFR 190-17  Joseph P. Hipps, Major, USAF Director of Information 19 Jan 79		
19. KEY WORDS (Continue on reverse side if necessary and identify by block number) Nitrogen Dioxide Fluorescence Lifetimes Quenching Rate Constants		
20. ABSTRACT (Continue on reverse side if necessary and identify by block number) A single counting technique is employed to measure the effective lifetime of excited NO <sub>2</sub> . These data are necessary for measurements of quenching rate constants of Ar, He and N <sub>2</sub> . A tuneable dye laser is used to raise the NO <sub>2</sub> to an excited electronic level. The NO <sub>2</sub> is held at a constant millitorr pressure while the foreign gas (Ar, He, N <sub>2</sub> ) pressure is varied. The results are compared to another investigator.		